6.0 FLIGHT CONTROL EFFECTORS

This section contains data pertaining to the requirements and capabilities of the flight control effectors used during ascent. These are SSME, OMS, and SRB engine gimbaling and Orbiter elevons as illustrated in Figure 6-1. The SSME and SRB gimbal deflection sign conventions are provided in Figure 6-2. The actuator/effector parameters of the SSME, OMS, and SRB TVC systems are tabulated in Table 6.1. Additional details of the capability of the ascent flight control effectors for operational vehicles are provided in Paragraph 2.1.

6.1 SSME GIMBAL

Figure 6-3 is a schematic showing the orientation of the SSME actuators which are designated Type I, Type II and Type III. There are two actuators per SSME, one for pitch and one for yaw. Each actuator is fastened to the Orbiter thrust structure and to the powerhead of one of the three SSMEs. Each of the six servoactuators respond to identical command voltages issued from four different drivers, each located in different ascent TVC channels. These voltages command the SSME hydraulic actuator to extend or retract, thus gimbaling the SSME to which it is attached, changing its thrust vector.

The geometry of the SSME pitch and yaw actuators is provided in Figure 6-4. The installed null position of SSME-1 is 0.0 degrees yaw and 16.0 degrees pitch above the Fuselage Reference Line (FRL). For SSME-2 and SSME-3, the installed null is 3.5 degrees yaw outboard and 10.0 degrees pitch above the FRL. As illustrated in Figures 6-5 and 6-6, the three pitch actuators gimbal the engines up or down a maximum of 10.5 degrees from the installed null position and the three yaw actuators gimbal the engines left or right a maximum of 8.5 degrees from the installed null position. Following SSME ignition, when all three engines exceed 90% RPL, SSME-2 and SSME-3 are commanded to gimbal in yaw 3.5 degrees inboard from their installed null positions. The SSME gimbal rate capability relative to TVC actuator load varies with actuation system tolerances and end-of-life factors. Figures 6-7 and 6-8 show the boundaries of the rate capabilities. For first stage, the SSME gimbal rate limits are set by software at 8 deg/sec, 5 deg/sec, and 4.0 deg/sec for zero, one and two hydraulic system failures, respectively. For second stage, the maximum gimbal rate limit is 10 deg/sec with priority rate limiting provided for both single and double hydraulic failures. The engine gimbal acceleration range is 0.78 rad/sec^2 to 30 rad/sec^2.

Structural interference exists between the three SSME nozzles for various combinations of SSME gimbal angles. The combinations of gimbal angles resulting in zero clearance between SSME-1 and -2, SSME-1 and -3, and SSME-2 and -3 are provided in Tables 6.2, 6.3 and 6.4, respectively. Clearances between the SSME nozzles are illustrated in Figures 6-9 and 6-10.

Structural interference can also exist between SSME-1 and the OMS. This consists of two possible types of interference: a) interference between the OMS pods and the SSME-1 nozzle and b) interference between the left and right OMS engines nozzles and the SSME-1 nozzle.

To prevent the SSME-1 nozzle from striking either the left or right OMS pod, the algebraic sum of the magnitudes of the pitch and yaw deflections of SSME-1 is limited to 13.7 degrees in the directions towards the two OMS pods (up-pitch half of the gimbal pattern). Based on this constraint, the pitch and yaw gimbal commands to SSME-1 are limited in the flight software. The resulting SSME-1 Gimbal Envelope is provided in Figure 6-11.

When the OMS engines are gimbaled down and inboard towards SSME-1, the OMS engines nozzles can strike the SSME-1 nozzle if SSME-1 is also gimbaled up towards the OMS engines. Clearances between the nozzles of SSME-1 and the OMS engines are provided in Tables 6.5, 6.6 and 6.7 and Figure 6-12. During ascent when the SSMEs are active, the OMS engines are stowed to preclude collisions with SSME-1 and when the OMS engines are active, SSME-1 is stowed in non-interference locations with respect to the OMS engines.

The body flap and the lower SSMEs (SSME-2 and -3) can collide for various combinations of body flap deflections and lower SSME pitch gimbal angles. This is shown in Figure 6-13.

6.2 OMS GIMBAL

The OMS TVC converts automatic and manual maneuver commands to OME deflections by means of actuator extend/retract voltages. The gimbal actuator assembly provides forces to gimbal the OME for thrust vector control. Each OME has one pitch and one yaw actuator. The OMS gimbal capability and installed null position are illustrated in Figure 6-14. The minimum gimbal rate with operational loads is 3.0 deg/sec and the minimum gimbal acceleration at zero rate with operational loads is 11.46 deg/sec^2.

The engine coordinate system is a right-handed system. The engine centerline in mechanical null is the X axis (+X forward), the engine XY plane is a plane perpendicular to the Orbiter XZ plane with an angle of 15 degrees 49 minutes 28 seconds with respect to the Orbiter XY plane and measured in the Orbiter XZ plane. The engine mechanical null position makes an angle of 6 degrees 30 minutes with respect to the Orbiter XZ plane, as measured in the engine XY plane.

6.3 SRB GIMBAL

During first stage of ascent, each SRM nozzle is gimballed along with the SSME nozzles for TVC. The TVC subsystem of each SRB consists of two self-contained,

independent Hydraulic Power Units (HPUs) and two hydraulic gimbal servoactuators (one for rock and one for tilt). Each HPU is connected to both servoactuators on that SRB. One acts as the primary hydraulic source and the other serves as the secondary source. The servoactuators provide the force and control to gimbal the Solid Rocket Motor (SRM) nozzle. Each SRB servoactuator consists of four independent two-stage servovalves that receive electrical signals proportional to Orbiter computer-commanded gimbal position. Each servovalve controls one power spool in each actuator which extends or retracts a dual-action piston in response to hydraulic pressure. The piston rods exert mechanical pressure on the nozzle causing it to gimbal about a pivot to control the direction of thrust. The orientation of the SRB actuators is illustrated in Figure 6-15. The nozzle gimbal capability is illustrated in Figure 6-16. The nominal nozzle gimbal rate and acceleration capability per axis under full load with two APUs operating is 5 deg/sec and 2 rad/sec^2, respectively. Figure 6-17 shows the rock or tilt SRB nozzle rate capability versus nozzle torque.

In the event of a hydraulic system failure, a switching valve in the actuator switches over to the remaining good system so that both actuators operate from a single hydraulic system. The maximum flow rate capability of a single hydraulic system corresponds approximately to 6.8 deg/sec for combined rock and tilt rates. Therefore, during operation of both rock and tilt actuators supplied by only one hydraulic system, when the actuators are commanded simultaneously, the achieved rates will be limited by flow rate so that the sum of the rates will be no greater than 6.8 deg/sec.

The SRB TVC gimbal position limits are ± 2 degrees for the first 2.5 seconds after SRB ignition and ± 4.5 degrees afterwards as shown in Figure 6-18. At event 27, SRB separation function moding, which occurs nominally at 1.7 seconds prior to the SRB separation command, both SRB nozzles are commanded to their null position of 0.0° rock and 0.0 degrees tilt.

6.4 ORBITER ELEVONS

The Orbiter elevons are the only aerodynamic surfaces which are actively controlled during ascent. There are four elevons - two inboard and two outboard. The elevon numbering and deflection sign conventions are illustrated in Figure 6-19.

The elevon actuator subsystem is an electro/hydromechanical subsystem that provides the necessary power to deflect the elevon surface panels that control the pitch and roll attitudes of the Orbiter. The inboard and outboard elevons are independently positioned - the maximum command elevon deflection rate during first stage is 2 deg/sec. The geometry of the elevon actuators is provided in Figure 6-20 and the maximum hardware and software elevon deflection limits are specified in Figure 6-21.

Due to Orbiter wing loading constraints, the elevons follow a predetermined deflection versus velocity profile during first stage as specified in NSTS 08209, Volume IV, Shuttle

Systems Design Criteria, Generic Ascent Flight Design Requirements. To prevent exceeding elevon structural loading limits during first stage, active elevon load relief logic is provided in the flight software as described in Paragraph 9.1. The primary load relief feedback indicator is the elevon actuator delta pressure. The maximum commanded elevon deflection rate during first stage is 2 deg/sec.

TABLE 6.1

ACTUATOR/EFFECTOR PARAMETERS OF TVC EFFECTOR SYSTEMS

		Top SSME Pitch	Low SSME Pitch	SSME Yaw	SRB Rock or Tilt	OMS Pitch	OMS Yaw
Stroke (in)		±5.449	±5.449	±4.413	±6.40	±3.79 min (±6 deg)	±4.38 min (±7 deg)
Piston Area (in^2)		24.83	20.03	20.03	32.32	N/A	N/A
Average Moment Arm (in)		29.74	29.74	29.74	71.60	N/A	N/A
Design Rate	deg/sec	10	10	10	5	3	3
	in/sec	5.19	5.19	5.19	6.25	0.983	0.983
Design Load (Hinge Moment Versus Rate)	lb	48,217	38,918	38,918	63,348	260+1.5 lb/sec^2/in inertia; 275 - lb breakaway; 2,500 static; ±3,500/lb dynamic	
	million in/lb	1.43	1.16	1.16	4.54		
No-load Rate Grain (0/sec/deg)		20.7	20.7	20.1	15.54	N/A	N/A
Operating Pressure (psid)		3,000 ± 100	3,000 ± 100	3,000 ± 100	2,940 - 3,250	N/A	N/A
Secondary Pressure Gain (psi/ma)		500 ± ×125	500 ± 125	500 ± 125	500 ± ×10%	N/A	N/A
Effector Inertia ($in/lb/sec^2$)		57,700	57,700	57,700	132,000		

TABLE 6.2

COMBINATIONS OF GIMBAL ANGLES FOR SSME-1 AND 2 THAT RESULT IN ZERO CLEARANCE BETWEEN NOZZLES (JUST TOUCHING)

Case	Combinations of Gimbal Angles That Result in Zero Clearance Between Nozzles			
	SSME-1		SSME-2	
	Pitch (w_{p1}), Degrees	Yaw (w_{y1}), Degrees	Pitch (w_{p2}), Degrees	Yaw (w_{y2}), Degrees
1	10.5*	0	−10.5*	2.95
2	10.5*	0	−7.52	0
3	10.5*	0	−1.95	−8.5*
4	10.5*	8.5*	0.69	−8.5*
5	10.5*	8.5*	0	−5.40
6	10.5*	8.5*	−1.96	0
7	10.5*	8.5*	−7.47	8.5*
8	10.5*	−8.5*	−10.5*	−5.53
9	10.5*	−8.5*	−7.50	−8.5*
10	0	8.5*	−10.5*	−5.40
11	0	8.5*	−9.81	−8.5*
12	10.5*	−2.94	−10.5*	0
13	7.52	0	−10.5*	0
14	1.96	8.5*	−10.5*	0
15	−0.69	8.5*	−10.5*	−8.5*
16	0	5.38	−10.5*	−8.5*
17	1.95	0	−10.5*	−8.5*
18	7.50	−8.5*	−10.5*	−8.5*
19	10.5*	5.48	−10.5*	8.5*
20	7.47	8.5*	−10.5*	8.5*
21	10.5*	5.38	0	−8.5*
22	9.81	8.5*	0	−8.5*

*Corresponds to thrust vector controller actuator hard stop.

TABLE 6.3

COMBINATIONS OF GIMBAL ANGLES FOR SSME-1 AND 3 THAT RESULT IN ZERO CLEARANCE BETWEEN NOZZLES (JUST TOUCHING)

Case	Combinations of Gimbal Angles That Result in Zero Clearance Between Nozzles			
	SSME-1		SSME-3	
	Pitch (w_{p2}), Degrees	Yaw (w_{y2}), Degrees	Pitch (w_{p3}), Degrees	Yaw (w_{y3}), Degrees
1	10.5*	0	– 10.5*	– 2.95
2	10.5*	0	– 7.52	0
3	10.5*	0	– 1.95	8.5*
4	10.5*	– 8.5*	0.69	8.5*
5	10.5*	– 8.5*	0	5.40
6	10.5*	– 8.5*	– 1.96	0
7	10.5*	– 8.5*	– 7.47	– 8.5*
8	10.5*	8.5*	– 10.5*	5.53
9	10.5*	8.5*	– 7.50	8.5*
10	0	– 8.5*	– 10.5*	5.40
11	0	– 8.5*	– 9.81	8.5*
12	10.5*	2.94	– 10.5*	0
13	7.52	0	– 10.5*	0
14	1.96	– 8.5*	– 10.5*	0
15	– 0.69	– 8.5*	– 10.5*	8.5*
16	0	– 5.38	– 10.5*	8.5*
17	1.95	0	– 10.5*	8.5*
18	7.50	8.5*	– 10.5*	8.5*
19	10.5*	– 5.48	– 10.5*	– 8.5*
20	7.47	– 8.5*	– 10.5*	– 8.5*
21	10.5*	– 5.38	0	8.5*
22	9.81	– 8.5*	0	8.5*

*Corresponds to thrust vector controller actuator hard stop.

TABLE 6.4

COMBINATIONS OF GIMBAL ANGLES FOR SSME-2 AND 3 THAT RESULT IN ZERO CLEARANCE BETWEEN NOZZLES (JUST TOUCHING)

Case	Combinations of Gimbal Angles That Result in Zero Clearance Between Nozzles			
	SSME-2		SSME-3	
	Pitch (w_{p2}), Degrees	Yaw (w_{y2}), Degrees	Pitch (w_{p3}), Degrees	Yaw (w_{y3}), Degrees
1**	0	– 5.69	0	5.69
2**	0	– 8.5	0	2.89
3**	0	– 2.89	0	8.5*
4	– 9.45	– 8.5*	9.45	8.5*
5	9.45	– 8.5*	– 9.45	8.5*
6	– 10.5*	– 8.5*	8.39	8.5*
7	– 10.5*	– 8.5*	0	4.52
8	10.5*	– 8.5*	– 8.43	8.5*
9	10.5*	– 8.5*	0	4.49
10	8.39	– 8.5*	– 10.5*	8.5*
11	0	– 4.52	– 10.5*	8.5*
12	– 8.43	– 8.5*	10.5*	8.5*
13	0	– 4.49	10.5*	8.5*

*Corresponds to thrust vector controller actuator hard stop.

**Zero clearance exists for given yaw angles w_{y2} and w_{y3} for all cases where the pitch angles w_{p2} and w_{p3} are equal.

TABLE 6.5

CLEARANCES BETWEEN NOZZLES OF SSME-1 AND OMS ENGINES (CASE 3)

Case 3 - SSME-1

Pitch: $w_p = -5.6$ degrees
Yaw: $w_y = 8.5$ degrees

		Left OMS Pitch Angle (w_{pL}), Degrees						
	w_{pL} / w_{yL}	$-7°$	$-4°$	$-2°$	$0°$	$2°$	$4°$	$7°$
Left OMS Yaw Angle (w_{yL}), Degrees	$0°$	6.10	5.56	5.26				
	$-2°$	4.46	3.89	3.56	3.28			
	$-4°$	2.86	2.25	1.90	1.60	1.36	1.15	0.94
	$-6°$	1.29	0.64	0.27	/ / / -0.05 / / /	/ / / -0.32 / / /	/ / / -0.54 / / /	/ / / -0.78 / / /
	$-8°$	/ / / -0.24 / / /	/ / / -0.93 / / /	/ / / -1.32 / / /	/ / / -1.66 / / /	/ / / -1.95 / / /	/ / / -2.27 / / /	/ / / -2.45 / / /

NOTE: Diagonally lined blocks correspond to regions of collision between nozzles of OMS and SSME-1.

Clearances between the nozzle of the SSME-1 and the right OMS can be determined from the table by changing the signs of the yaw gimbal angles for SSME-1 and the OMS engine and replacing the left OMS with right OMS.

Clearances between the OMS and SSME-1 nozzle are shown in inches.

TABLE 6.6

CLEARANCES BETWEEN NOZZLES OF SSME-1 AND OMS ENGINES (CASE 4)

Case 4 - SSME-1

Pitch: $w_p = -4.5$ degrees
Yaw: $w_y = 8.5$ degrees

		Left OMS Pitch Angle (w_{pL}), Degrees						
	w_{pL}	$-7°$	$-4°$	$-2°$	$0°$	$2°$	$4°$	$7°$
Left OMS Yaw Angle (w_{yL}), Degrees	w_{yL} $0°$	6.73	6.09	5.72				
	$-2°$	5.11	4.43	4.03	3.69			
	$-4°$	3.51	2.80	2.38	2.01	1.70	1.43	1.11
	$-6°$	1.96	1.20	0.76	0.38	0.04	/ / / -0.25 / / /	/ / / -0.59 / / /
	$-8°$	0.43	/ / / -0.35 / / /	/ / / -0.81 / / /	/ / / -1.22 / / /	/ / / -1.58 / / /	/ / / -1.89 / / /	/ / / -2.25 / / /

NOTE: Diagonally lined blocks correspond to regions of collision between nozzles of OMS and SSME-1.

Clearances for the right OMS nozzle can be obtained by changing the signs of the yaw gimbal angles for SSME-1 and the OMS engine.

Clearances between the OMS and SSME-1 nozzle are shown in inches.

TABLE 6.7

CLEARANCES BETWEEN NOZZLES OF SSME-1 AND OMS ENGINES (CASE 5)

Case 5 - SSME-1

Pitch: w_p = 0 degrees
Yaw: w_y = 8.5 degrees

		Left OMS Pitch Angle (w_{pL}), Degrees						
	w_{pL}	−7°	−4°	−2°	0°	2°	4°	7°
Left OMS Yaw Angle (w_{yL}), Degrees	w_{yL} 0°	10.3	9.30	8.67				
	−2°	8.75	7.68	7.03	6.42			
	−4°	7.21	6.11	5.43	4.80	4.22	3.68	
	−6°	1.96	1.20	0.76	0.38	0.04	−0.25	−0.59
	−8°	4.24	3.07	2.34	1.55	1.05	0.48	/ / / −0.28 / / /

NOTE: Diagonally lined blocks correspond to regions of collision between nozzles of OMS and SSME-1.

Clearances for the right OMS nozzle can be obtained by changing the signs of the yaw gimbal angles for SSME-1 and the OMS engine.

Clearances between the OMS and SSME-1 nozzle are shown in inches.

THIS PAGE INTENTIONALLY LEFT BLANK

FIGURE 6-1

FCS EFFECTORS

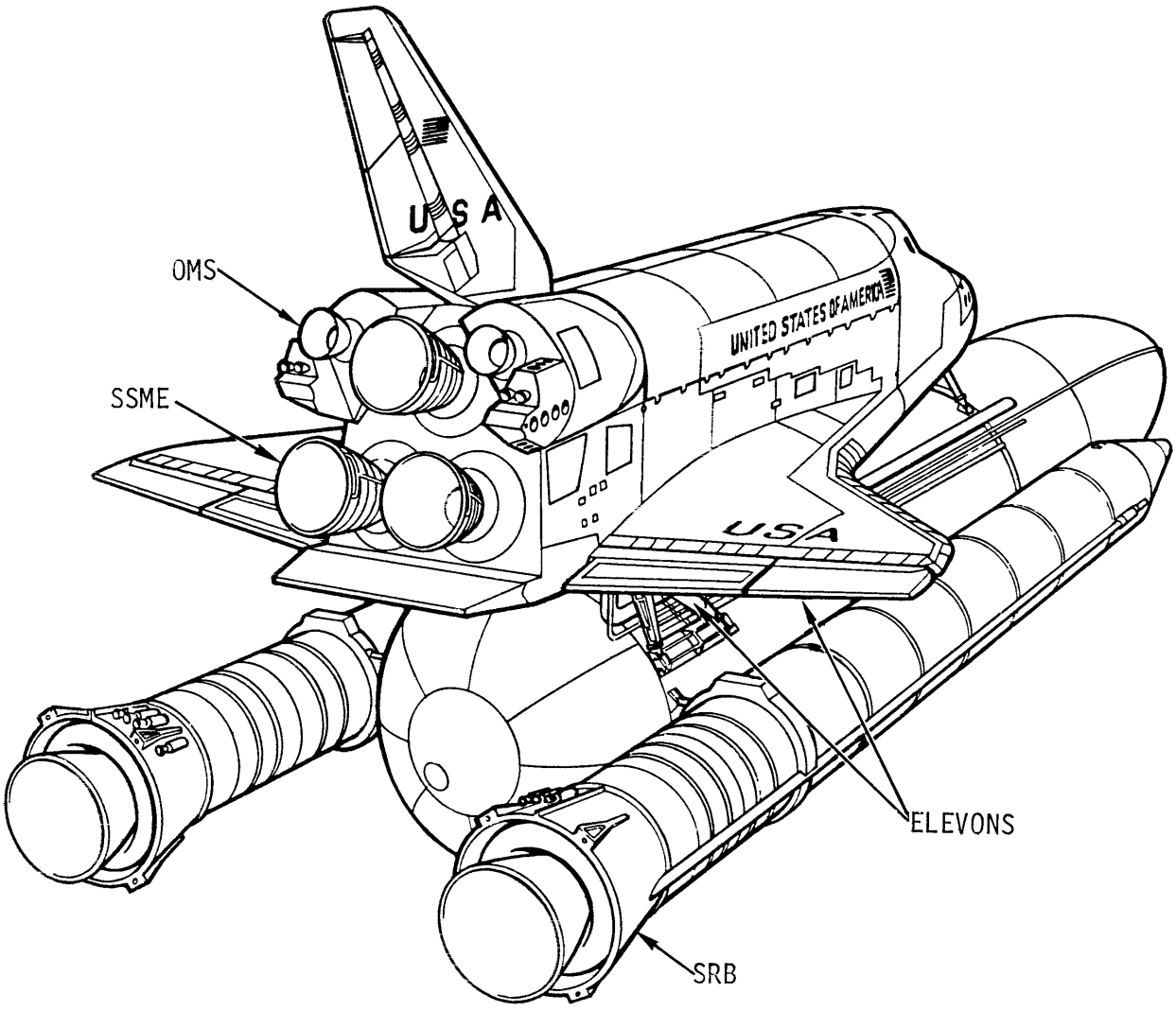

FIGURE 6-2

SSME/SRB GIMBAL DEFLECTION SIGN CONVENTIONS

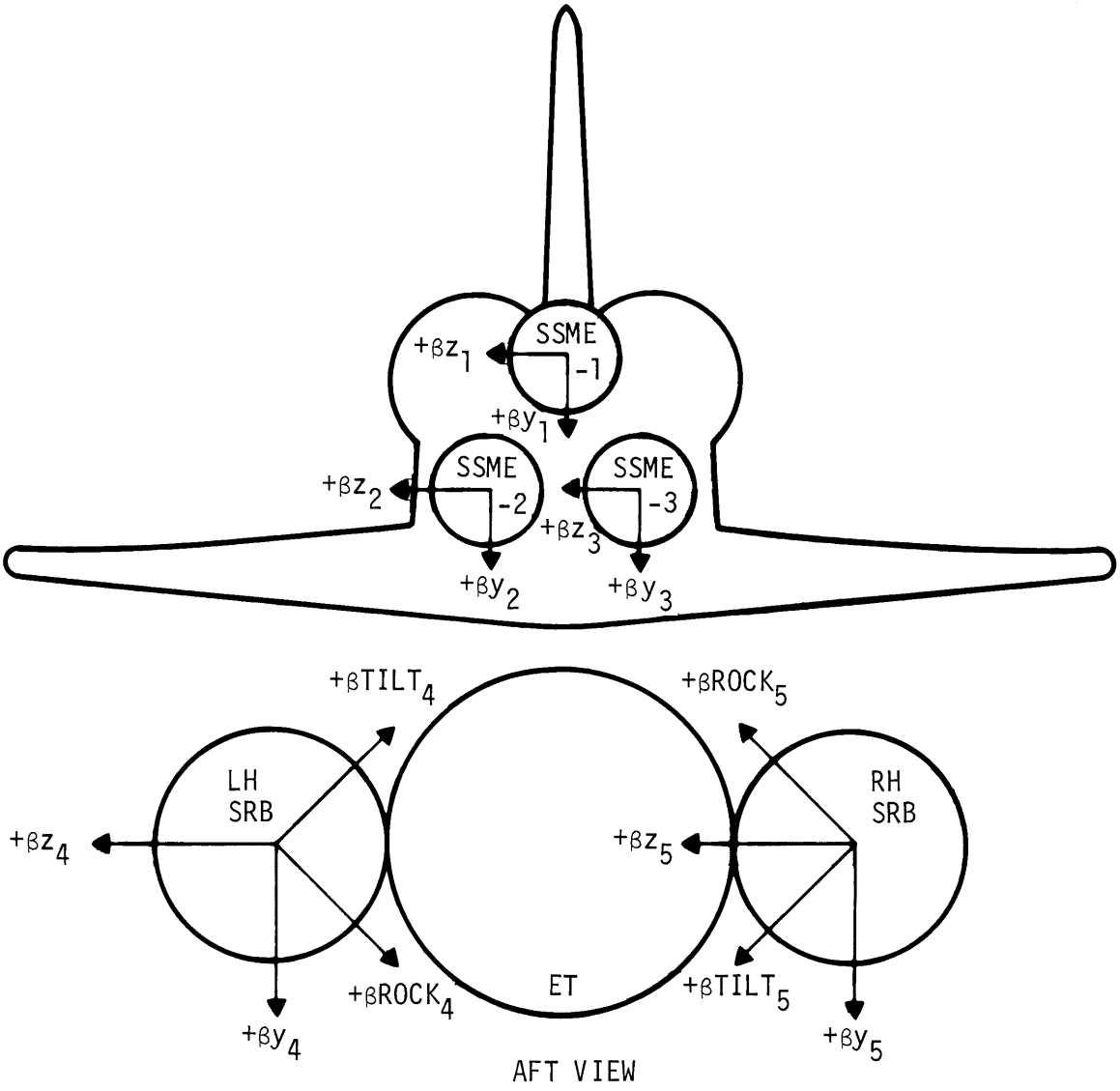

FIGURE 6-3

MPS ENGINE ACTUATOR ORIENTATION - VIEW LOOKING FORWARD

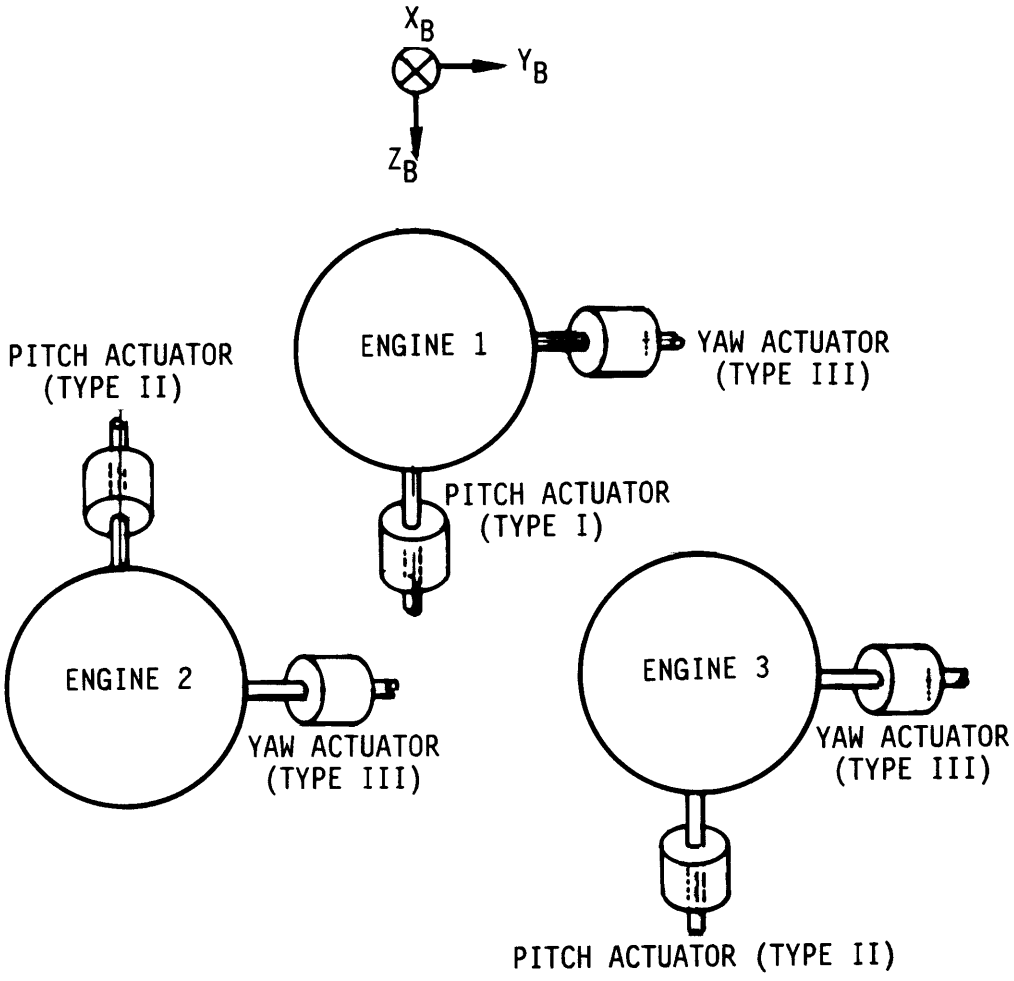

NOTE: ACTUATORS ARE ATTACHED TO THE ENGINES AFT OF THE GIMBAL POINT

FIGURE 6-4

NOMINAL SSME AND ACTUATOR GEOMETRY

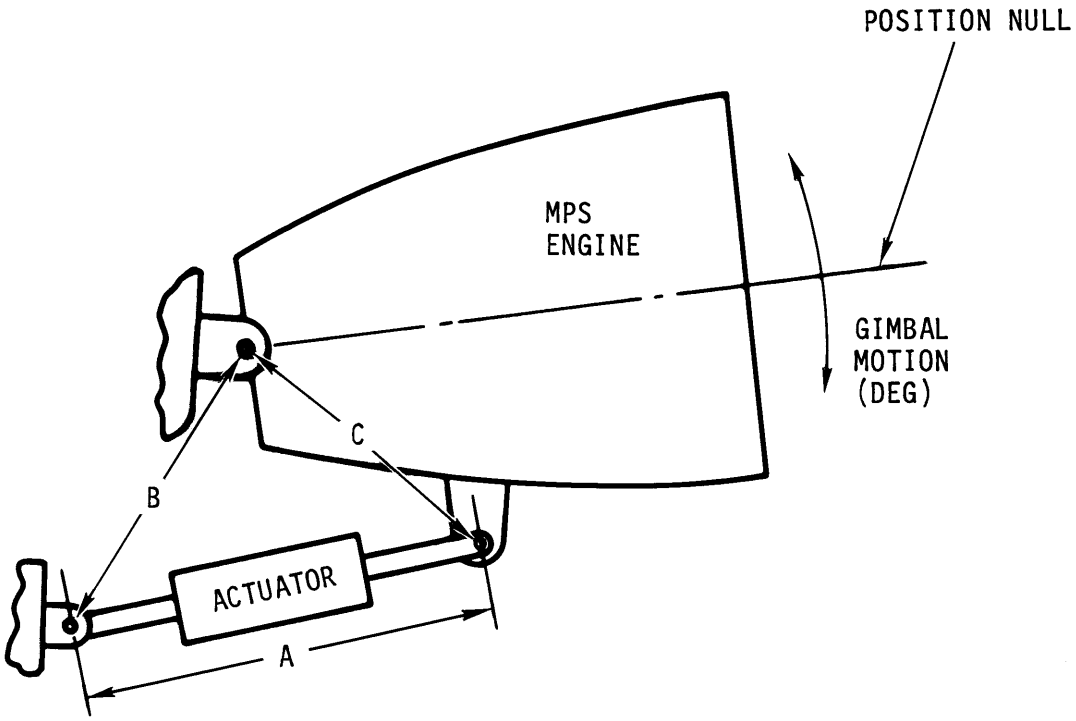

ACTUATOR NULL PARAMETER, CURRENT = 0	ENGINE 1		ENGINE 2		ENGINE 3	
	PITCH	YAW	PITCH	YAW	PITCH	YAW
A (IN.)	47.33	43.91	47.33	43.91	47.33	43.91
B (IN.)	33.514	32.062	33.514	32.062	33.514	32.062
C (IN.)	43.829	43.829	43.829	43.829	43.829	43.829

FIGURE 6-5

MAIN ENGINE GIMBAL PITCH AXIS

MPS GIMBAL LOCATION IN ORBITER COORDINATES

	NUMBER	X	Y	Z
TOP ENGINE	1	1,445	0	443
LEFT ENGINE	2	1,468.17	-53	342.64
RIGHT ENGINE	3	1,468.17	53	342.64

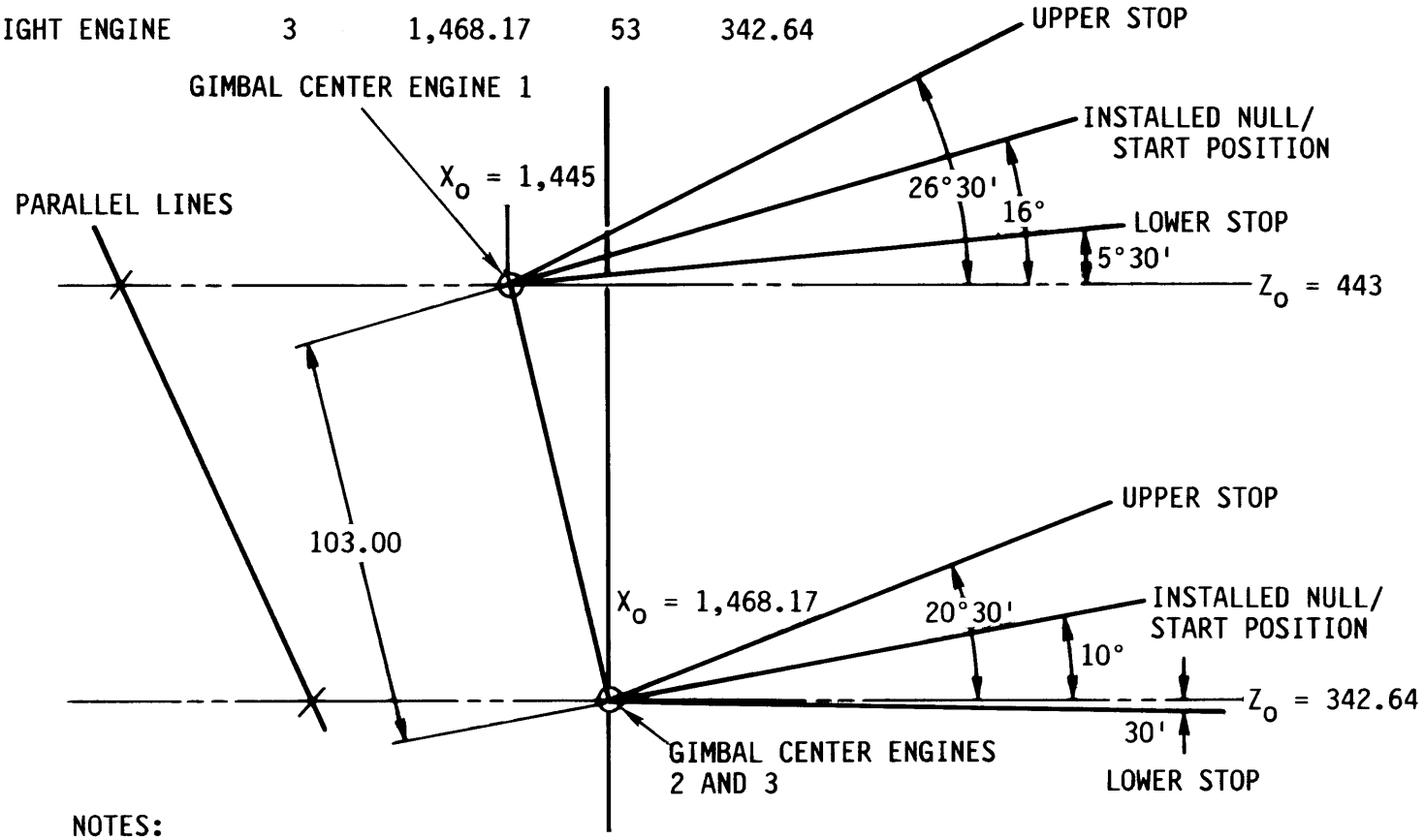

NOTES:

1. ADDITIONAL 30 MINUTES ALLOWED FOR OVERTRAVEL.
2. DOES NOT INCLUDE STRUCTURAL DEFLECTION DUE TO ENGINE THRUST OR INERTIAL LOADS.

FIGURE 6-6

MAIN ENGINE GIMBAL YAW AXIS

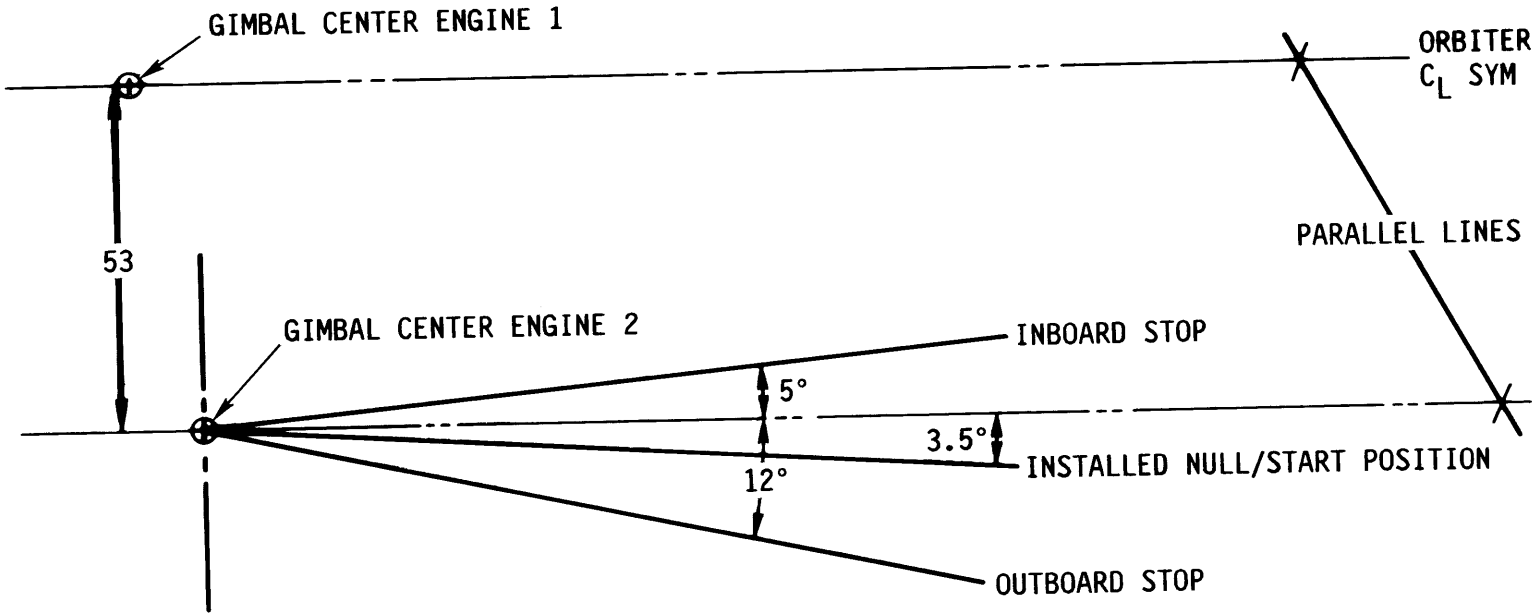

NOTES: 1. ADDITIONAL 30 MINUTES ALLOWED FOR OVERTRAVEL.

2. DOES NOT INCLUDE STRUCTURAL DEFLECTION DUE TO ENGINE THRUST OR INERTIAL LOADS.

FIGURE 6-7

RATE CAPABILITY VERSUS EXTERNAL LOAD OF THE MPS I ACTUATOR SUBSYSTEM*

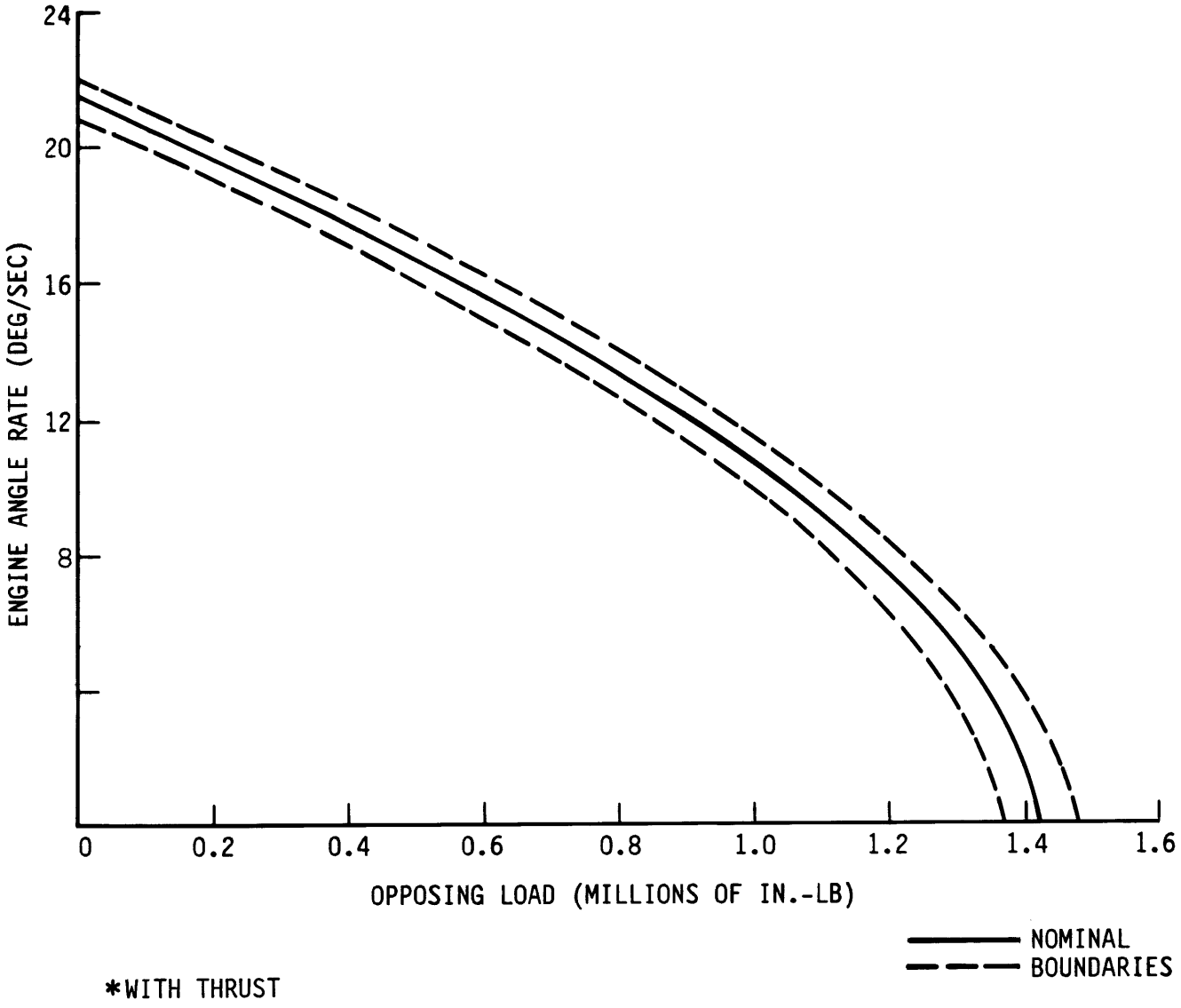

FIGURE 6-8

RATE CAPABILITY VERSUS EXTERNAL LOAD OF THE MPS TYPE II AND III ACTUATION SUBSYSTEM*

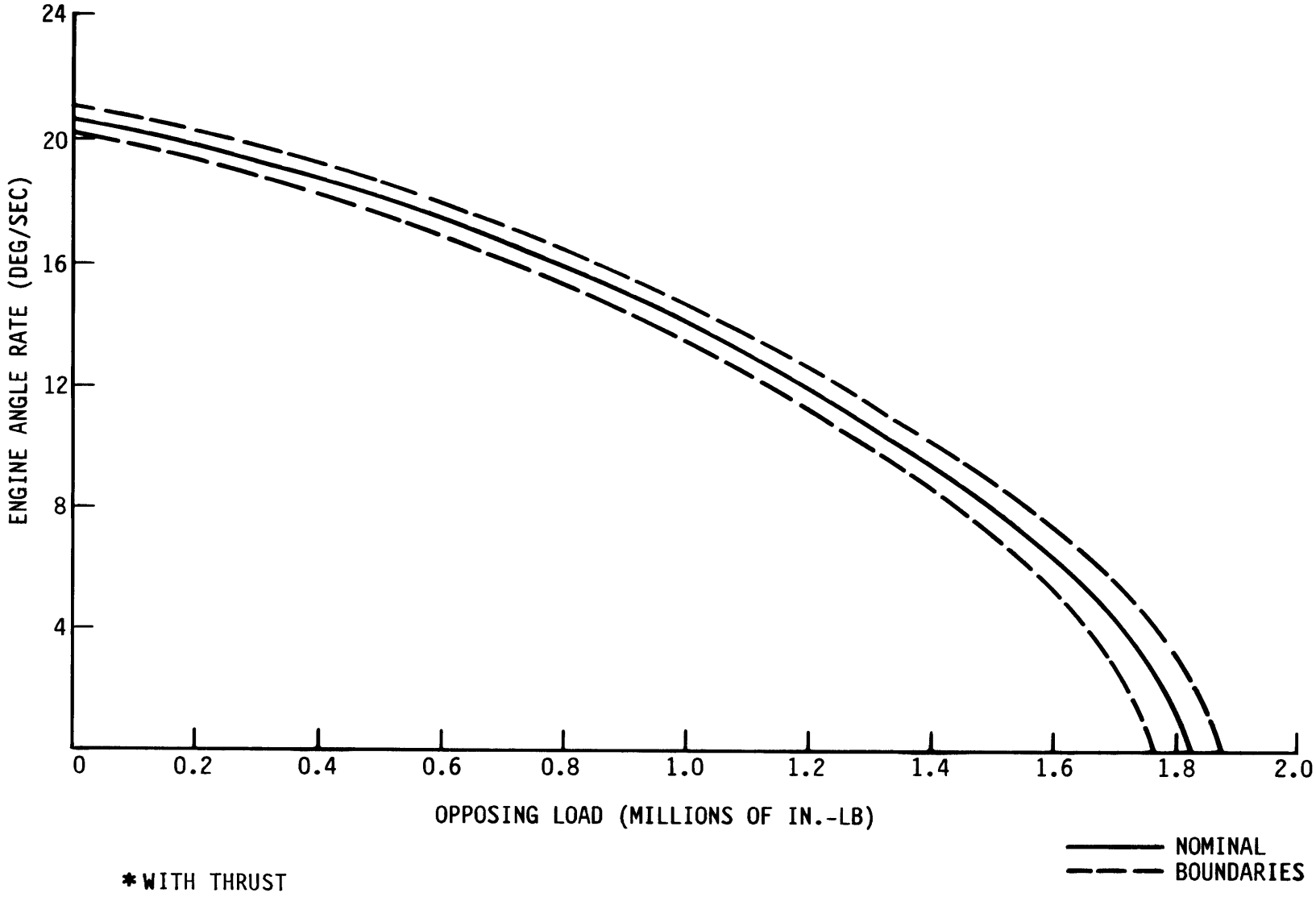

FIGURE 6-9

CLEARANCES BETWEEN SSME-1, SSME-2 (D_{12}), AND SSME-3 (D_{13}) AS A FUNCTION OF SSME-1 GIMBAL ANGLES, δ_{yl} AND δ_{p2}, WITH SSME-2 AND 3 HELD IN THEIR NULL POSITIONS

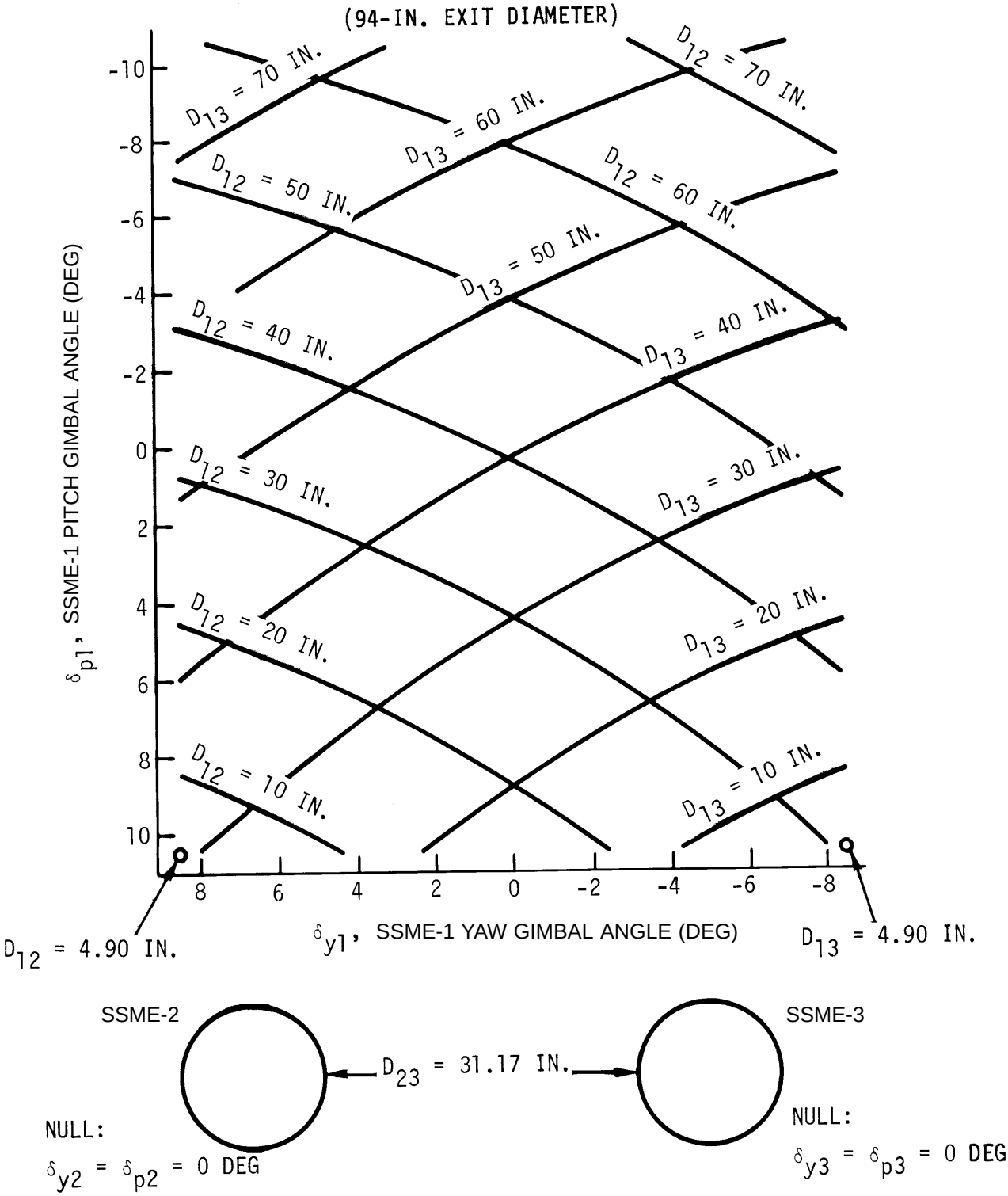

FIGURE 6-10

CLEARANCES BETWEEN SSME-2, SSME-1 (D_{12}), AND SSME-3 (D_{23}) AS A FUNCTION OF SSME-2 GIMBAL ANGLES, δ_{y2} AND δ_{p2}, WITH SSME-1 AND 3 HELD IN THEIR NULL POSITIONS

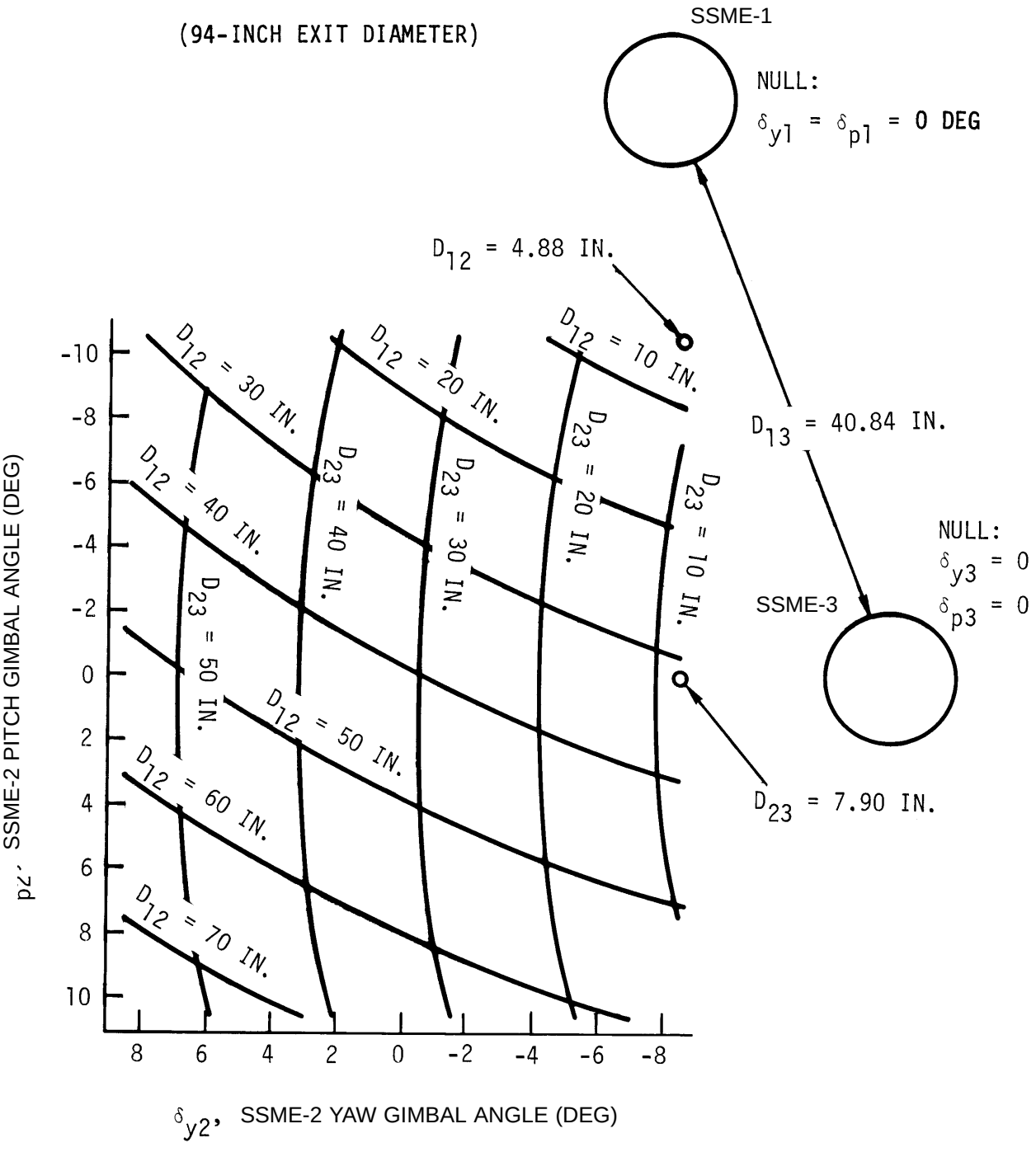

FIGURE 6-11

GIMBAL ENVELOPE OF SSME-1 WITH SOFTWARE LIMITS TO PREVENT INTERFERENCE BETWEEN SSME-1 AND OMS PODS

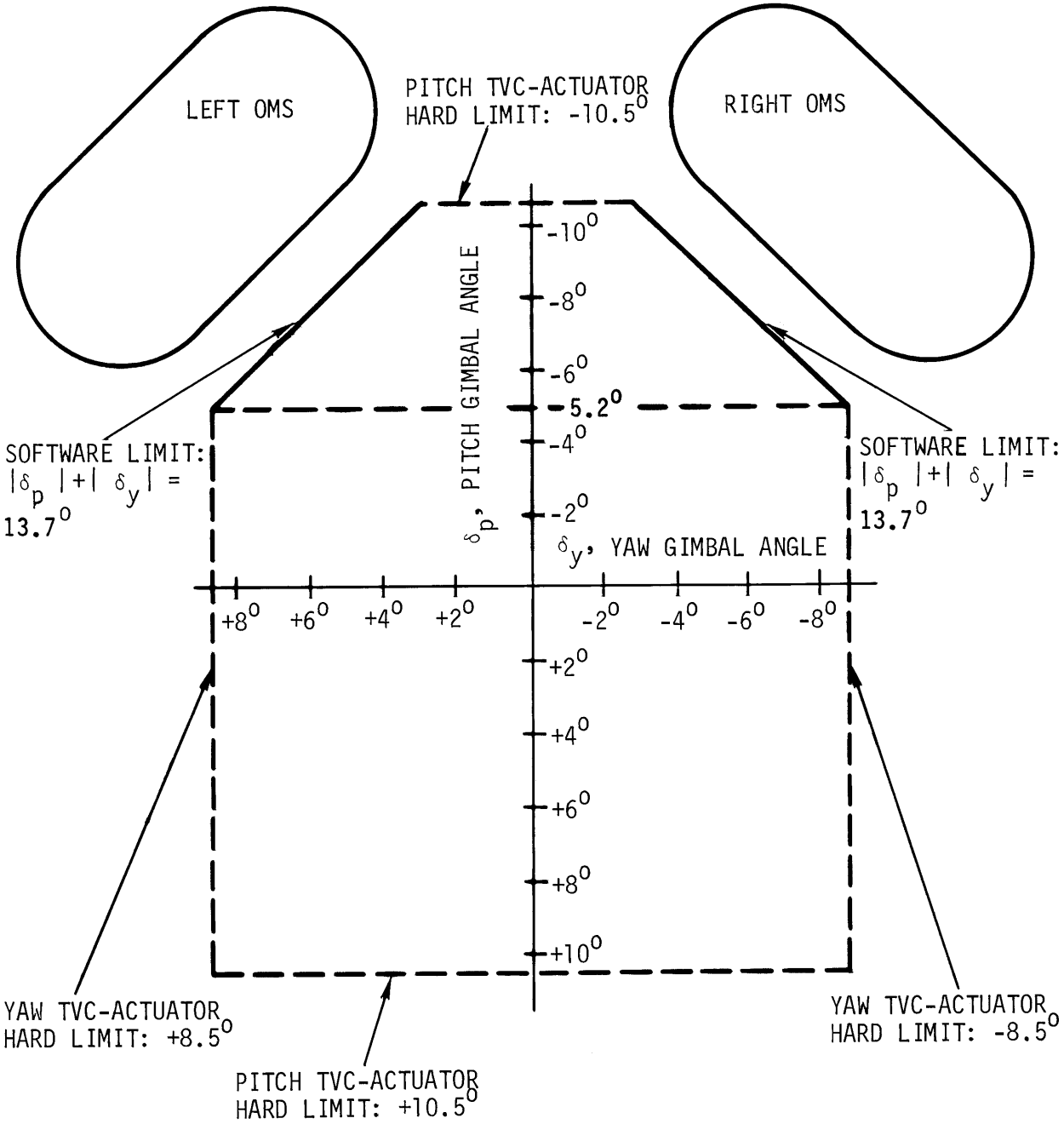

FIGURE 6-12

REGIONS OF POTENTIAL COLLISION BETWEEN NOZZLES OF SSME-1 AND LEFT AND RIGHT OMS ENGINES

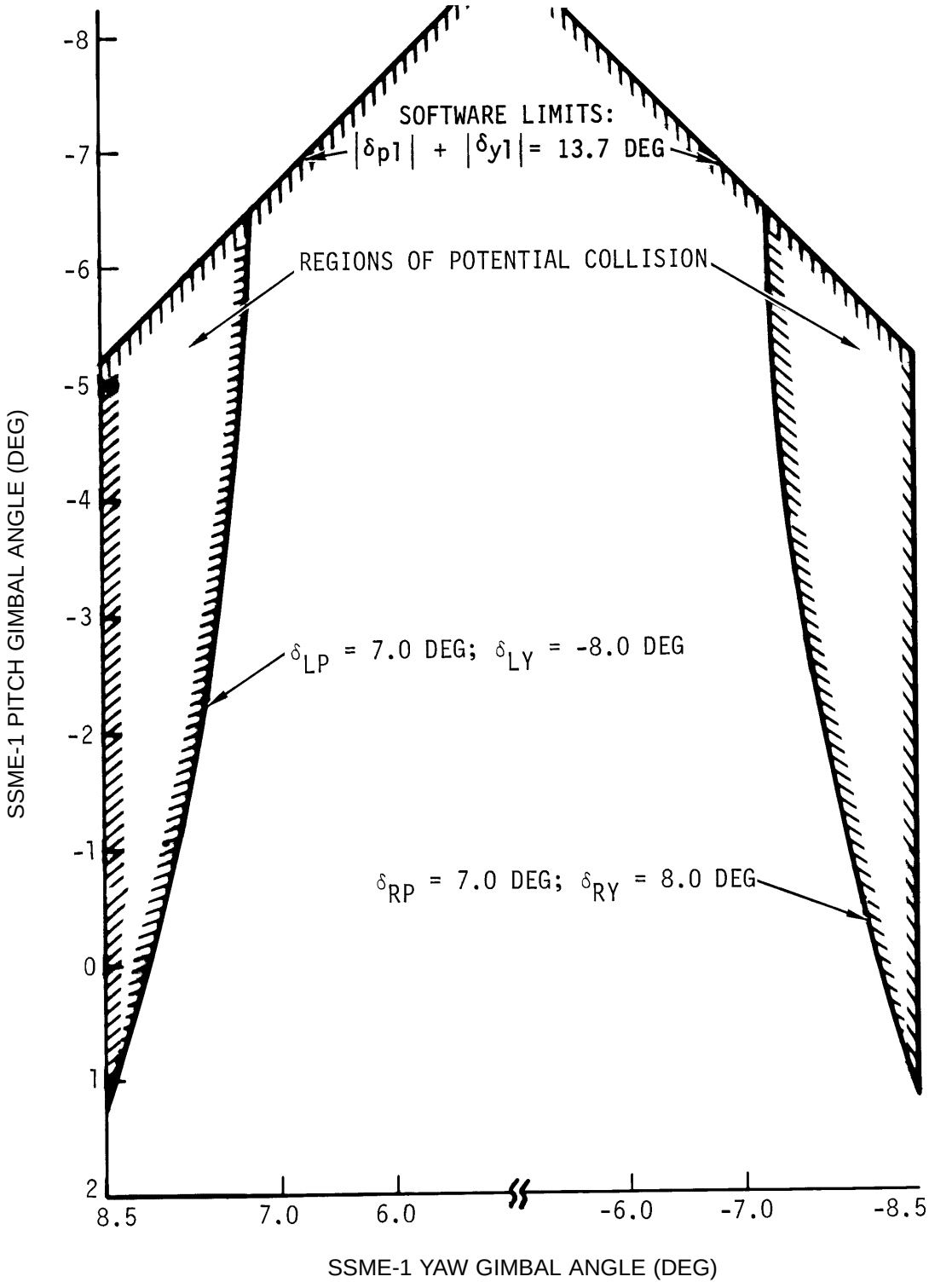

FIGURE 6-13

CLEARANCE BETWEEN LOWER SSME AND BODY FLAP AS A FUNCTION OF PITCH GIMBAL ANGLE (δ) FOR LOWER SSME AND BODY FLAP DEFLECTION (δ_{BF})

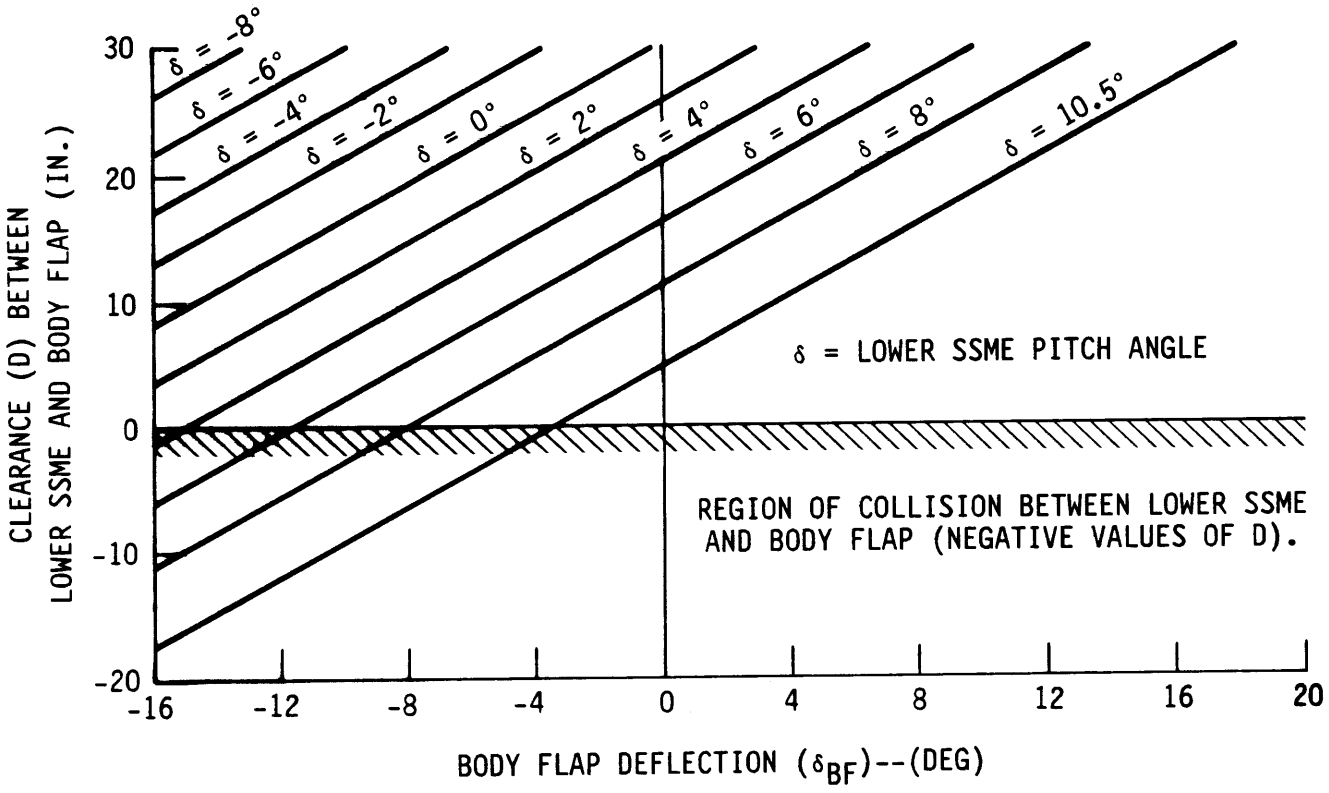

FIGURE 6-14

OMS GIMBAL YAW/PITCH AND NULL ANGLES

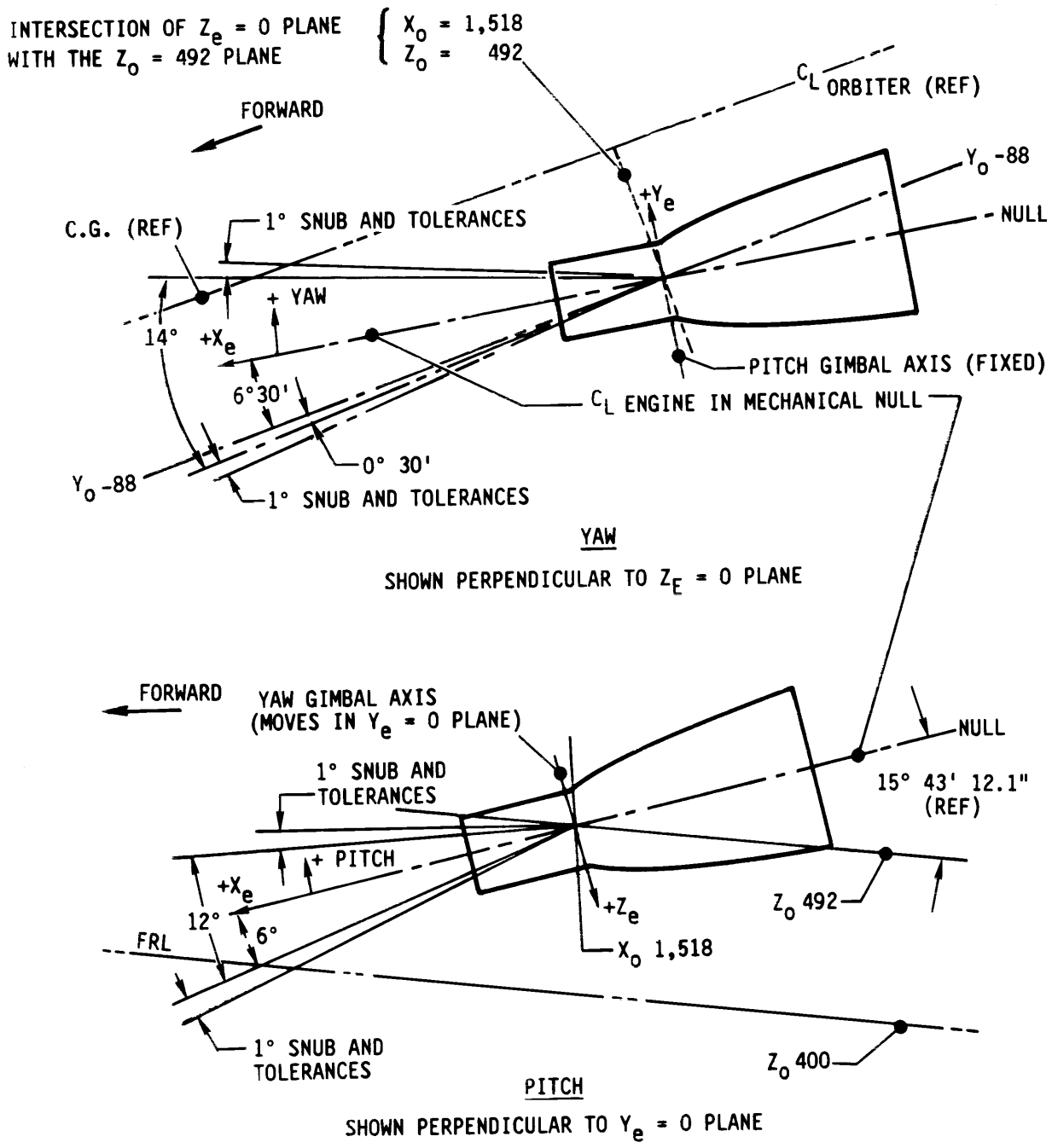

FIGURE 6-15

SRB ACTUATOR ORIENTATION - VIEW LOOKING FORWARD

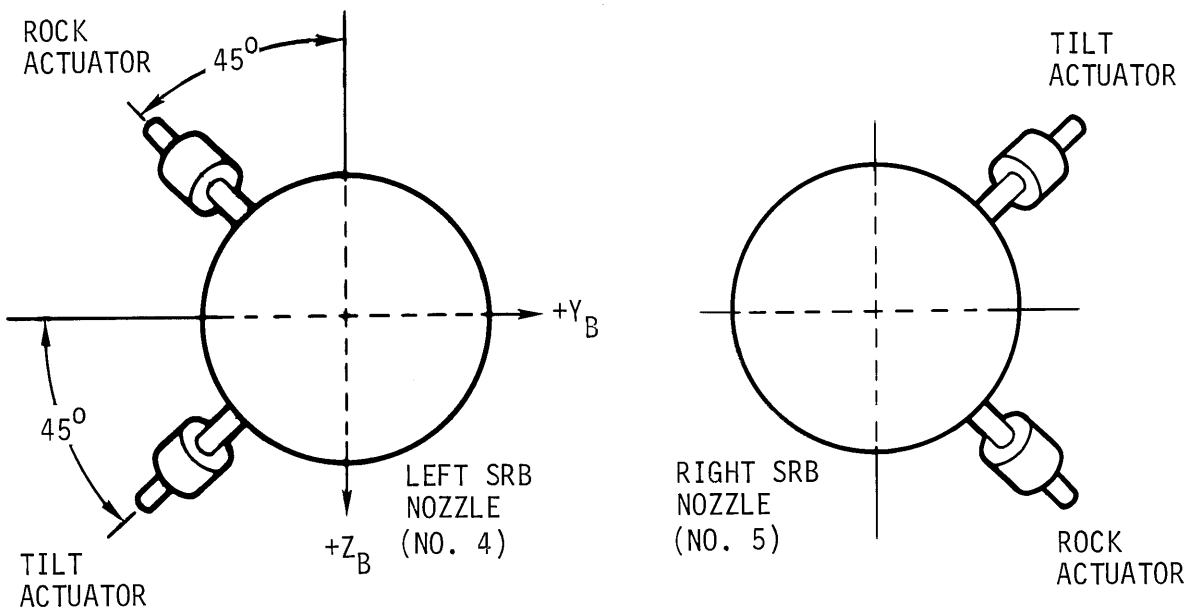

NOTES: 1) ROCK AND TILT GIMBAL DEFLECTIONS ARE POSITIVE FOR ACTUATOR EXTENSIONS FROM THE NULL POSITION.

2) SRB GIMBAL PIVOT POINT LOCATIONS ARE AT X_S = 2406.458, Y_S = ±250.5, Z_S = 400.0.

FIGURE 6-16

SRM NOZZLE DEFLECTION

SRM NOZZLE DEFLECTIONS

7.1° CONTROL
0.5° GEOMETRICAL MISALIGNMENT } SEE NOTE
0.4° OVERTRAVEL
8.0° TOTAL

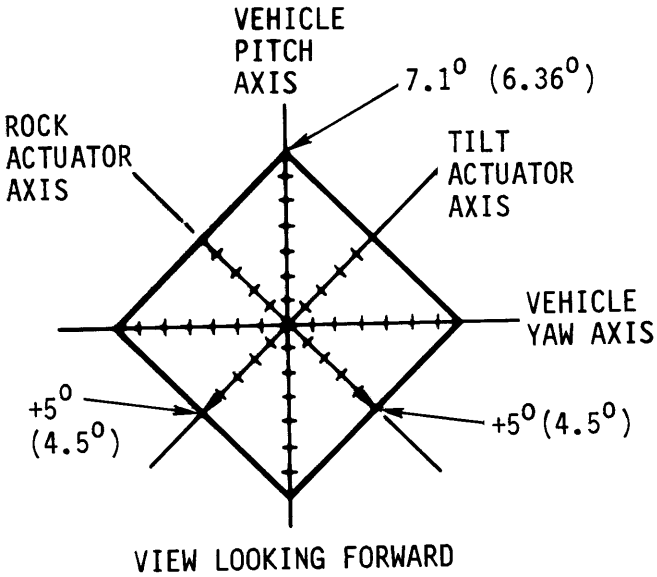

NOTE: THE 7.1° . 0.5°, AND 0.4° INCREMENTS ARE TAKEN IN VEHICLE PITCH/YAW AXIS: ACTUATOR TRAVEL REQUIREMENTS FOR FLIGHT CONTROL ARE ± 5° TRAVEL. NUMBERS IN PARENTHESES ARE SOFTWARE LIMITS. THE DETAILED SRM GIMBAL REQUIREMENTS ARE SPECIFIED IN NSTS 07700, VOLUME X - BOOK 1, PARAGRAPH 3.3.2.2.1.4.

FIGURE 6-17

SRB NOZZLE RATE CAPABILITY VERSUS NOZZLE TORQUE FOR LOW, NOMINAL, AND HIGH PERFORMANCE RESPONSES

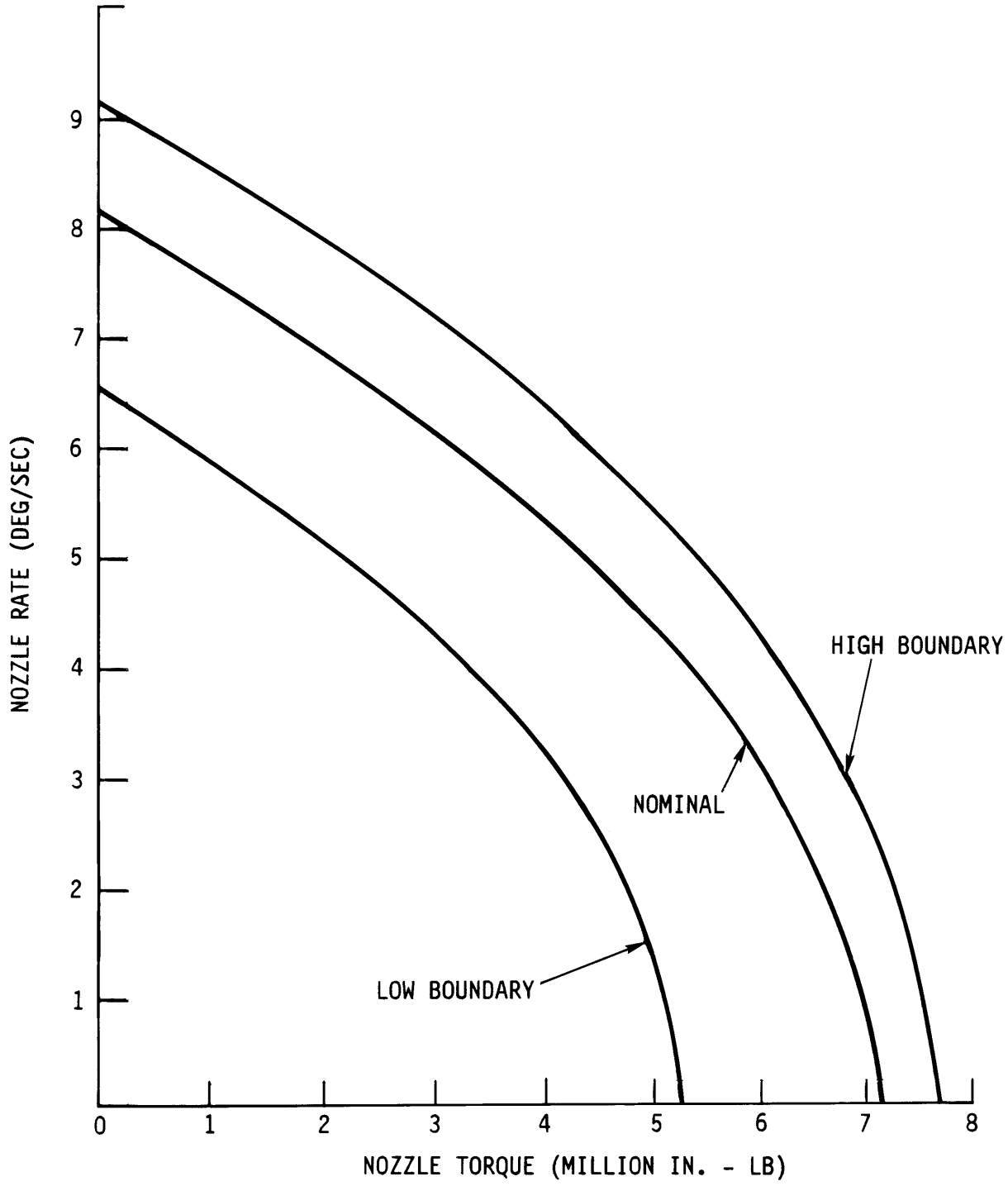

FIGURE 6-18

SRB TVC GIMBAL ROCK AND TILT COMMAND LIMITS

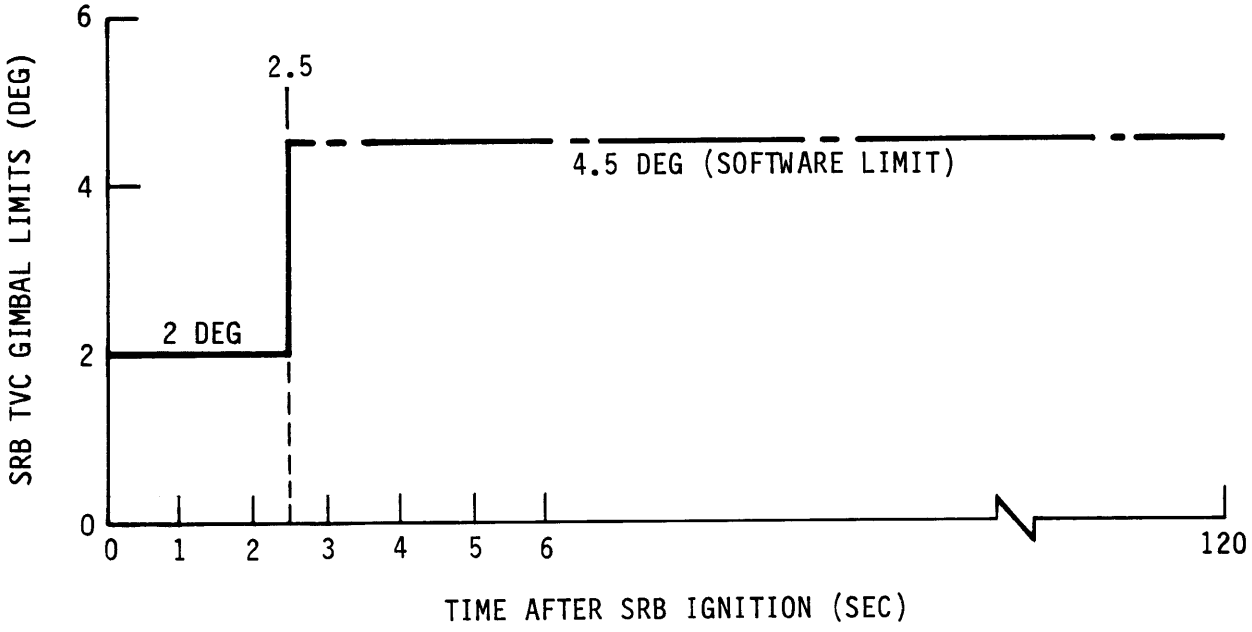

FIGURE 6-19

ELEVON NUMBERING AND SIGN CONVENTION

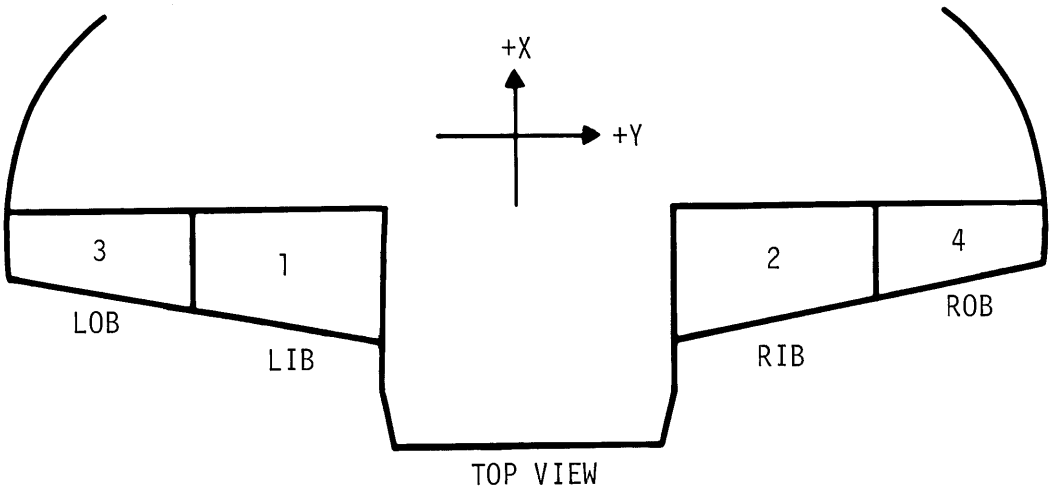

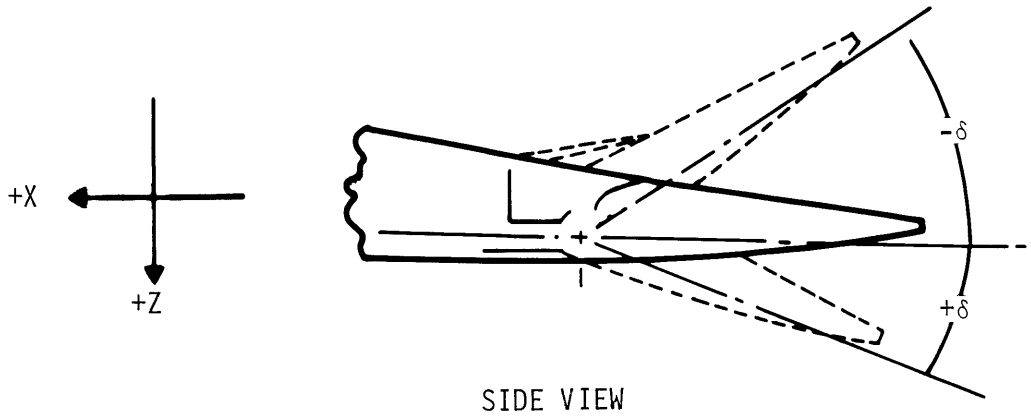

FIGURE 6-20

ELEVON ACTUATOR GEOMETRY

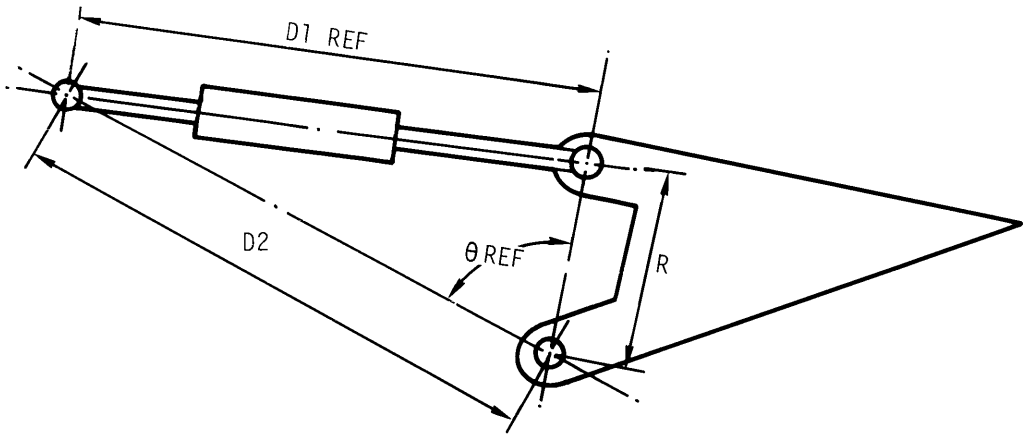

PICTORIAL CONFIGURATION
(SHOWN IN TRAIL POSITION)

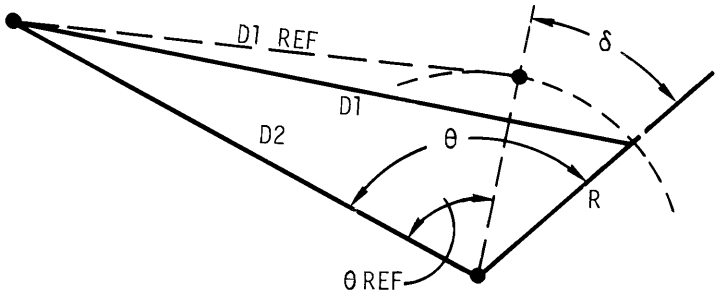

GEOMETRIC CONFIGURATION

	ACTUATOR DIMENSION	INBOARD (TYPE I)		OUTBOARD (TYPE II)	
		ADJUSTED*	REFERENCE*	ADJUSTED*	REFERENCE*
	MIN D1 (IN.)	47.3221	47.23	34.3417	34.32
	MIDSTROKE (IN.)	54.6421	54.55	38.6017	38.58
	MAX D1 (IN.)	61.9621	61.87	42.8617	42.84
** TRAIL	D1 REF (IN.)	56.6310	56.5389	39.7783	39.7566
** TRAIL	θREF (DEG)	83.6128		87.0437	
	TOTAL STROKE (IN.)	14.64		8.52	
	D2 (IN.)	56.2865		39.2492	
	R (IN.)	15.1		8.8	

*THE "REFERENCE LENGTH" IS THE LENGTH SPECIFIED IN THE ELEVON ACTUATOR PROCUREMENT SPECIFICATION, MC621-0014. THE LENGTH OF THE ACTUATOR CAN BE INCREASED OR DECREASED FROM THIS REFERENCE LENGTH BY ADJUSTMENT OF THE ROD-END AND/OR HEAD-END FITTINGS.
THE "ADJUSTED LENGTH" IS THE LENGTH AFTER THIS ADJUSTMENT HAS BEEN MADE TO MATCH THE ACTUATOR TO THE WING AND ELEVON PROPERLY.

**"MIDSTROKE" = (MIN D1 + MAX D1)/2.

FIGURE 6-21

MAXIMUM ELEVON DEFLECTIONS

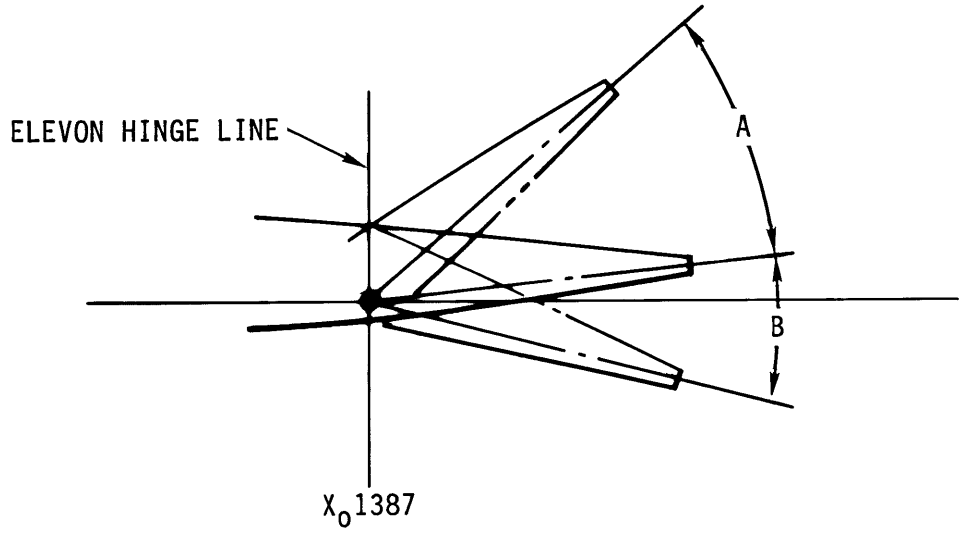

HARDWARE MAXIMUM LIMIT	SOFTWARE MAXIMUM LIMIT
A = 36.5^o ± 0.25	33^o
B = 21.5^o ± 0.25	18^o

THIS PAGE INTENTIONALLY LEFT BLANK

7.0 TRAJECTORY AND PERFORMANCE ASSESSMENT

The primary objective of shaping the Space Shuttle ascent trajectories is to maximize vehicle performance (i.e., payload capability) while observing all system constraints for flight as specified in this volume, NSTS 08209, Volume IV and NSTS 07700, Volume X. This is accomplished through optimization of the steering and SSME throttle variables.

The detailed trajectory design requirements are maintained in NSTS 21075, Space Shuttle Operational Flight Design Standard Groundrules and Constraints. This section is intended to provide a descriptive explanation only. The major trajectory shaping flight constraints that were involved in the PE certification (reference NSTS 08209, Volume VII for details) and would likely be involved in the next certification activity consist of (see Figure 7-1):

a. First stage transonic region loads

b. Aeroheating

c. Separation and disposal of the SRBs and ET

d. Maintenance of continuous intact abort capability

e. State vector targets at MECO

In addition to these major constraints, a provision is made in the shaping process for dispersions which can occur during ascent. This provision includes consideration for dispersions associated with winds aloft and miscellaneous system performance variations that could drive the flight trajectory towards one or more of the flight constraint limits. These dispersions are described in NSTS 08209, Volume III, Shuttle Systems Design Criteria, Systems and Environmental Dispersions.

Nominal ascent trajectory design criteria pertinent to vehicle structural limitations are:

a. Predicted RSRM performance

b. Dispersed SRB separation dynamic pressure maximum limit defined in NSTS 07700, Volume X - Book 1, Paragraph 3.2.1.1.9.1.3.

c. Maximum acceleration ≤ 3.0 g

d. SSME throttling for maximum dynamic pressure control

e. Elevon hinge moment limits

f. Wing bending, shear and torsion limits

g. Mach-varying ET protuberance squatcheloids and Orbiter q-planes

h. Load indicators (see NSTS 08209, Volume IV)

The procedure for first stage trajectory design consists of the following steps:

a. Develop AOA and elevon schedules compatible with q α structure limits

b. Select loft and SSME throttle schedule to satisfy dynamic pressure constraints

c. Develop yaw bias policy so that $+ q\,\beta DISP = 1 - q\,\beta DISP^{1}$ for $0.9 < M < 1.4$

d. Select flight azimuth to minimize second stage steering

Trajectory shaping for the best balance of vehicle loads is accomplished through q α shaping in the transonic region. The adequacy of the trajectory is verified using a method developed to protect the vehicle structural safety margins against the effects of ascent systems dispersions and in-flight winds. The method uses a representative set of 150 wind profiles for the launch month to predict external vehicle loads along the trajectory. Structural margins are then predicted for each wind profile. The number of trajectories that show no load indicator exceedances divided by the 150 wind sample gives a launch probability prediction. To ensure a reasonable probability for launch on any specific date, a probability in excess of 85% is desirable. If the launch probability is lower, modifications are made to the q profile and the procedure is repeated.

The major ascent trajectory shaping constraints are maximum dynamic pressure, aerodynamic loads and heating, acceleration, intact abort, SRB and ET disposal, lift-off loads, and propulsion. These constraints are illustrated in Figures 7-2 through 7-10. Details of these are provided in this section and NSTS 08209, Volume IV.

7.1 MISSION PROFILE

As illustrated in Figure 7-11, the Shuttle is launched with the three Orbiter SSMEs burning in parallel with the two SRBs. After approximately two minutes, the SRB propellants are depleted, and the SRBs are staged to be recovered and returned to the launch site. The Orbiter ascent is continued using the three SSMEs, which provide thrust vector control until MECO conditions assure a safe disposal of the ET. The Orbiter is in an elliptical orbit with perigee inside the Earth's atmosphere. The ET is separated after MECO, and the main propulsion system is purged. At apogee, the Orbiter initiates a maneuver to circularize the orbit or raise the perigee altitude. Additional maneuvers may be executed, as required, for the orbital operations of a specific mission.

Following the completion of orbital operations, the Orbiter is oriented to a tail-first attitude, and the OMS provides the deceleration thrust necessary for deorbiting. The Orbiter is reoriented nose-forward to the proper attitude for entry. The orientation of the Orbiter is established and maintained by the RCS down to the altitude where the atmospheric density is sufficient for the pitch and roll aerodynamic control surfaces to be

effective, about the 250,000-foot altitude. The yaw RCS remains active until the vehicle reaches the 80,000-foot altitude, approximately.

The Orbiter entry trajectory provides lateral flight range to the landing site and energy management for an unpowered landing. The trajectory, lateral range, and heating are controlled through the attitude of the vehicle by AOA and bank angle. The Orbiter has a lateral or cross-range capability of approximately 1,150 nm. Terminal Area Energy Management (TAEM) is initiated approximately 50 nm from the landing site and provides the proper vehicle approach to the runway with respect to position, altitude, velocity, and heading. Final touch-down occurs at a nominal landing speed of about 210 knots.

Typical Shuttle Orbiter ascent and descent trajectory profiles are presented in Figure 7-12 and illustrate altitude as a function of range. Major events as well as mission elapsed time are noted on the profiles.

7.1.1 Ascent Trajectory

After approximately 8 seconds of vertical rise to clear the launch pad, the vehicle rolls at a rate of 15 deg/sec to the desired azimuth. It then gradually pitches over into a heads down attitude as it flies downrange. The typical ascent trajectory reaches a maximum dynamic pressure approximately 60 seconds after launch at an altitude of about 33,600 feet. At approximately 108 seconds, the total load factor reaches the first stage maximum value of about 2.6 g's. SRB separation occurs at between 121 seconds and 131 seconds at an altitude of about 160,000 feet, 28 nm downrange from the launch site. After SRB separation, the Orbiter continues to ascend, using the three SSMEs. The total load factor reaches a maximum value of 3.0 g's and remains at that value until the MECO sequence is initiated.

MECO takes place about 515 seconds after lift-off, when the Orbiter has reached an altitude of about 360,000 feet. The ET separation occurs after MECO. Direct insertion, with the vehicle achieving orbital velocity at MECO, is now standard. An OMS burn at apogee is required to circularize the orbit or raise the perigee altitude.

7.1.1.1 Ascent Abort Modes Definitions

Abort characteristics are illustrated in Figure 7-13. Selection of an ascent abort mode may become necessary if there is a failure that affects vehicle performance, such as the failure of a Main Engine or an OMS failure. Other failures requiring early termination of a flight, such as a cabin leak, might require the selection of an abort mode.

There are two basic types of ascent abort modes for Space Shuttle missions: intact aborts and contingency aborts. Intact aborts are designed to provide a safe return of

the Orbiter to a planned landing site following full or partial loss of thrust from one engine. Contingency aborts are designed to permit crew survival following more severe failures when an intact abort is not possible. A contingency abort caused by multiple engine failures will often result in a ditch operation. Systems aborts are a special class of contingency aborts that provide the earliest landing opportunity following certain failures such as a cabin leak. Reference NSTS 07700, Volume X - Book 1, Paragraph 3.2.1.5 for abort operations requirements.

To achieve an orbit, the SRBs and the Main Engines provide thrust to achieve a MECO target, and then the OMS engines provide an additional velocity increment (ΔV) to insert the vehicle into a stable orbit. Main Engine failures can affect the ability to attain the desired velocity and altitude at MECO, and OMS failures can affect the performance available for orbital insertion and deorbit.

A MECO velocity which is less than the target velocity is called an underspeed. The most probable cause of a significant MECO underspeed is a Main Engine failure. The ascent trajectory is designed to provide at least one intact abort option in the event of a single Main Engine failure at any time during flight. The abort mode available depends on the time of the engine failure. An early failure might require an RTLS or TAL, whereas a later failure might allow the vehicle to continue on toward MECO, although an ATO or AOA might subsequently be required. A plot of the abort mode boundaries for a typical mission is shown in Figure 7-15.

The failure of two or three Main Engines would result in a contingency abort unless the failure occurred very near MECO. No abort procedures exist for an SRB failure. When a Main Engine fails, there are several engine-safing functions that are performed automatically.

a. The remaining engines will be commanded to the full thrust level if not already there. They will still be throttled down to maintain the 3 g limit, if necessary.

b. The nozzle of the failed engine is moved to the null position to prevent a collision with the other engine nozzles.

c. The velocity at which the engine failed is stored by Guidance and used subsequently by the abort targeting logic as a decision boundary.

d. If the failure occurs during first stage, Guidance switches to a separate table of steering commands that can loft the vehicle slightly to improve the initial conditions for RTLS.

If the onboard computers are not informed of an engine failure (as in a data path failure), then the crew should depress the Main Engine shutdown pushbutton (on Panel C3) for the failed engine to enable the engine-safing functions.

There are four types of intact abort modes: ATO, AOA, TAL, and RTLS. In addition to the abort modes, there is Press to MECO (PTM) capability for late engine failures which result in relatively small MECO underspeeds. In this case, the lower than planned orbit at MECO can be raised to the planned orbit using available OMS propellant.

7.1.1.1.1 Abort Mode Preference

The type of failure and the time of the failure determine which type of abort is selected. In cases where performance loss is the only factor, the preferred modes would be ATO, AOA, TAL, and RTLS, in that order. Since the AOA window is usually within the ATO window, this mode is not often used for a single engine-out, and then only for a small window (several seconds). It is available for certain two engine-out scenarios and for systems aborts. The mode chosen is the highest one that can be completed with the remaining vehicle performance. In the case of some support systems failures, such as cabin leaks or vehicle cooling problems, the preferred mode might be the one that will end the mission most quickly. In these cases, TAL or RTLS might be preferable to AOA or ATO.

7.1.1.1.2 ATO/AOA Powered Flight Phase

The ATO mode is designed to allow the vehicle to achieve a temporary orbit that is lower than the nominal orbit. This mode requires less performance and allows time to evaluate problems and then choose either an early deorbit burn or an OMS maneuver to raise the orbit and continue the mission.

The AOA mode is designed to allow the vehicle to fly once around the Earth and make a normal entry and landing. This mode generally involves two OMS burns, with the second burn being a deorbit maneuver. There are two types of AOA trajectories: a normal AOA and a shallow AOA. The entry trajectory for the normal AOA is similar to the nominal entry trajectory. The shallow AOA results in a flatter entry trajectory, which is less desirable than that of the normal AOA but uses less propellant in the OMS maneuvers. The shallow entry trajectory is less desirable because it exposes the vehicle to a longer period of atmospheric heating and to less predictable aerodynamic drag forces. A shallow ATO, using the AOA targets, is another variation and involves three orbits prior to entry and landing.

ATO and AOA may be required either for performance reasons due to an engine failure or for system failures such as cabin leak.

In these abort modes, the velocity lost due to an underspeed can be made up by increasing the ΔV provided by the OMS burns. Large underspeeds will require large ΔV contributions from the OMS, and the ΔV capability is limited by the amount of OMS propellant onboard although, OMS and RCS propellant that would have been used for

on-orbit operations is available for the critical OMS maneuvers. Examples of OMS capability are given in Figure 7-16.

The orbital altitude achieved with the ATO OMS-1 and OMS-2 targets will be lower than the orbital altitude for a nominal mission. In the case of an ATO, the OMS ΔV capability necessary to perform a deorbit must still be preserved.

For the AOA OMS-1 maneuver, the orbital altitude is lower than nominal as with the ATO, but the OMS-2 maneuver is actually a deorbit burn. This reduces the OMS maneuver sequence from three burns to two burns and saves a significant amount of ΔV capability. The shallow AOA targets require even less ΔV than the normal AOA targets and are therefore useful for the most severe underspeed cases or for the loss of OMS due to a tank failure or leak.

As with all intact abort modes, the implementation of the ATO and AOA options is highly dependent on specific flight planning. The payload weight, orbital inclination, orbital altitude, and propellant loading all have their effects on the performance capabilities and requirements for a flight. The flight software is designed to accommodate the varying mission requirements for guidance, navigation, and flight control by defining I-Loads that can be changed for specific flights.

7.1.1.1.3 Transoceanic Abort Landing

The TAL mode is designed to permit an intact landing in western Europe or Africa, depending on mission parameters. This mode results in a ballistic trajectory, which does not require an OMS maneuver for performance although a 100 fps post ET separation burn is required for separation. Additional pre-MECO, and in some cases Post MECO, propellant dumps are required for CG and landing weight control. TAL provides an intact abort option for the one-engine-failure case during the time between the last RTLS opportunity and the earliest press to ATO (PTA) point. It also provides an abort option for two-engine-failure situations much earlier than the single-engine PTM point. The TAL mode is also useful for support system failures that occur after the last RTLS opportunity. If a cabin leak or vehicle-cooling problem was found to be too severe to permit an AOA, then a TAL could be initiated to permit an early landing. Also, if OMS tank failures during ascent reduced the ΔV capability below that necessary for an AOA, then a TAL could be initiated.

The implementation of the TAL mode, like that of ATO and AOA, is very dependent on specific flight planning. Vehicle performance and especially the azimuth of the launch trajectory have an effect on the availability of this option.

To provide highest probability of a successful launch without a delay, two TAL sites will be maintained during the flight design process. The preferred TAL sites are:

28.5 Degree Inclination	39, 51.6 and 57 Degree Inclination
Banjul (prime)	Zaragoza (prime)
Ben Guerir (alt.)	Moron (alt.)
Moron (alt.)	Ben Guerir (alt.)

If a landing site falls along the launch groundtrack, then less performance is required to reach it and the TAL abort region is relatively long. If the landing site is very far from the groundtrack, then the crossrange is large and some performance must be expended to reach it. This expenditure shortens the time in ascent during which the TAL mode is available.

The TAL sites can be changed by changing software target I-Loads and runway and Tactical Air Navigation I-Loads.

7.1.1.1.4 Return to Launch Site

If an engine fails too early to accomplish a TAL, the Shuttle must return to the runway at KSC. The RTLS mode involves flying downrange to dissipate propellant and then turning around under power to return directly to a landing near the launch site.

The turn to reverse course is called Powered Pitch Around (PPA), and the timing of PPA is critically important. Since the Orbiter is powerless once the Main Engines are shut down, these engines must be shut down when the Orbiter has exactly enough speed and altitude to glide to the runway. Also, in order to safely separate the Orbiter from the ET, the ET should have no more than 2% propellant remaining. Having more than 2% remaining could result in slosh forces large enough to cause collision with the Orbiter during separation. Thus the Shuttle must turn back toward the launch site at the correct time that will allow it to arrive at MECO with the desired speed, altitude, and propellant level.

If the RTLS is declared before the time of PPA, the Shuttle will have to perform what is called fuel wasting. This means lofting the Shuttle to provide desirable initial flyback conditions. This continues until the Shuttle must execute PPA and turn back toward the launch site. From this point on, the Shuttle thrusts back toward the runway until it reaches MECO conditions. These conditions are specified as 2% propellant remaining with the right speed, direction, and altitude to glide to a landing. Then the Shuttle Orbiter separates from the ET and begins to glide back to the runway. During this gliding flight (called Glide RTLS or Glide Return to Launch Site [GRTLS]), the Orbiter may perform certain maneuvers to fine tune its glide range. Finally, as the Orbiter approaches the runway, it will perform a wide turn to align itself with the direction of the runway and then glide down to a landing. A typical RTLS trajectory is shown in Figure 7-17.

7.1.2 Descent Trajectory

Descent trajectory design requirements are also maintained in NSTS 21075. The Orbiter entry restrictions are documented in NSTS 08934, Space Shuttle Operational Databook, Volume V, Orbiter Flight Capability.

The descent or entry phase of a Shuttle mission is initiated by a Deorbit OMS burn approximately one hour prior to the desired landing time. Following the deorbit burn, the Orbiter maneuvers to a desired attitude of zero bank angle with +40 degrees of pitch in preparation for entry. Entry guidance and flight control is initiated by crew action five minutes prior to Entry Interface (EI) (400,000-foot altitude).

From EI-5 minutes to TAEM (VREL=2,500 fps), entry guidance controls the trajectory by bank angle commands while following a design alpha versus velocity profile. The alpha profile is designed to keep the Orbiter within thermal and stability constraints. Roll reversals are commanded at appropriate times to control the vehicle heading angle. Alpha modulation is used to control the drag profile during roll reversals.

From TAEM to Approach and Landing (~15,000 ft, 288 KEAS), TAEM guidance controls the trajectory by bank angle, alpha and speedbrake position commands. Altitude errors are corrected by changes in alpha. Dynamic pressure errors are corrected by changes in speedbrake position. Range errors are corrected by changes in bank angle.

Approach and Landing guidance commands the vehicle to follow an approach trajectory to the runway from TAEM termination until touchdown. The Orbiter is commanded to acquire a steep glide slope, follow it, then flare and follow a shallow glide slope. A final flare is performed just prior to touchdown in order to reduce the sink rate to near zero.

7.2 LAUNCH SITE LOCATION AND VEHICLE ORIENTATION

Two launch complexes are in operation for the launch of the Space Shuttle: LC-39A and LC-39B, located at KSC for launches from the ETR. The precise locations of the launch sites are provided in Table 7.1. For LC-39A and LC-39B, the Space Shuttle launch vehicle is oriented with the Orbiter vertical stabilizer pointing at 180 degrees geodetic azimuth measured clockwise from north. Nominal performance shall be based on the data in these tables.

7.3 LAUNCH WINDOW

The launch window is determined by Orbiter and payload requirements. When this window is greater than three hours, or multiple launch opportunities exist in the same day, the weather database for the launch, RTLS, TAL, and End of Mission (EOM) sites will be used to select the best launch time of day. It is highly desirable to strive for the

optimum weather launch window that exists at midday between October and March and in the early morning from April through September.

There is no MPS/OMS/RCS allowance for launch holds in determining ascent/abort performance. Therefore, any launch hold impacting performance reduces the mission propellant margin, hence reducing guided MECO probability. One example of a hold which affects performance would be a launch hold on a rendezvous mission which requires injection into a fixed inertial orbit. Launching ahead of the in-plane launch time (to maximize total launch window duration) or beyond the in-plane launch time (due to a hold condition) requires out-of-plane steering during boost which reduces propellant margin.

Another example is the case involving a launch hold which occurs between the end of LO_2 replenish (T-4 min 55 sec) and launch. Prior to Launch, a LO_2 drainback is performed to condition the SSMEs for start-up. If a hold is exercised once replenish is completed and drainback started, LOX is lost at a rate of 20.89 lb/sec based on the formula for Drainback Rate given in Table 4.1.2 of this document and the value of LO_2 Drainback given in Table 4.93. This reduces usable propellant and changes its balance resulting in increased fuel bias and reduced propellant margin. Figure 7-18 shows the effect of a launch delay initiated after LO_2 drainback has started. The data is plotted to provide hold capability if predicted usable propellant remaining at MECO is known (obtained from DOL trajectory simulation). If more hold capability is desired it may be available if a lower FPR protection level was defined for the specific mission.

The maximum hold capability provided by the predicted margin may be greater than that allowed by system constraints. For example, the Orbiter APU has the capability to operate 12 minutes prior to launch for each of two launch opportunities without any APU servicing and still support a mission. This represents a 7-minute hold time following APU start at T-5 minutes for each launch opportunity.

7.4 ASCENT/ABORT PERFORMANCE

Nominal performance will be based on the criteria listed in NSTS 08209, Volume IV, Paragraph 3.1.1.2.

For Flight Performance Reserve (FPR) requirements, see NSTS 08209, Volume IV, Paragraph 3.1.1.1.

All flights will be flown with SSME pitch parallel turned ON to enhance performance.

At all points on the ascent profile, the Orbiter will have with one SSME out either RTLS, TAL, AOA, or ATO capability. Additionally, systems AOA capability up to OMS-2 deorbit Time of Ignition (TIG) is required. Although the remainder of this section provides guidelines for various abort boundary determinations, NSTS 21075 is the official source of abort design requirements.

a. The following guidelines will be used in determining the last RTLS boundary:

   1. SSME failure at the latest time that satisfies items (2) to (6) below
   2. Fifteen-second abort decision delay
   3. Powered Pitch Around immediately after RTLS selection with flyback at the maximum intact abort SSME power level
   4. Guided MECO with 3-sigma MPS FPR
   5. Twenty-second powered pitchdown
   6. MECO targeting consistent with overhead approach to the preferred runway

b. The following guidelines will be used in determining the first TAL boundary:

   1. SSME failure at the earliest time that satisfies items (2) to (4) below
   2. Fifteen-second abort decision delay or TAL selected 10 seconds prior to last RTLS boundary, whichever is later in time
   3. Guided MECO with 2-sigma MPS FPR
   4. Maximum intact abort SSME power level

c. The following guidelines will be used in determining the last auto TAL boundary:

   1. Fifteen-second abort decision delay
   2. Guided MECO with at least 2-sigma MPS FPR and acceptable altitude and flight path angle MECO target misses
   3. SSME power level, as required, to extend last TAL capability (throttledown to 65% for in-plane TAL landing sites)
   4. Sufficient time in TAL powered flight to complete roll-to-heads-up and achieve acceptable weight and CG

d. The following guidelines will be used in determining the earliest single-engine TAL boundary:

   1. Two simultaneous SSME failures at earliest time that satisfy items 2 to 6 below
   2. Fifteen-second abort decision delay to the flight-specific in-plane TAL site
   3. Maximum contingency abort SSME power level

4. Minimum droop altitude of 265,000 feet

5. MECO attitude and rates within acceptable limits required to maintain control at ET separation

6. Nominal SSME performance

e. The earliest PTA and PTM abort mode boundaries will be based on the ability to achieve the design MECO underspeed. The design MECO underspeed is based on the most constraining of the following:

1. ET impact constraints - Critical land masses as defined in Paragraph 7.11 will be protected from the 3-sigma ET impact footprint.

2. Maximum AOA capability - The maximum underspeed off which an AOA to steep targets may be flown, assuming commitment of usable OMS and Aft Reaction Control System (ARCS) to ARCS PRESS QUANTITY.

(a) Usable OMS which can be committed to AOA is defined as loaded (level A mission-specific GandC).

(1) Minus trapped (891 lb for OV-102 and 799 lb for other Orbiters)

(2) Minus OMS FPR

(3) Minus sequential shutdown (120 lbs)

(4) Minus CG ballast (mission dependent)

NOTE: The OMS FPR allowance is defined as the Root-Sum-Squared (RSS) of

- Flow rate and MR error based on nominal load with 2% error

- Loading error based on good benchmark of 40-pound oxidizer (OX)/pod and 24-pound fuel/pod.

(b) Aft RCS PRESS quantity.

(1) Trapped (378 lbs)

(2) Gauge error (168 lbs)

(3) Sequential shutdown (70 lbs)

(4) MECO to deorbit usage (290 lbs)

(5) Deorbit to EI usage (160 lbs)

(6) CG ballast (mission dependent)

(7) Entry redline (level A mission-specific GandC, function of CG)

The above usage requirements include an allotment for dispersions.

3. Minimum altitude constraints - The maximum underspeed will be limited to a value which protects against low-altitude ($\leq$ 55nm) trajectory conditions between MECO and OMS-2 TIG.

4. Minimum SSME NPSP constraints - The maximum underspeed will be limited to 500 fps which protects against violation of SSME NPSP requirements during the MECO shutdown sequence.

f. The following guidelines will be used in determining the earliest PTA boundary:

1. Common OMS-1 targets for AOA/ATO.

2. A pre-MECO OMS burn will be utilized to achieve the design underspeed if excess OMS is available.

3. SSME failure at earliest time and still achieve design underspeed with 2-sigma MPS FPR.

4. AOA OMS-2 entry target line for minimum ΔV at prebank of 0 degrees, consistent with skipout protection and target standardization.

5. No forward RCS propellant use for ΔV.

6. Fifteen-second decision delay.

7. Maximum intact abort SSME power level.

8. Abort MECO targets (if required).

9. Variable Iy steering (if required).

g. The following guidelines will be used in determining the earliest PTM boundary:

1. SSME failure at earliest time and still achieve design MECO underspeed with 2-sigma MPS FPR

2. No forward RCS propellant for ΔV

3. Maximum intact abort SSME power level

h. The following guidelines will be used in determining the earliest single-engine PTM boundary:

1. Two simultaneous SSME failures at earliest time and still achieve design MECO underspeed with 2-sigma MPS FPR
2. No forward RCS propellant for ΔV
3. Maximum intact abort SSME power level

i. A 15-second delay from the abort condition to initiation of the abort sequence will be provided to allow for the abort mode decision process on the ground and abort initiation by the crew. The ground is prime for abort mode determination.

   If the maximum SSME power level is required for ditch avoidance, a 10-second delay will be provided from abort select to enabling maximum throttles.

7.4.1 Performance Adjustments

Post-flight analysis of the Space Shuttle System has identified variations from expected operations in several areas. These empirical observations require that adjustments be made to performance predictions. Predictions used in manifesting and preflight planning require that performance margins predictions account for DOL variations.

7.4.1.1 Inert Weight

Reconstruction of Space Shuttle ascent trajectories has shown that the predicted inert weight for the Orbiter, External Tank, SSMEs and payloads can differ significantly from the post-flight reconstruction. The SSP has decided the mean flight-derived inert weight delta should be applied to all mission assessments. The current value of this delta, based on flights STS-26R through STS-106 is 339 pounds. All missions shall have 339 pounds added to the total inert weight at lift-off via TDDP “Reconstructed Ascent Performance Collector”.

7.4.1.2 Predicted Liquid Hydrogen (LH_2) Load

Reconstruction of LH_2 usage has shown that, on average, 460 lb_m less LH_2 remains at MECO than predictions indicate. The cause of this difference could be either lower than predicted LH_2 loads at engine start, or higher than accounted for usage of LH_2 during ascent. The SSP has determined that this difference will be accounted for in preflight predictions. The 460 lb_m of LH_2 has been removed at lift-off by increasing the H_2 bubble volume from 58.25 ft^3 to 162.50 ft^3. This volume change applies to both the current LWT (R0103L) and SLWT (R0104S) inventories.

7.4.1.3 Day-of-Launch Performance Protection

The Manager’s Reserve Policy (NSTS 07700, Volume III, Flight Definition and Requirements Directive, Paragraph 3.1q) defines performance margin requirements for various

stages during mission planning. The ascent performance margin trajectory result calculation is reduced by 700 pounds prior to comparison with the Manager's Reserve Policy. The 700 pounds protects for DOL performance variations due to wind and atmospheric variations and variations in MPS propellant loads. This value protects for 95% of reconstructed mission results. Ascent performance margin calculations in support of the flight readiness review process do not require this DOL reserve protection and should only be quoted against 3-sigma flight performance reserve protection.

7.5 TRAJECTORY SHAPING

Trajectory shaping was optimized for best nominal payload capability during the PE certification activity. The resulting nominal trajectory design options were discussed in Paragraph 7.0. The required constraints and placards are specified in NSTS 08209, Volume IV. Any new certification activities will perform the required trajectory design trade studies, assess the resulting certification trajectories, and then update NSTS 08209, Volume IV with any new constraints and placards. The remainder of this section lists engine-out design requirements.

First-stage engine-out trajectory design shall satisfy the following criteria:

a. Profiles will be shaped to accommodate a single (top or side) SSME-out anytime from lift-off to SRB staging.

b. Engine-out steering will be the same as nominal steering for vertical rise.

c. Alpha versus Mach number heating constraints defined in NSTS 08209, Volume IV, will be satisfied.

d. SRB separation conditions will be designed to alleviate RTLS guidance problems and the total pressure behind the shock described in the next paragraph.

Second stage engine-out trajectory design shall satisfy the following criteria:

a. A 20-second powered pitchdown phase just prior to MECO will be provided for RTLS to enhance manual pitchdown capability.

b. A roll-to-heads-up maneuver will be performed before MECO for TAL to facilitate time-critical post-MECO activities and to relieve ET heating.

c. Abort propellant management groundrules affecting trajectory shaping are defined in Paragraph 7.14.

d. The SSME retrim mass I-Load will be defined such that retrim occurs at Time To Go = 60 seconds.

e. The mass I-Load that arms ET low level sensors will be defined such that the arm occurs when there is 31,000 pounds usable MPS propellant remaining.

7.6 (DELETED)

7.7 (DELETED)

7.8 (DELETED)

7.9 (DELETED)

7.10 SSME PITCH AND YAW PARALLEL

All three Shuttle Main Engines are gimballed to parallel their thrust vectors beginning 12 seconds after the SRB separation command through MECO command. The SSMEs are paralleled in yaw from lift-off through MECO command. Several changes were incorporated during the performance enhancements certification effort including deletion of the ramp to unparallel position between MECO - 60 seconds and MECO, gaining 125 pounds of additional performance margin. Parallel position is now held until MECO command. With the deletion of the ramp, SSME bias limiting logic was added to prevent gimbal saturation that may occur near MECO. For SSME pitch and yaw parallel requirements, see NSTS 08209, Volume IV, Paragraph 3.1.3.2.

Another performance enhancement was to increase the parallel between the SSME and SRB thrust vectors in first stage by adding time varying biases to the SSME pitch trim commands. This increased payload capability by an additional 270 pounds.

7.11 MECO TARGETS

The original standard insertion technique of achieving orbit used a post-MECO OMS-1 burn. This technique limited the Shuttle to a maximum orbital altitude of about 200 nm. Today's direct insertion technique enables the Shuttle to attain higher orbital altitudes by targeting the ascent trajectory to a higher speed at MECO, resulting in a higher apogee at insertion. This technique eliminates the need for the OMS burn necessary to establish the apogee. Due to a steeper flight path angle and higher MECO velocity, the ET impact footprint is in the Pacific Ocean for a due east launch from ETR.

MECO target lines (inertial velocity versus inertial flight path angle) for direct insertion into orbits of 28.45 degrees and 57.0 degrees inclinations for launches from ETR are shown in Figures 7-24 and 7-25, respectively. A tabular listing of MECO targets for ETR launches is provided in Table 7.4. The MECO target lines satisfy all requirements for safe ET disposal. The apogee lines superimposed on the MECO target lines account for second zonal harmonic effects and have 4.5 nm added to accommodate the ΔV expected from the MPS Dump. For additional information, see NSTS 08209, Volume IV, Paragraph 3.1.3.4.

For ETR launches, only direct insertion targets will be considered for use on all 28.45 through 57-degree inclination missions. Powered flight MECO targets for RTLS and TAL will be consistent with the five navigation operational (OPS) 1/6 landing sites areas defined in NSTS 21075, Section 5.4, Paragraph 9.

MECO targeting for RTLS will support the following criteria at ET separation:

a. Undispersed separation q between 7 and 9 psf

b. Less than 2% MPS propellant excess remaining

c. Flightpath angle of 0 degrees

d. Range-velocity relationship specified by a target line

e. Twenty-second powered pitchdown

MECO targeting for TAL will support the following criteria at ET separation:

a. Geodetic altitude of 360,000 ft

b. Zero degree inertial flightpath angle

c. Range-velocity relationship specified by a target line

d. Inertial plane within a specified crossrange

For additional requirements, see NSTS 08209, Volume IV, Paragraph 3.1.3.3.

7.12 ET SEPARATION

For nominal, AOA, and ATO, the Orbiter will perform a $-Z$ body axis translation maneuver for a minimum ΔV of 4 fps The maneuver begins at ET separation at the separation inertial attitude with the measured attitude rates being within $\pm$ 0.7 deg/sec of zero for each body axis. The ET separation conditions must be within the following limits for no-fail and AOA/ATO:

a.	Pitch rate	$\pm$ 0.7 deg/sec
b.	Roll rate	$\pm$ 0.7 deg/sec
c.	Yaw rate	$\pm$ 0.7 deg/sec
d.	Dynamic Pressure	< 0.1 psf for 57 nm MECO < 0.22 psf for 52 nm MECO

For RTLS, the Orbiter will perform a *Z body axis translation maneuver beginning at ET separation. This translation maneuver is terminated no earlier than 10 seconds after

separation with an AOA greater than 10 degrees. The ET separation conditions must be within the following limits for RTLS:

a.	Pitch rate	-0.25 ± 0.5 deg/sec
b.	Roll rate	0.0 ± 2.0 deg/sec
c.	Yaw rate	0.0 ± 0.5 deg/sec
d.	Dynamic Pressure	$6.0 < q < 9.5$ psf
e.	Angle of Attack	-2.5 ± 1.0 deg
f.	Angle of Sideslip	0.0 ± 2.0 deg
g.	Bank Angle	0.0 ± 20.0 sec
h.	MPS prop remaining in tank	$\leq 2\%$

For TAL, the Orbiter will perform a *Z body axis translation maneuver for a minimum ΔV of 11 fps beginning at ET separation. The ET separation conditions must be within the following limits for TAL:

a.	Pitch rate	± 0.7 deg/sec
b.	Roll rate	± 0.7 deg/sec
c.	Yaw rate	± 0.7 deg/sec

For TAL, the following attitude and rate limits will be met after ET separation and prior to transfer to the OPS-3 descent flight software mode (note that pitch angle and sideslip angle are manually controlled by the crew after Major Mode (MM) 104, not by the flight control system):

a.	Euler pitch angle	(θ) ≥ 15 deg
b.	Sideslip angle	(β) 0 ± 30 deg
c.	Body roll rate	(p) 0 ± 0.5 deg/sec
d.	Body pitch rate	(q) 0 ± 0.5 deg/sec
e.	Body yaw rate	(r) 0 ± 0.5 deg/sec

For all TAL aborts, a post-MECO OMS burn of 100 fps will be conducted following MM304 in order to minimize the probability of the Orbiter being hit by ET debris following ET rupture. The OMS burn will occur after 15 seconds of a 20 second +X RCS settling burn is performed. The settling burn occurs as soon as the flight control system

satisfies the following OMS burn inhibit limits (note that it may take as long as 55 seconds past MM304 to meet these constraints):

a. Angle of attack (α) 43 ± 20 deg

b. Euler roll angle (Φ) 0 ± 40 deg

c. Body roll rate (p) 0 ± 3.0 deg/sec

d. Body pitch rate (q) 0 ± 2.5 deg/sec

e. Body yaw rate (r) 0 ± 2.0 deg/sec

For a contingency abort, the fast separation sequence will be utilized with the separation mode selection defined by the contingency abort flight regime (except for the high-speed regime, where autoguidance continue is employed and nominal sequence and nominal ET separation are utilized). There are no MPS propellant remaining restrictions.

For additional ET separation constraints as related to TAL hit requirements, see NSTS 08209, Volume IV, Paragraph 3.3.3.3.

For GRTLS, the Orbiter attitude and rates at the end of the *Z RCS separation burn phase will be within the RCS aerosurface recovery limits. The GRTLS attitude and attitude rate control requirements at the end of the *Z translational burn phase (separation termination) specified in NSTS 07700, Volume X, Figure 3.2.1.1.10.2.4, are as follows:

Axis	Angle	Angle Limits	Rate
Roll	Roll	$-30 \text{ deg} \leq \emptyset \leq 30 \text{ deg}$	$-2 \text{ deg/sec} \leq p \leq 2 \text{ deg/sec}$
Pitch	Angle of attack	$\alpha = 20 \text{ deg} \pm 10 \text{ deg}$	$0 \text{ deg/sec} \leq q \leq 5 \text{ deg/sec}$
Yaw	Angle of sideslip	$-3 \text{ deg} \leq \beta \leq 3 \text{ deg}$	$-1 \text{ deg/sec} \leq r \leq 1 \text{ deg/sec}$

7.13 POST-MECO THROUGH ORBIT INSERTION

This section will discuss the flight phases which begin after MECO and end after the OMS-2 burn. Flight phases which exist during this period are defined as nominal, ATO and AOA. RTLS and TAL aborts have no orbit insertion burns. These sub-orbital abort flight phases transition into the entry flight phase following the ET separation maneuver.

Mated Coast flight phase (for nominal, ATO and AOA) begins at the Software Zero Thrust Event. At this time, the attitude control of the Shuttle transitions from the Main Engines to the RCS. The Transition Digital Auto Pilot (TRANS DAP) commands the forward and aft RCS jets ON and OFF as it tries to minimize (attempts to drive to 0 deg/sec) the attitude rates.

During Mated Coast:

Attitude Deadband = +/3 deg (all axes)

Attitude Rate Deadbands = $\pm$0.5 deg/sec (all axes)

The purpose of the Mated Coast flight phase is to keep the Shuttle at the proper attitude and body rates in preparation for the ET separation burn. Approximately 19 seconds after MECO, the ET separation burn is commanded. ET separation consists of firing four forward and six aft downfiring RCS jets. This burn drives the Orbiter away from the ET.

During ET separation burn:

Attitude Deadband = $\pm$3 deg (all axes)

Attitude Rate Deadbands = $\pm$0.5 deg/sec (all axes)

Duration of the burn = time required to build up 4 fps of Z direction delta-V (by the Orbiter)

At the end of the ET separation burn, the first orbit insertion flight phase begins, called MM104. The OMS burn performed during MM104 is called the OMS-1 burn. This burn is done to place the Orbiter into an elliptical orbit, that later will be circularized (for nominal and ATO) or changed to a different ellipse (for AOA).

The OMS-1 burn is not performed for a DI nominal mission. DI refers to MECO targets (radius, velocity, and flight path angle) which result in a trajectory that has an apogee over 105 nm. For these trajectories, an OMS-1 burn is not required because the Orbiter inserts directly in an orbit that has a high enough apogee.

An ATO OMS-1 burn is performed when an SSME failed during ascent resulting in an underspeed (velocity miss) at MECO of approximately 150 fps to 500 fps. Start time of the burn is chosen to be two minutes prior to the apogee established at MECO.

An AOA OMS-1 burn is performed when an SSME failed during ascent resulting in a larger underspeed than an ATO can make up or not enough OMS is available to perform an ATO mission. Start time of the burn is chosen to be two minutes prior to the apogee established at MECO, but no sooner than two minutes after MECO.

At the end of MM104, the crew transitions to MM105. The OMS burn performed during MM105 is called the OMS-2 burn. This burn is usually done at the apogee of elliptical orbit established by the OMS-1 burn or by the MECO conditions (if a DI trajectory). OMS-2 will establish the final nominal orbit and ATO orbit (usually circular) and the AOA orbit (elliptical).

For nominal OMS-2, the burn is started at a time when apogee will occur half-way through the burn. OMS-2 raises the perigee only. The perigee target is usually the same as the current apogee for non-rendezvous missions. For rendezvous missions, the perigee target is a function of how quickly the Orbiter is to catch-up with the target. The lower the perigee, the faster the Orbiter will catch up to a target that is in a higher orbit. Perigee can be no lower than 85 nm, due to excessive atmospheric drag below that altitude.

An ATO OMS-2 burn is done at the apogee established by the ATO OMS-1 burn (usually 105 nm). The OMS-2 burn raises the perigee to 105 nm, in order to circularize the orbit. This orbit allows the crew and ground to assess whether an early deorbit is required or whether an additional orbit insertion burn can be performed to raise the orbit and continue on with the mission.

The AOA OMS-2 burn is actually a deorbit burn. Following this burn, the Orbiter will be on a sub-orbital trajectory which falls back into the atmosphere. Start time for the AOA OMS-2 burn is determined by entry ranging requirements. At the point where the trajectory reenters the atmosphere (400,000 feet), flight software targets a range to landing site and a flight path angle that are both functions of the inertial velocity at that point.

AOA OMS-2 burns can target for either a “steep” entry trajectory or “shallow” trajectory. Steep and shallow refer to the flight path angle of the trajectory as it reaches the 400,000-foot altitude point. Shallow flight path angles are approximately minus one degree. Shallow entry trajectories have longer range to landing site distances (5,000 nm). Longer range to landing site and shallow flight path angle results in longer entry trajectory durations and higher heating. Steep is preferred over shallow for this reason. Shallow deorbit burns, however, require less change in orbit and therefore less OMS to accomplish. Shallow deorbit burns are used for OMS system failures.

The orbit insertion flight phase ends for the nominal and ATO trajectory, following the OMS-2 burn, when the crew begins the on-orbit preparation activities.

Orbit insertion (deorbit) ends for the AOA case, five minutes prior to 400,000-foot altitude, when the crew transitions the GPCs to MM304 (the first entry flight phase).

Table 7.8 defines a typical set of OMS target options for nominal, ATO, AOA-steep and AOA-shallow.

7.14 ASCENT PROPELLANT MANAGEMENT

After SSME shutdown and ET separation, the Orbiter will dump propellants remaining trapped in the MPS feedlines and Main Engine. When dumping through the SSMEs, the minimum time between engine shutdown and the start of propellant dumping is 20

seconds to provide time for the engines to complete the shutdown sequence, although the dump normally begins two minutes after MECO. The maximum time from engine cutoff to completion of propellant dumping is five minutes to limit consumables required to provide hydraulic power to the engines. For nominal missions and AOA, the dump will be completed by the MPS recirculation system. For RTLS and TAL the dump will be completed by vacuum inerting.

Either the OMS engines alone, or the OMS engines in combination with the aft 24 RCS engines, shall be used to dump OMS propellant in parallel with SSME dumps. During RTLS and TAL this is for Orbiter CG and landing weight control. During ATO this is for performance.

The capability to use the OMS engines during nominal second stage flight has been added as a performance enhancement. The typical OMS assist burn will begin at SRB separation + 10 seconds and last for 102 seconds. Four thousand pounds of propellant is consumed gaining approximately 250 pounds of ascent performance margin. The maximum certified OMS assist burn is for 178 seconds, using 7,000 pounds of propellant and gaining 400 pounds of ascent performance margin.

The MPS, OMS and RCS propellant dump sequences for nominal, RTLS, TAL, and ATO are provided in Figures 7-26 through 7-29, respectively (reference NSTS 08934, Space Shuttle Operational Databook, Volume VI, Orbiter Propellant Dump Reference Data, Tables 4.1.10 through 4.1.13).

The following list of propellant dump groundrules should be used to define the OMS, RCS, and MPS Dump I-Loads. These groundrules are compatible with the Orbiter Propellant Dump Reference Document.

a. Pre-MECO, the OMS/RCS interconnect will be inhibited:
    1. The latest RTLS abort dumps can be completed without the interconnect.
    2. The TAL pre-MECO OMS dump performed at the PTA call can be completed without the interconnect.
    3. The ATO pre-MECO OMS dump will be performed non-interconnected.

b. Post-MECO, for nominal/AOA/ATO
    1. Always perform MPS LH_2 vent at MECO $\pm$10 seconds to relieve pressures in the LH_2 feedline manifold.
    2. Always initiate LH_2 and LO_2 pressurized MPS Dumps at MECO $+2$ minutes.

c. For AOA/ATO
    1. A pre-MECO OMS dump will be performed with excess OMS propellant to provide the earliest PTA time.

(a) A constant dump will be used if an SSME failure at the PTM time with a constant dump and $+2\sigma$ SSME performance does not achieve a guided MECO.

(b) A ramp dump will be used if an SSME failure at the PTM time with a constant dump and $+2\sigma$ SSME performance achieves a guided MECO.

2. During AOA deorbit burns, excess OMS propellant will be burned out of plane to protect the OMS tank landing constraint (OMS < 22% gauge). The out-of-plane portion of the burn will be in a direction that reduces cross-range at EI.

3. After the AOA deorbit burn, a manual forward RCS dump to 0% gage will be performed in MM 303 to minimize the Orbiter landing weight.

d. For TAL

1. A pre-MECO OMS dump will initiate immediately after the TAL abort is declared.

2. The pre-MECO OMS dump design will reserve 100 fps for the OMS separation burn from the external tank.

3. The TAL MPS Dump will automatically initiate at MM304 and will terminate at a relative velocity less than or equal to 4,500 fps.

4. A 4 + X aft RCS burn will be performed in MM304 to reduce the Orbiter's landing weight and to protect for aft CG critical flights.

5. A post-MECO OMS burn will be conducted in MM304, up to 85 seconds after ET separation. The exact time depends on the number of available RCS jets at ET separation as well as the attitude of the Orbiter at OPS-3 transition.

e. For RTLS

1. A pre-MECO OMS dump will be initiated at RTLS abort selection.

2. The RTLS MPS Dump will automatically initiate at the MM602 transition and will terminate at a relative velocity less than or equal to 3,800 fps.

3. A 4 + X RCS burn will be performed at MM602 + 20 seconds to reduce the vehicle's landing weight and to protect for aft CG critical flights.

7.15 REFERENCE MISSION PERFORMANCE TRACKING

Reference Missions 1 and 9 in NSTS 07700, Volume X - Book 1, Paragraph 3.2.1.1.3, are to be tracked for performance margin. Mission descriptions and performance margins relative to the payload requirements for the missions are shown in Table 7.12.

Detailed mission mass properties and requirements are provided in the trajectory design data packages referenced in Table 7.12.

7.15.1 Mission 1

Mission 1 is a payload delivery mission to a 150 nm circular orbit. The mission will be launched due east and require a payload capability of 65,000 pounds. The purpose of this mission is either the placement in orbit of 65,000-pound satellite or the placement in orbit of a 65,000-pound satellite and retrieval from orbit of a 32,000-pound satellite.

7.15.2 Mission 9

This International Space Station (ISS) mission is a direct insertion design to 173 nm with a rendezvous occurring at 220 nm. This mission is launched from KSC to an inclination of 51.6 degrees. The crew size is five with a mission duration of seven days. The total mission performance requirement is 39,400 pounds, of which 36,200 pounds is provided for ISS cargo.

7.15.2.1 (Deleted)

7.15.2.2 (Deleted)

7.16 (DELETED)

7.17 I-LOAD SELECTION

With the complete implementation of DOLILU II trajectory designs, as part of the performance enhancement certification activity, mission-specific ascent designs have been simplified. First stage nominal ascent design now consists of determining the following:

a. An alpha profile (max, mid, or min)

b. A q-level (high or low)

c. A design season for q (summer or winter)

d. A design month (Jan through Dec)

e. A commanded throttle profile (104-67-104, 104-72-104, or 106-72-106)

Second stage nominal ascent design now consists of determining the following:

a. A MECO altitude (52 nm or 57 nm)

b. OMS_Assist (on/off and amount)

NSTS 07700, Volume III contains the listing of performance enhancements changes and the guidelines for their use, along with the Ascent Performance Manager's Reserve Guidelines. The remaining design considerations for nominal and abort designs are determined by NSTS 21075.

7.18 MINIMUM ORBITER LIFT-OFF WEIGHT

The following is the basis for the minimum Orbiter lift-off weight referenced in NSTS 07700, Volume III and NSTS 07700, Volume X - Books 1 and 2. Flight history and mission content were evaluated to determine the minimum Orbiter weight at lift-off. Missions with low payload and high propellant consumables are expected to result in the lightest weight Orbiter. The following data does not represent any specific proposed mission but is representative of light weight missions.

Orbiter	154,200 lbs
Block II SSMEs	23,100 lbs
Crew Compartment	5,200 lbs
Non-propulsive Consumables @ Launch	6,200 lbs
RCS	7,500 lbs
OMS	25,100 lbs
MPS Propellant @ SRB Ignition	5,200 lbs
Payload	4,600 lbs
STS Operator	3,900 lbs
Total Orbiter Weight @ SRB Ignition	235,000 lbs

Flights planned with an Orbiter weight at lift-off of less than 235,000 pounds will require a mission-unique assessment to accommodate surface wind constraints.

TABLE 7.1

LOCATION OF SPACE SHUTTLE LAUNCH SITES

	ETR	
	LC-39A	LC-39B
Geodetic Latitude (deg)	28.608422 N	28.627213 N
Geodetic Longitude (deg)	279.395910	279.379203
Elevation (Feet)		
• Above MSL	95.0	92.66
• Above Fisher 1960 Ellipsoid	−112.8*	−115.14

NOTES: 1. Locations are for the ET C/L and top of the mobile launch pad corresponding to Orbiter coordinates (inches) X = 1744.0, Y = 0.0, Z = −336.5.

2. Elevations are consistent with Shuttle navigation inputs for NavBase altitude (−2.4 feet at 39A, −4.74 feet at 39B).

3. Mean Sea Level (MSL) is taken to be 207.8 feet below Fischer Ellipsoid.

TABLE 7.2 (DELETED)

TABLE 7.3 (DELETED)

TABLE 7.4

ETR - TARGETS

DIRECT INSERTION

Inclination (DEG)	HA/HT (NM)	VI (FPS)	GAMI (DEG)	RI (FT)	Flight Effectivity
28.45	150/57	25869.	0.60	21272079.	STS-87
28.45	153/57	25872.	0.60	21272079.	STS-93
28.45	160/57	25873.	0.77	21272079.	STS-87
28.45	300/57	26102.	1.30	21272079.	STS-95
39.0	150/57	25861.	0.60	21272079.	STS-90
51.6	150/57	25973.	0.60	21272079.	STS-89
51.6	170/52	25923.	0.60	21241700.	STS-88 (Eng)
51.6	173/52	25928.	0.60	21241700.	STS-91
57.0	160/52	25829.	0.99	21241700.	STS-85

HA - Apogee Altitude

HT - MECO Target Altitude

VI - Inertial Velocity of MECO Target

GAMI - Inertial Flight Path Angle of MECO Target

RI - Inertial Radius of MECO Target

Eng - Engineering Cycle

TABLE 7.5 (DELETED)

TABLE 7.6 (DELETED)

TABLE 7.7 (DELETED)

TABLE 7.8

DIRECT INSERTION OMS TARGETS FOR 28.45 TO 57-DEGREE INCLINATION (APOGEE ≤ 250 NM)

		OMS-1			OMS-2		
Target Option	MECO Underspeed**	Target	TIG	ITGT	Target	ITGT	Notes
1	0 - 25 fps				Nominal	0	Auto software select
2	0 - 138 fps				Nom PEG 7	Key in	Raise Hp to 95 nm**
3	138 - 161 fps				Nom PEG 7	Key in	Raise Ha to 105 nm**
4	0 - 33 fps				AOA	10	
5	0 - 33 fps				AOA shallow	11	
6	33 - 161 fps				AOA	8	
7	33 - 161 fps				AOA shallow	9	
8	161 - 695 fps	ATO-DEL	MECO + 2* TTA − 2	1	ATO	1	Auto software select Delay OMS-1 exec
9	161 - 695 fps	ATO-DEL	MECO + 2* TTA − 2	1	AOA	6	Delay OMS-1 exec
10	161 - 695 fps	ATO-DEL	MECO + 2* TTA − 2	1	AOA shallow	7	Delay OMS-1 exec
11	695 - 786 fps	AOA-DEL	MECO + 2* TTA − 2	1	AOA MIN Hp	2	Hp = 90 nm**
12	265 fps (design u/s)	AOA	MECO + 4	4	AOA	4	Optimum AOA Full ATO Dump
13	265 fps (design u/s)	AOA	MECO + 4	4	AOA shallow	3	Optimum AOA Full ATO Dump
14	786-832 fps	DEL AOA-S	MECO + 2* TTA − 2	5	AOA shallow	5	Delayed AOA

NOTE: Additional targets may be required if the nominal MECO apogee is greater than 250 nm.

*For ATO-OMS-1, the I-Loaded TIG time will be MECO plus 2 minutes; (MECO + 2); however, OMS ignition will occur at either APOGEE minus 2 minutes (TTA - 2 min) or MECO + 2, whichever is later.

**Values for typical Space Station mission.

TABLE 7.9 (DELETED)

TABLE 7.10 (DELETED)

TABLE 7.11 (DELETED)

TABLE 7.12

SPACE SHUTTLE/SPACE STATION REFERENCE MISSION PERFORMANCE DESCRIPTION

	REFERENCE MISSION NUMBER	
	1	9b
Launch Month	June	February
Max Dispersed Q (psf)	819	PE High q
Min Nominal Q Alpha (psf deg)	– 3,000	N/A
PE Design Alpha Target	N/A	PE max Alpha
Altitude (nm)	150	173
Inclination (deg)	28.45	51.6
Crew Size	4	5
Mission Duration (days)	5	7
Ground*up Rendezvous	No	Yes
SRM	RSRM	RSRM
RMS	Not Installed	Installed
FWD RCS	1862	Full
OMS Load	19,700	22,900
CRYO Tanks	3 tanks	4 tanks offloaded to 3 equiv
Ascent Performance Margin Target (lbs) (Including Yaw Steering)	3,000	5,000
Ascent Performance Margin	TBD	TBD
Max Nominal Q	TBD	TBD
Min Nominal Q Alpha	TBD	TBD
Staging Gamma	TBD	TBD
MECO Weight	TBD	TBD
TDDP Reference	ASPLBS09	SPLFS084

FIGURE 7-1

ASCENT TRAJECTORY MAJOR SHAPING CONSTRAINTS

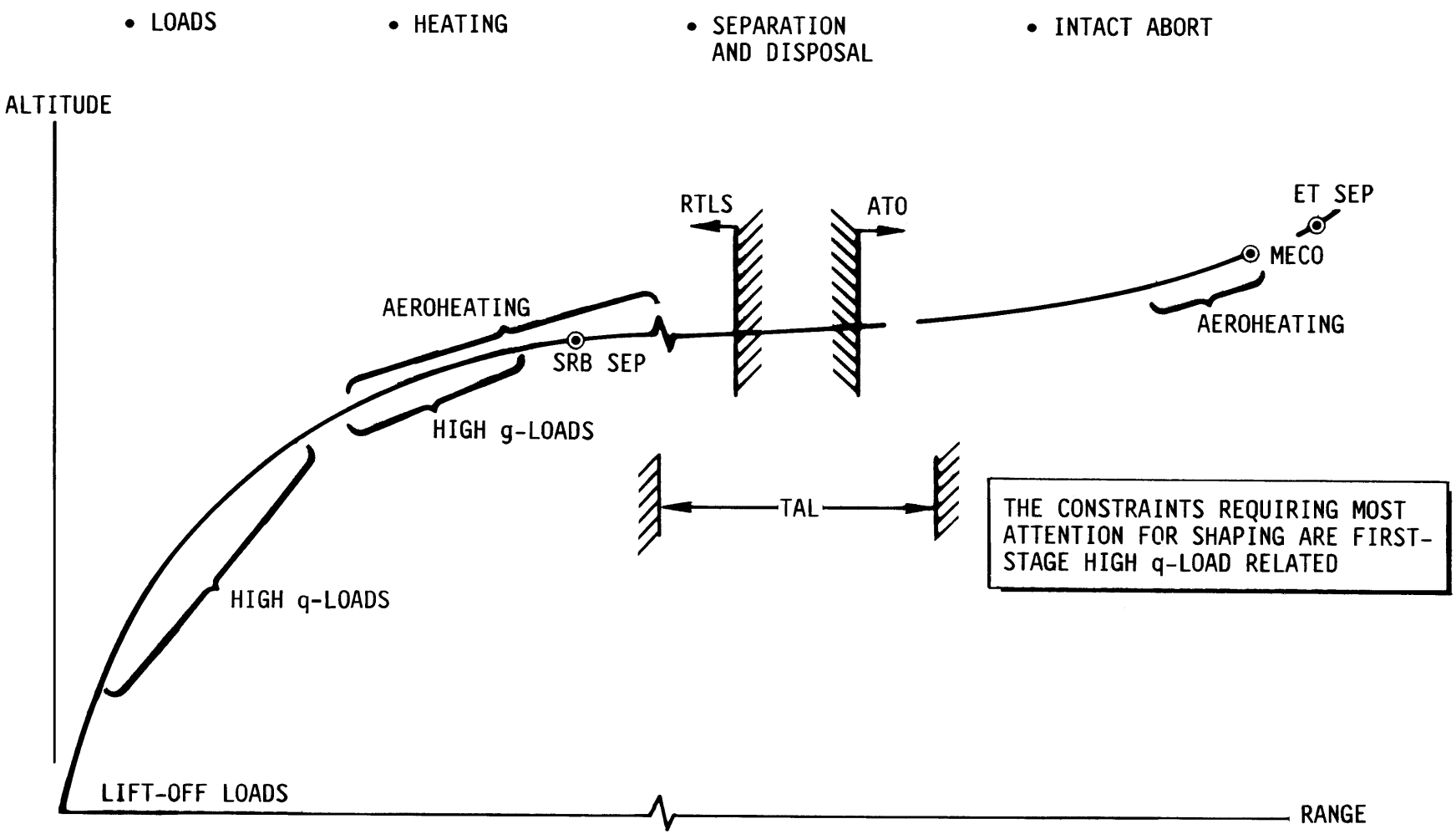

FIGURE 7-2

TRAJECTORY DESIGN/FLIGHT CONSTRAINTS

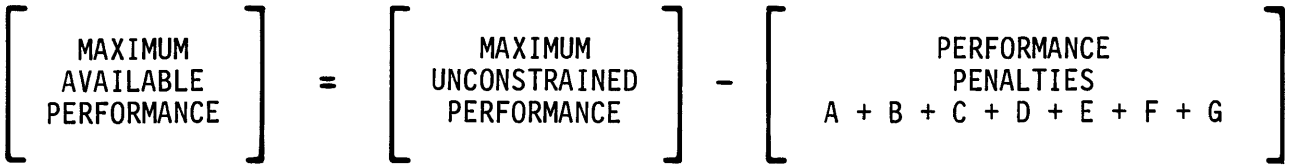

PERFORMANCE PENALTY	TRAJECTORY DESIGN/FLIGHT CONSTRAINT
A	MAXIMUM DYNAMIC PRESSURE
B	AERODYNAMIC LOADS
C	AERODYNAMIC HEATING
D	ACCELERATION
E	INTACT ABORT
F	ET DISPOSAL
G	LIFT-OFF LOADS AND PROPULSION SYSTEM

FIGURE 7-3

MAXIMUM DYNAMIC PRESSURE LIMITING (A)

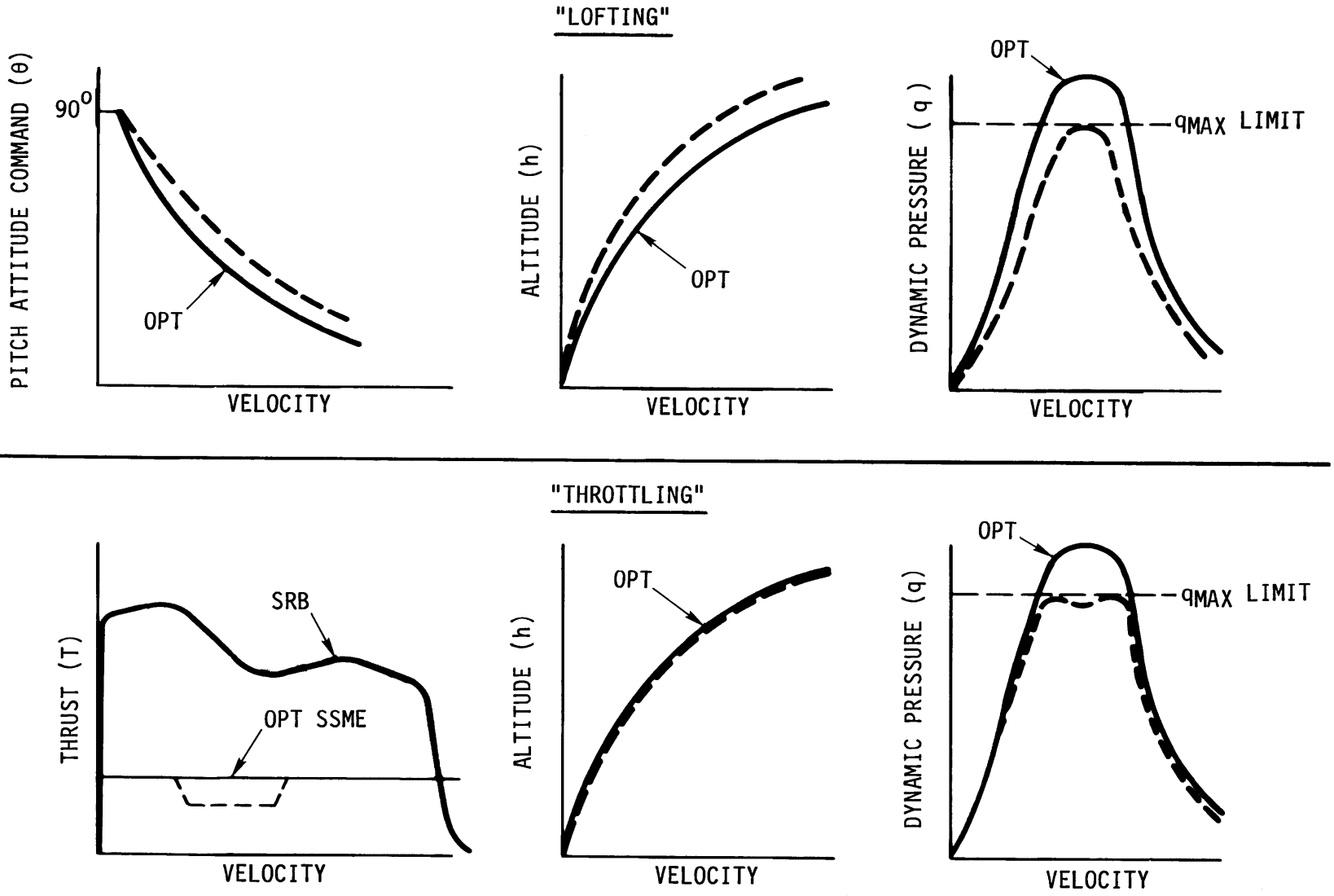

FIGURE 7-4

AERODYNAMIC LOADS LIMITING (B)

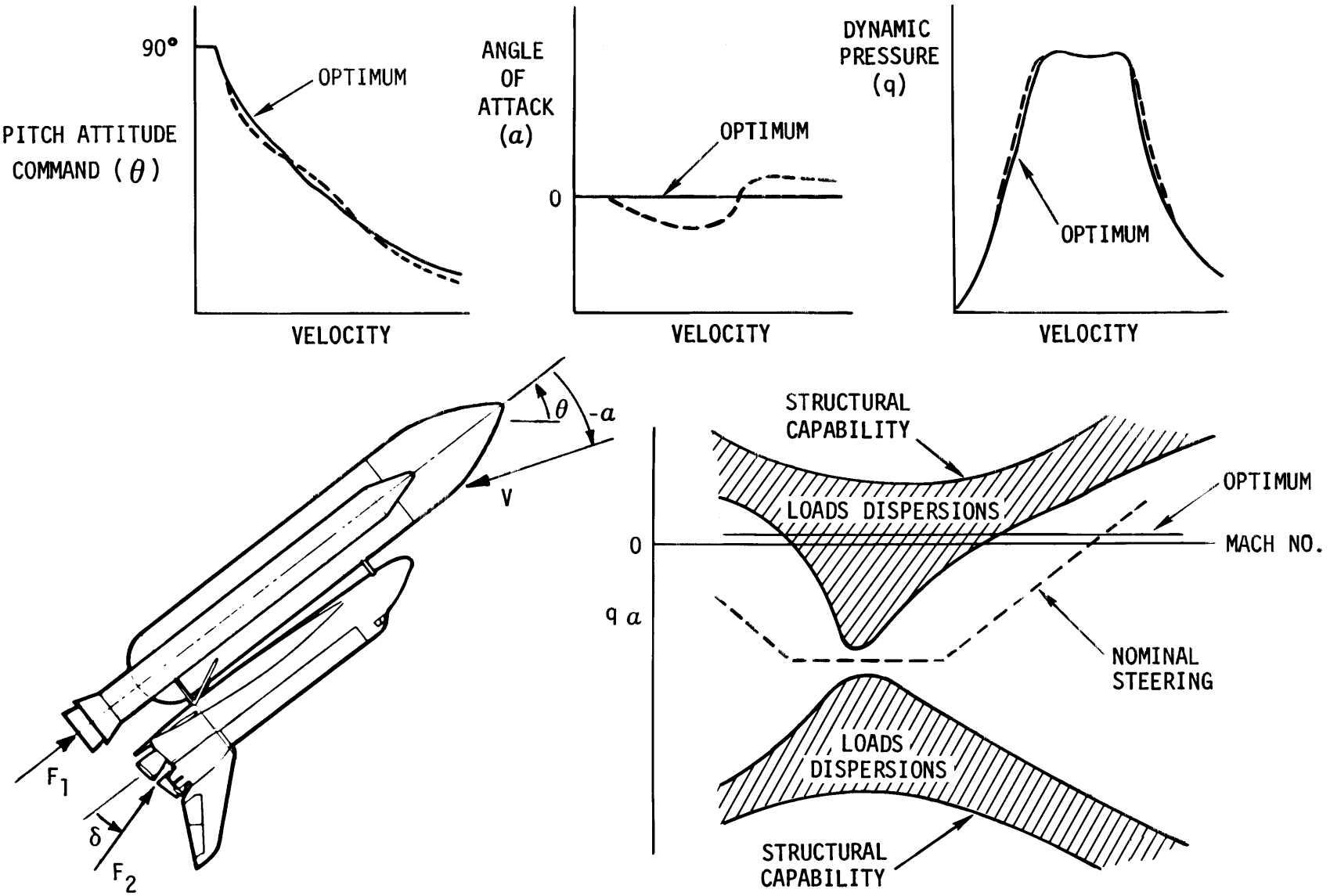

FIGURE 7-5

AERODYNAMIC HEATING LIMITING (C)

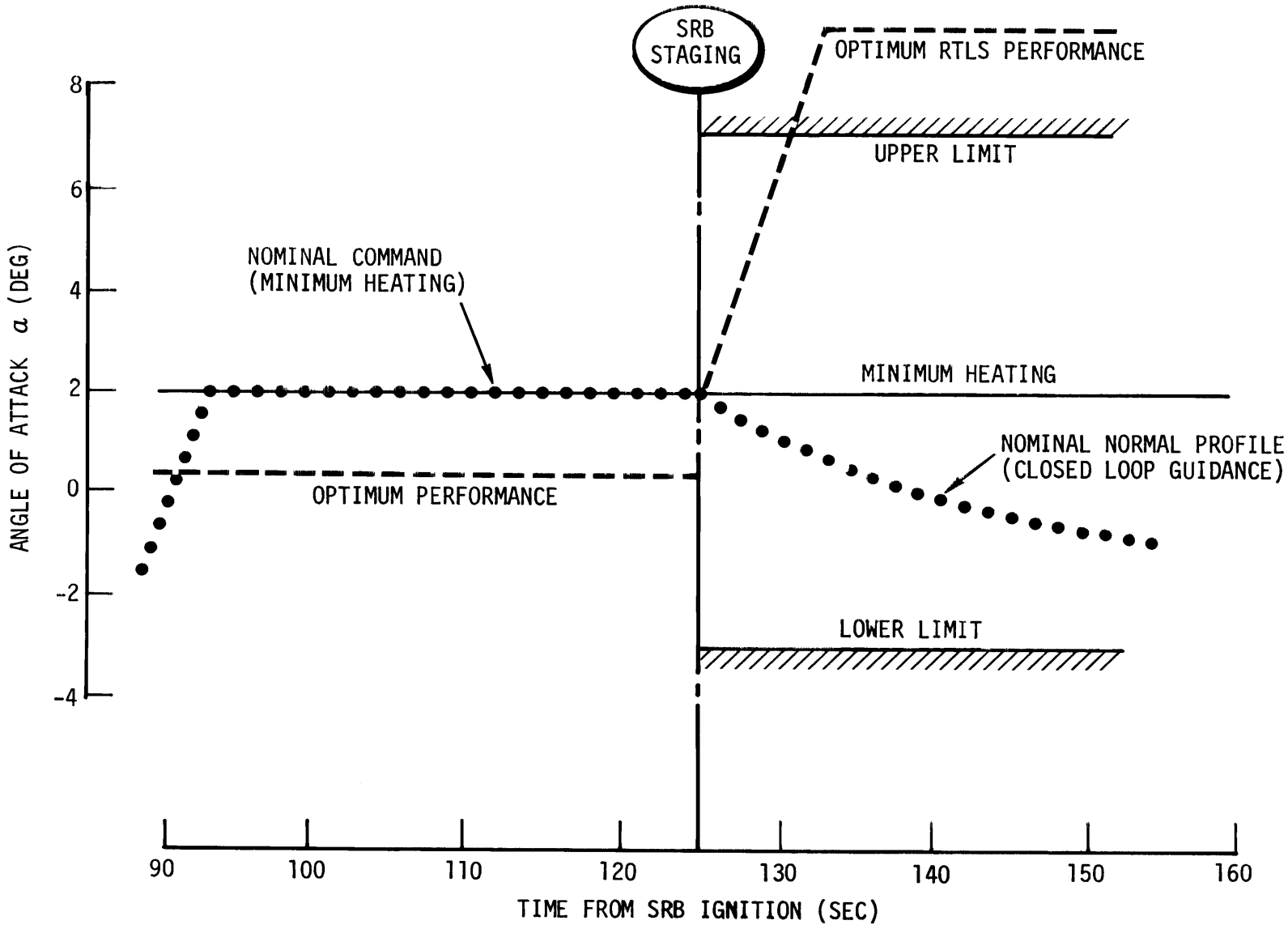

FIGURE 7-6

ACCELERATION LIMITING (D)

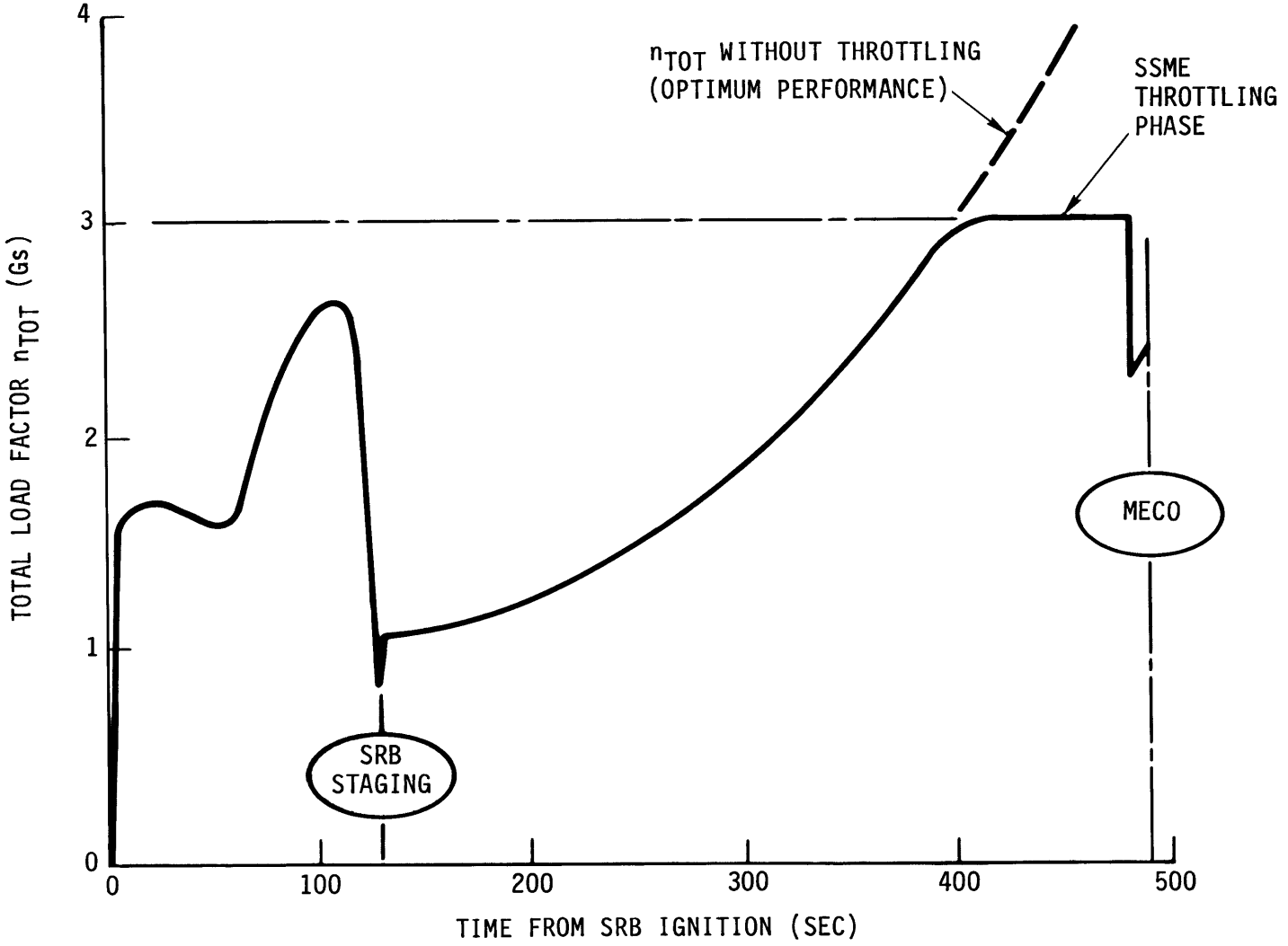

FIGURE 7-7

SHAPING FOR INTACT ABORT (E)

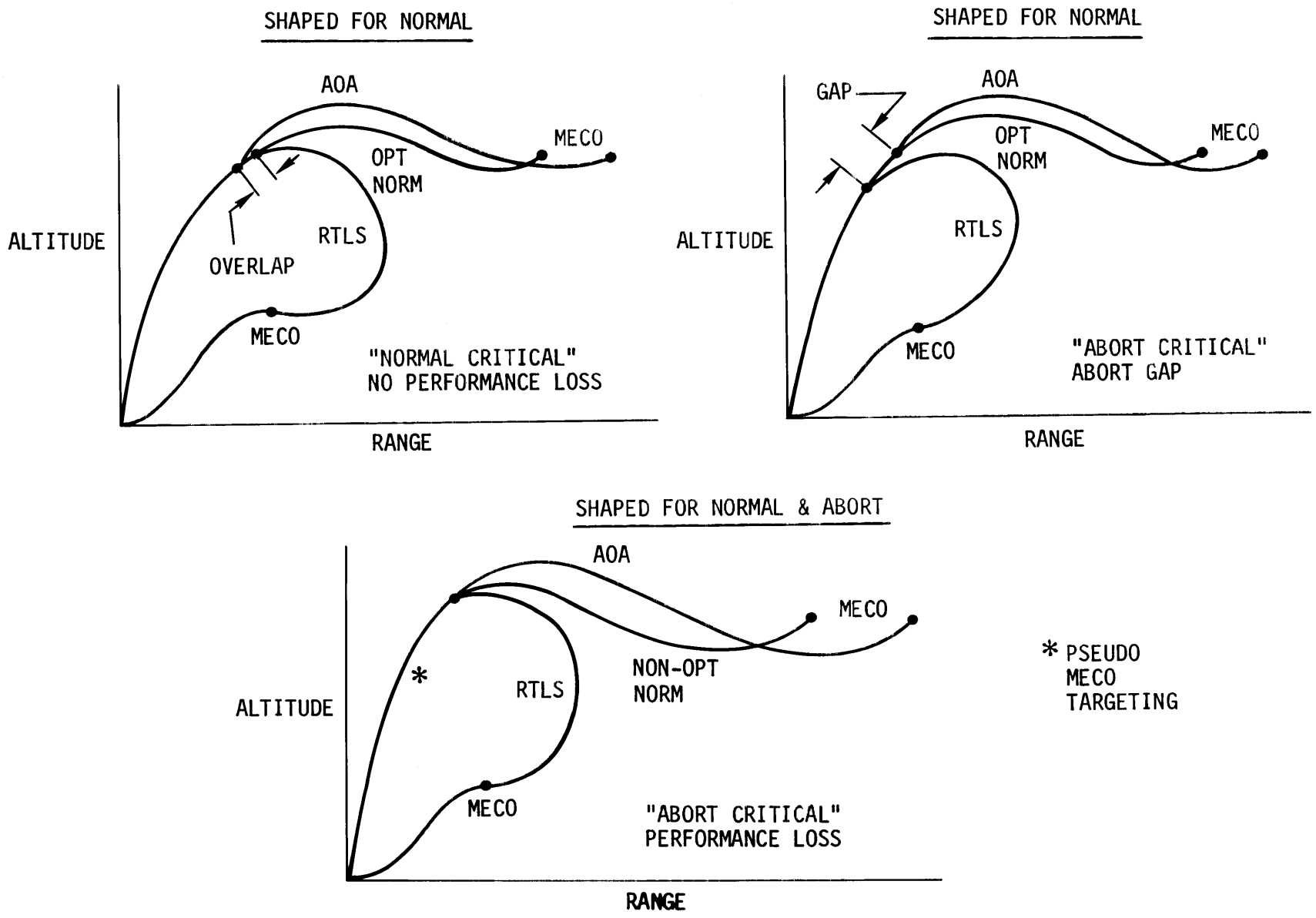

FIGURE 7-8

MECO TARGETING FOR ET DISPOSAL (F)

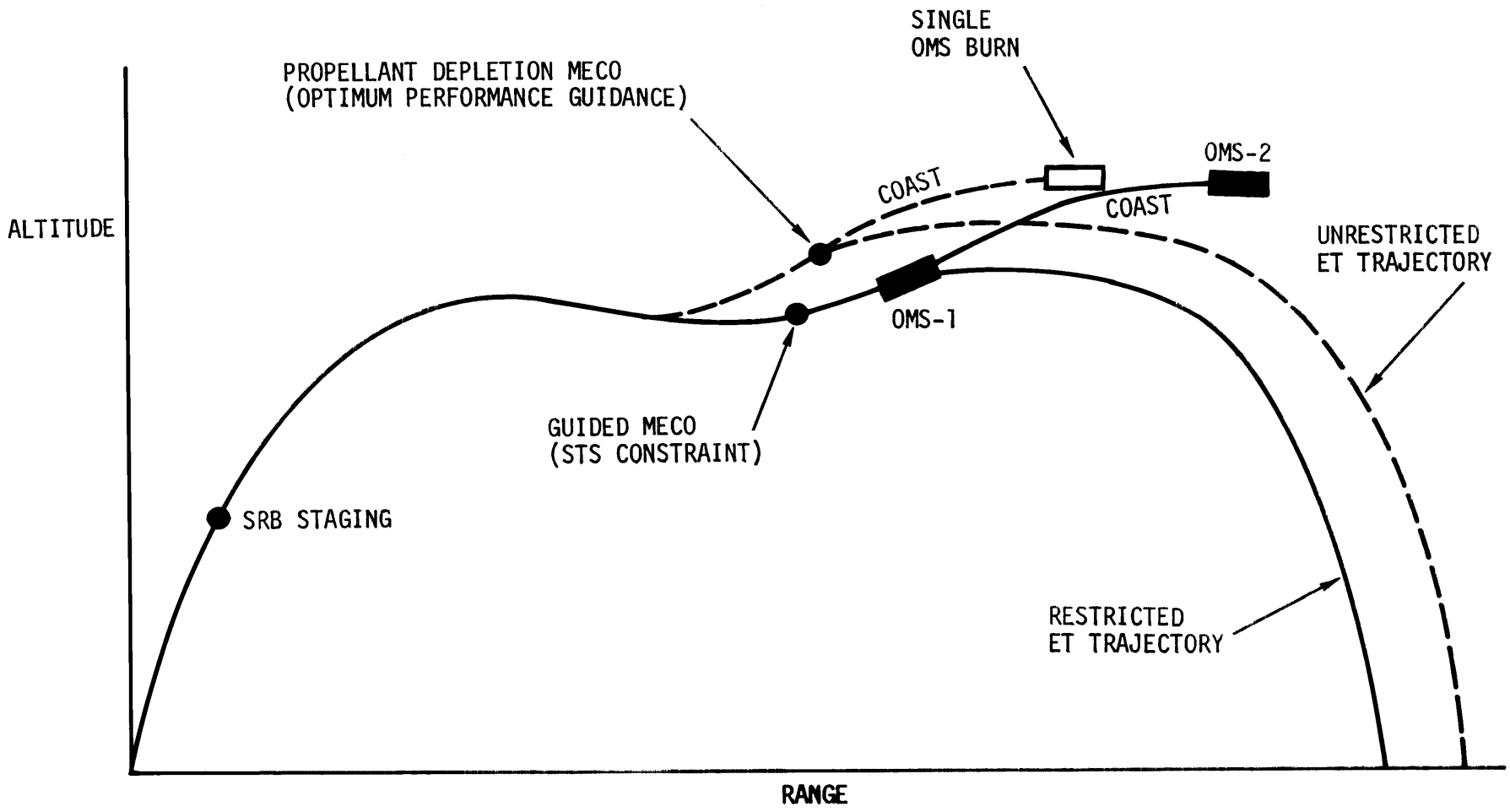

FIGURE 7-9

LIFT-OFF LOADS LIMITING (G)

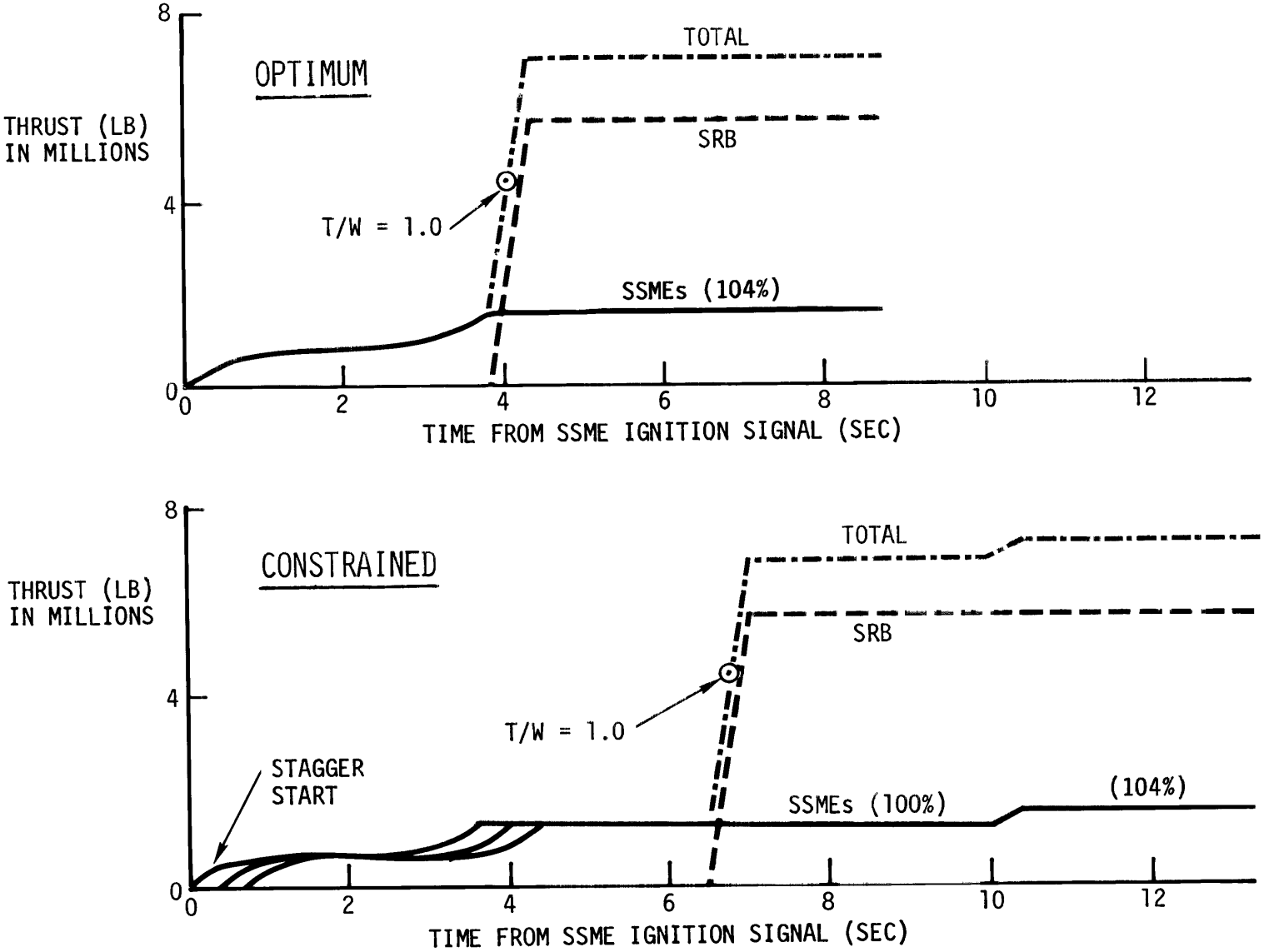

FIGURE 7-10

PROPULSION SYSTEM CONSTRAINT (G)

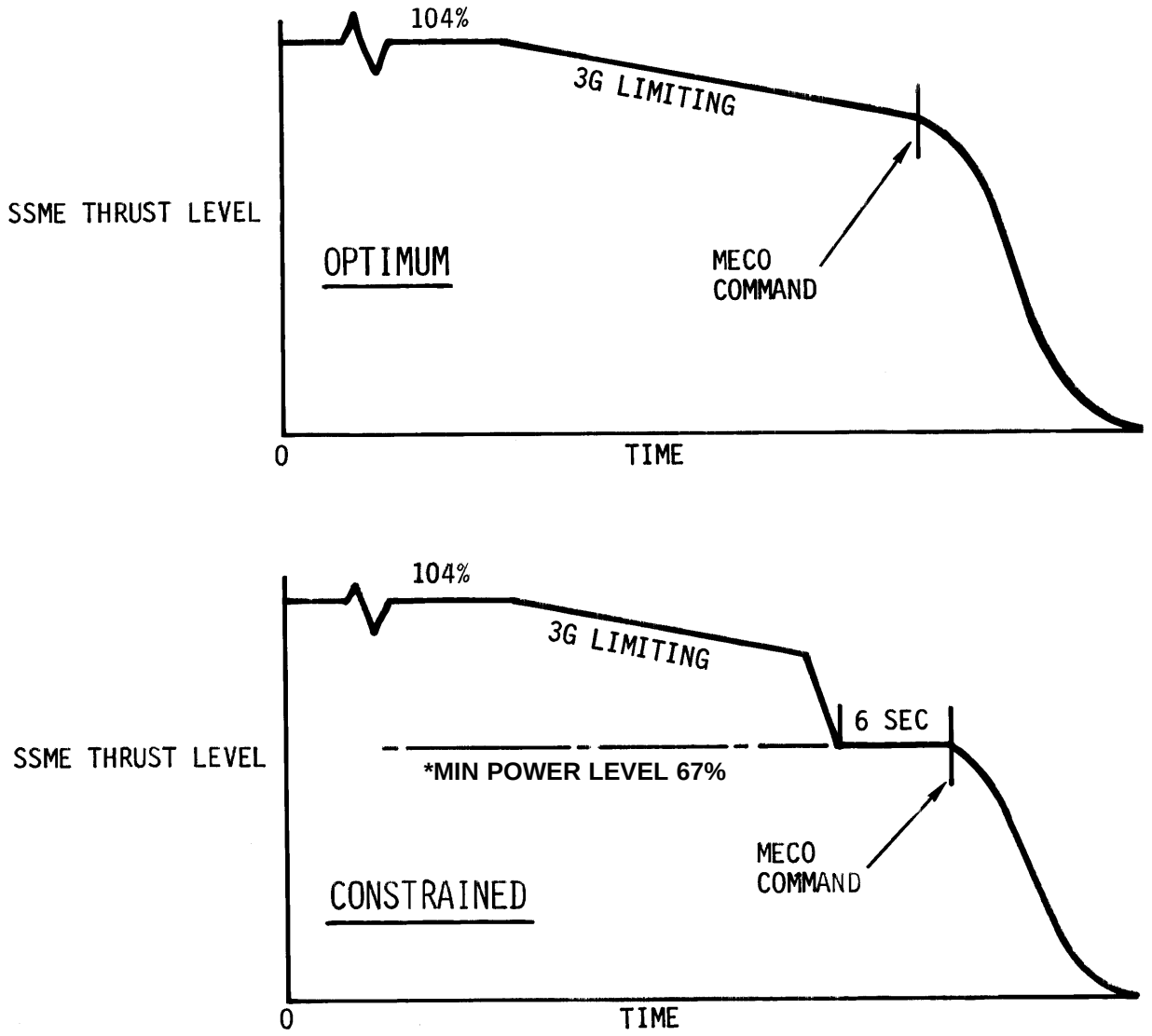

*** 67% is a flight design constraint; the SSME constraint is 65%**

FIGURE 7-11

TYPICAL MISSION PROFILE

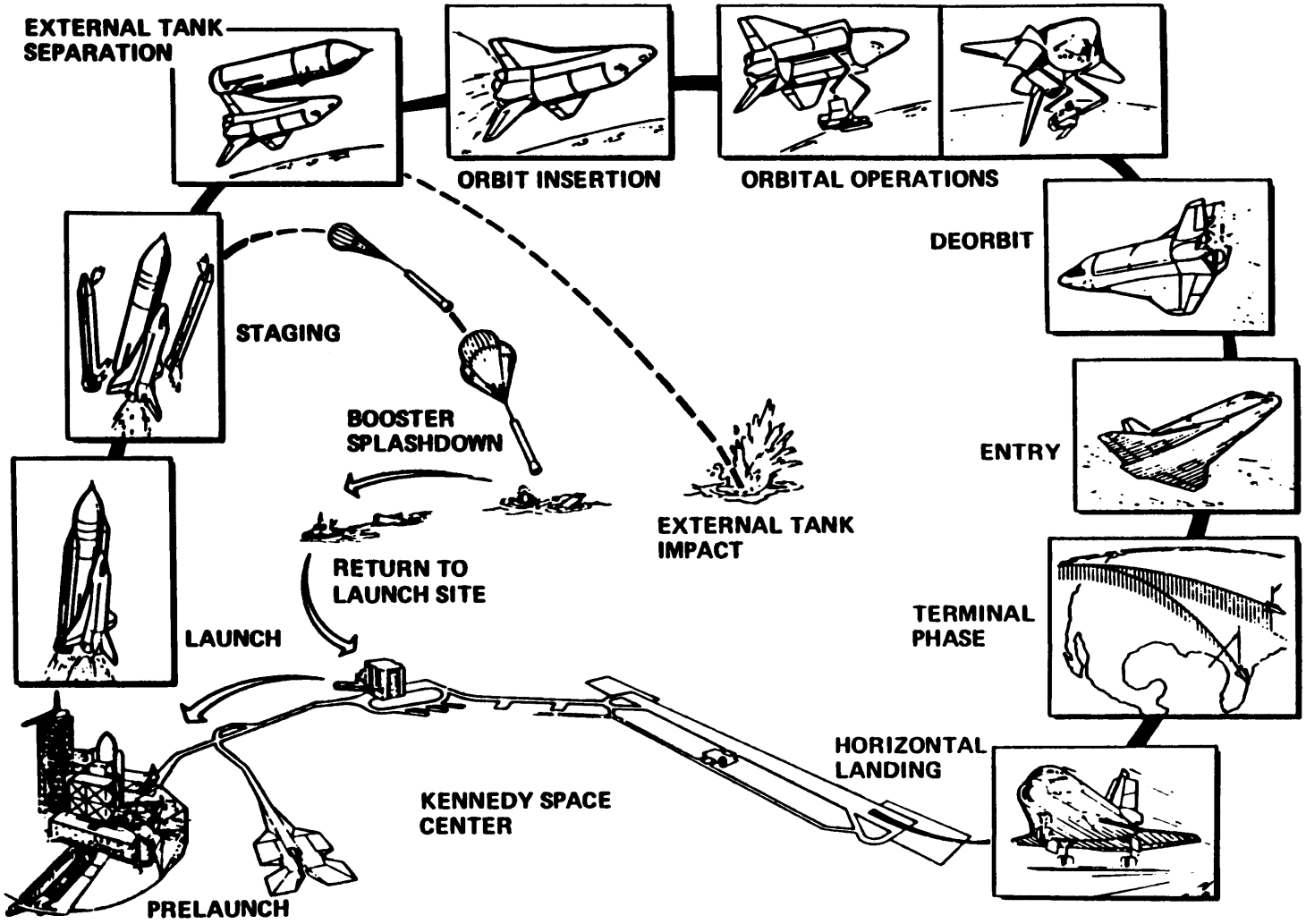

FIGURE 7-12

TYPICAL ASCENT AND DESCENT TRAJECTORY PROFILES

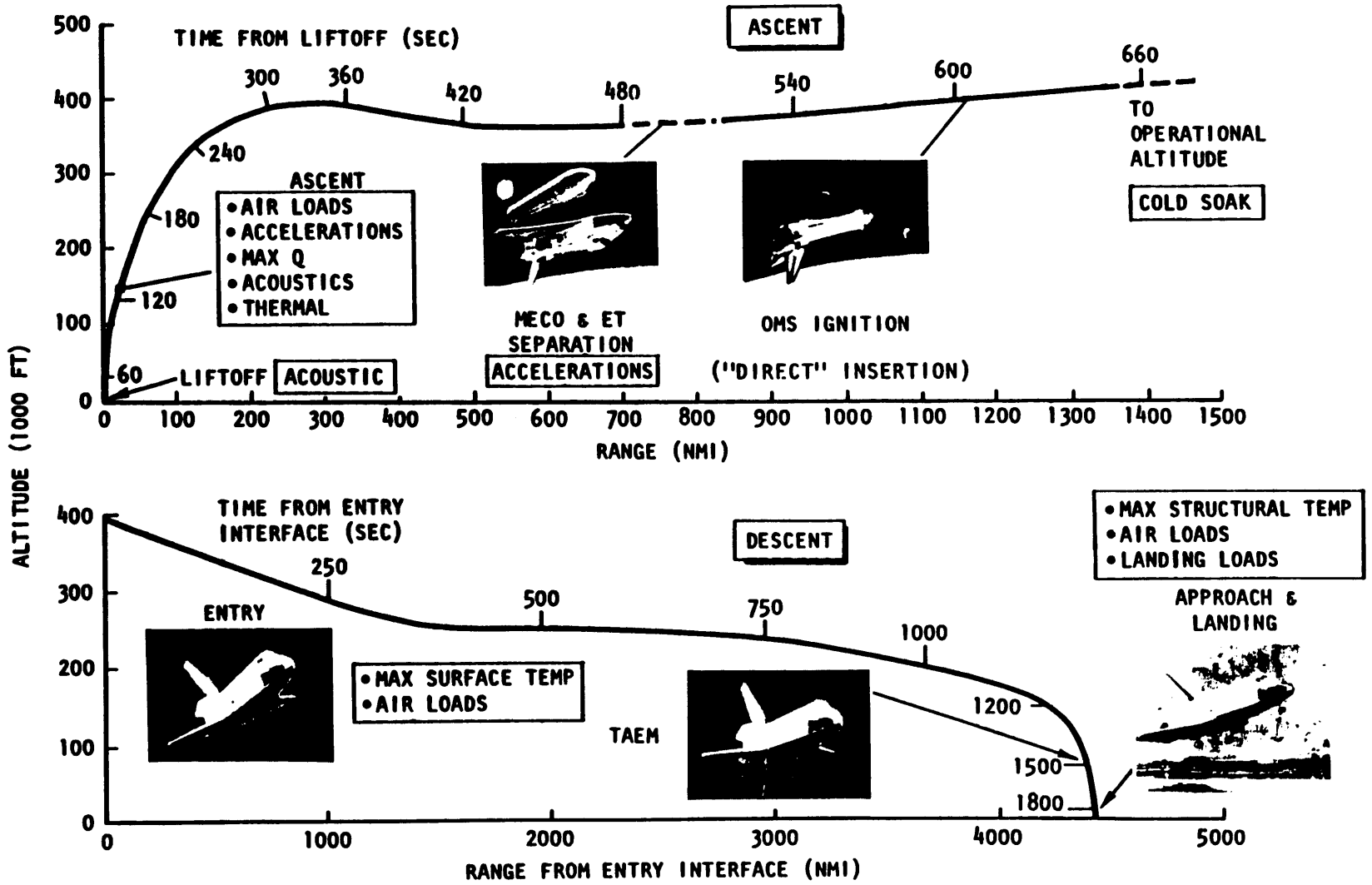

FIGURE 7-13

SPACE SHUTTLE ABORT CHARACTERISTICS

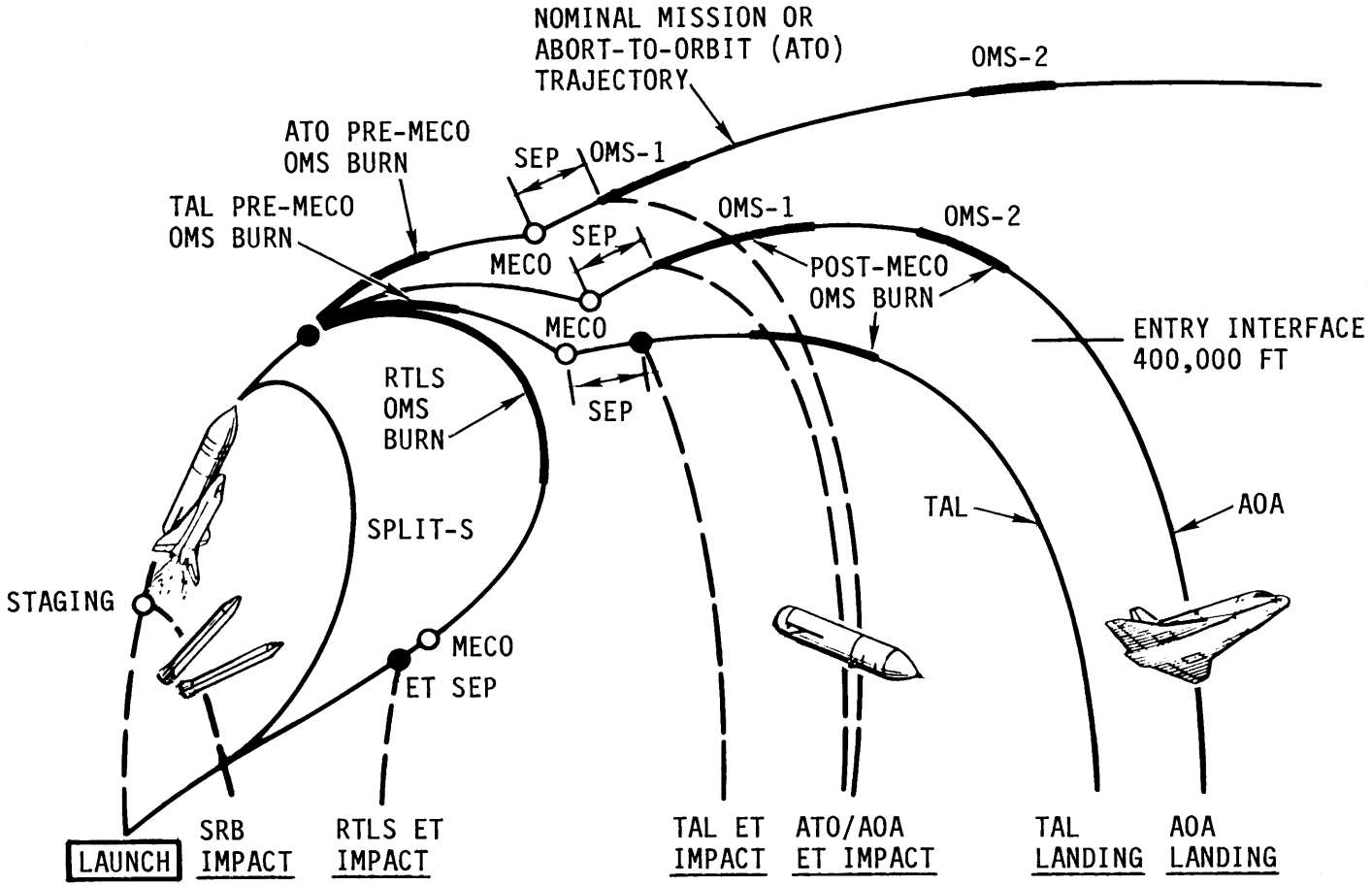

FIGURE 7-14 (DELETED)

FIGURE 7-15

ABORT MODE AVAILABILITY VS. ENGINE OUT TIME FOR TYPICAL 51.6-INCLINATION MISSION

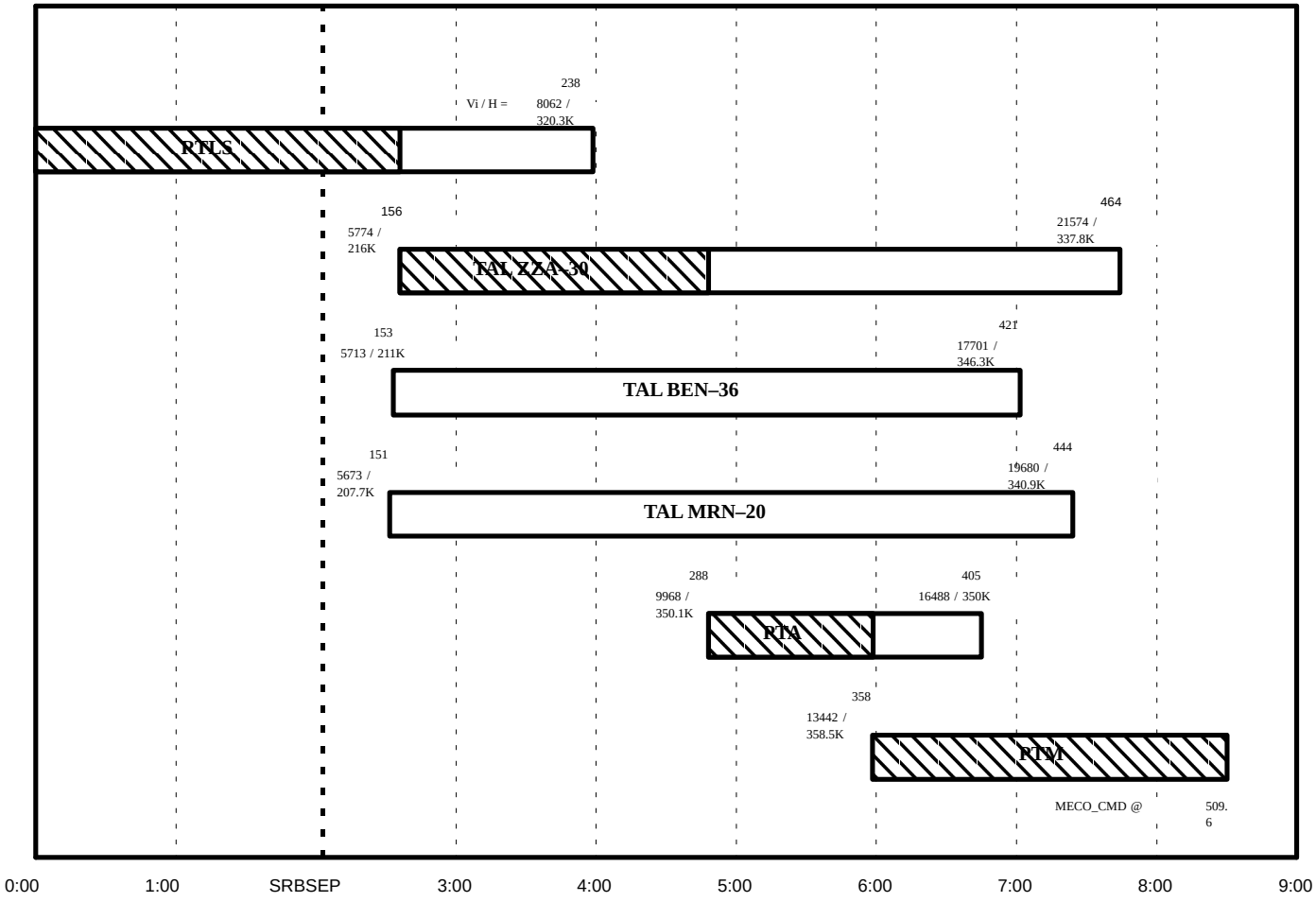

FIGURE 7-16

OMS CAPABILITY EXAMPLES

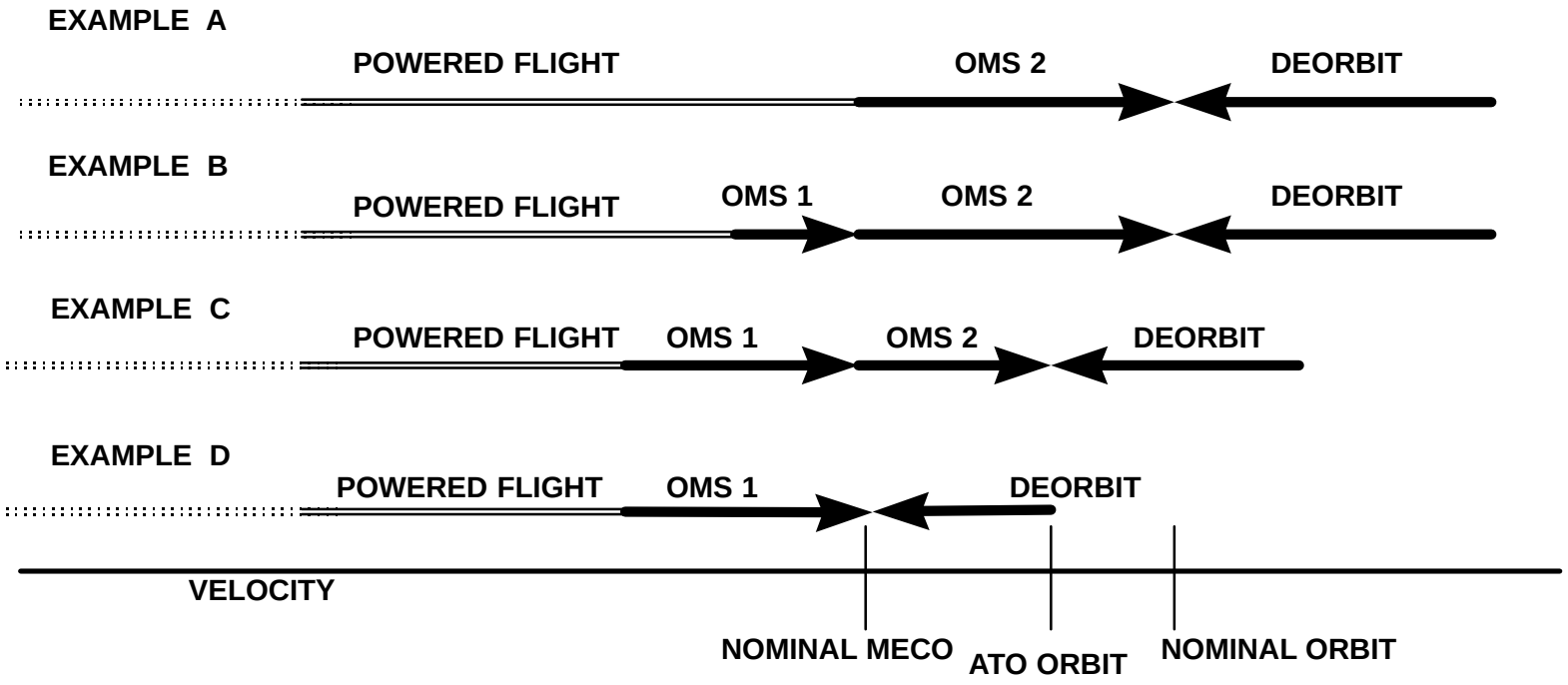

Example A: Nominal Case. There is more than enough OMS capability to achieve the nominal orbit.

Example B: PTM to MECO. With a slight underspeed at MECO, the nominal orbit can still be achieved by using all of the available OMS capability.

Example C: ATO. With a larger underspeed at MECO, there is not enough OMS capability to reach the nominal orbit, but the lower ATO orbit can be achieved.

Example D: AOA. Quick return to Earth is required. Deorbit burn on first rev.

FIGURE 7-17

TYPICAL RTLS PROFILE

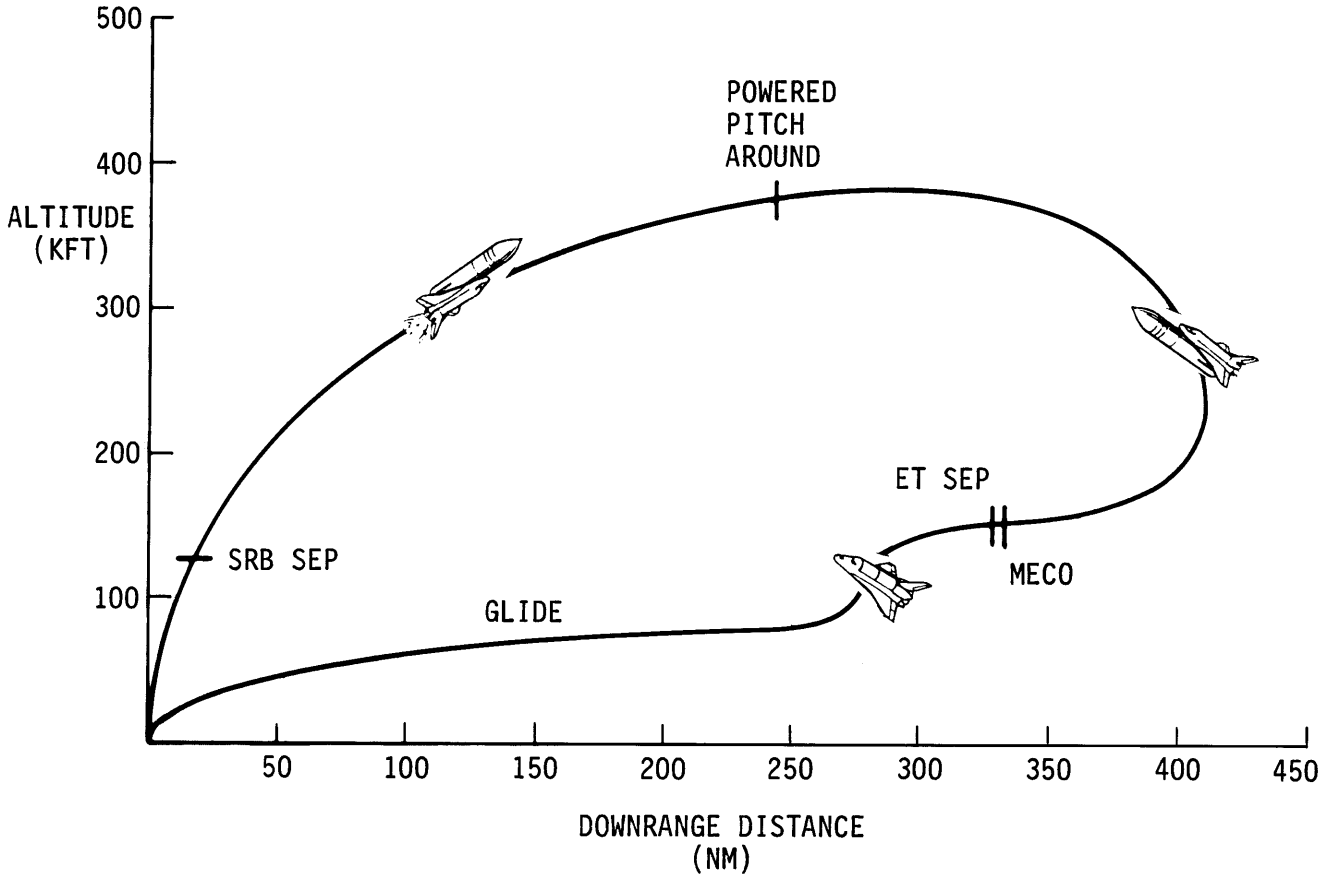

FIGURE 7-18

LAUNCH HOLD CAPABILITY

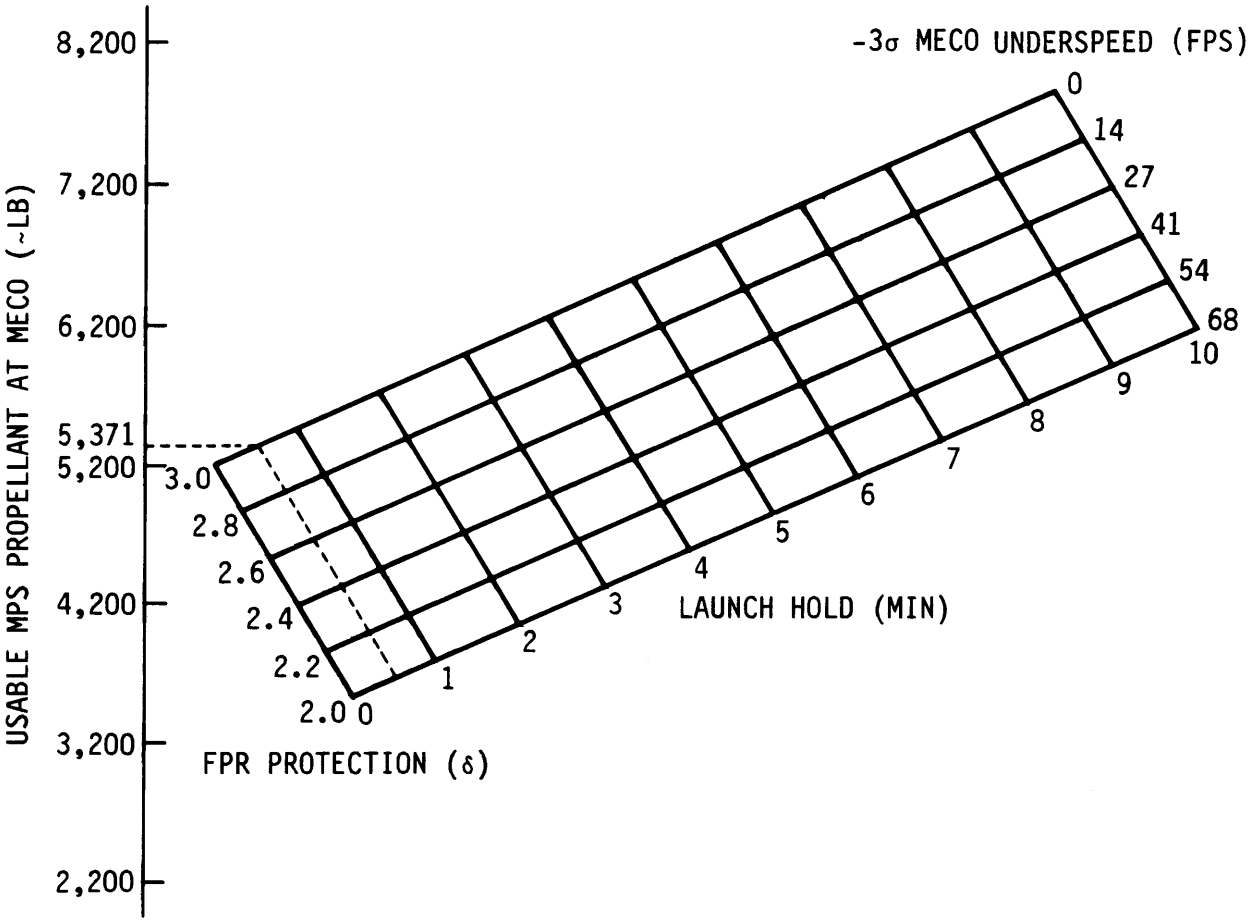

FIGURE 7-19 (DELETED)

FIGURE 7-20 (DELETED)

FIGURE 7-21 (DELETED)

FIGURE 7-22 (DELETED)

FIGURE 7-23 (DELETED)

FIGURE 7-24

ETR 28.450 DIRECT INSERTION MECO TARGET LINES

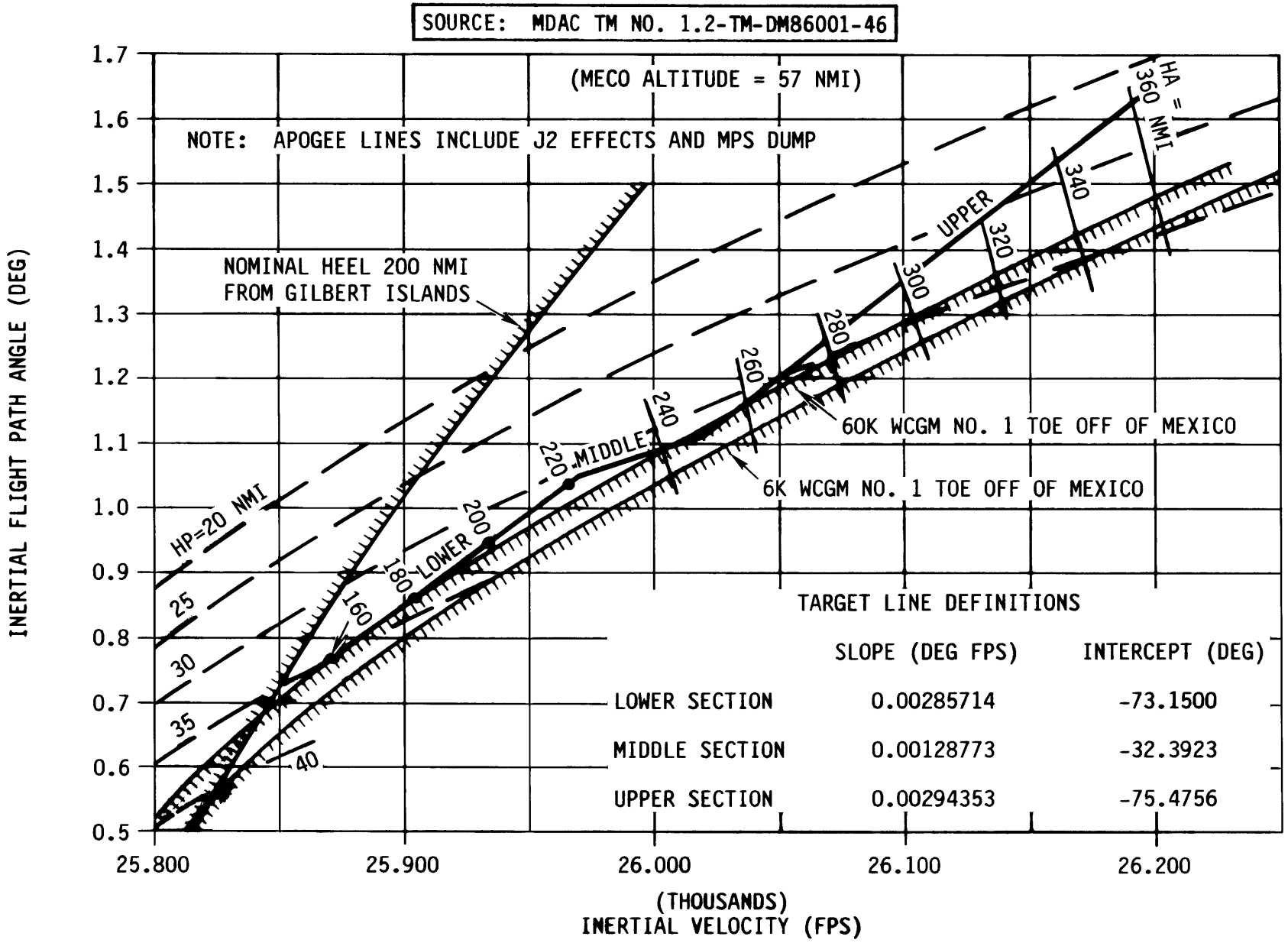

FIGURE 7-25

ETR 57.0-DEGREE INCLINATION DI TARGET LINES

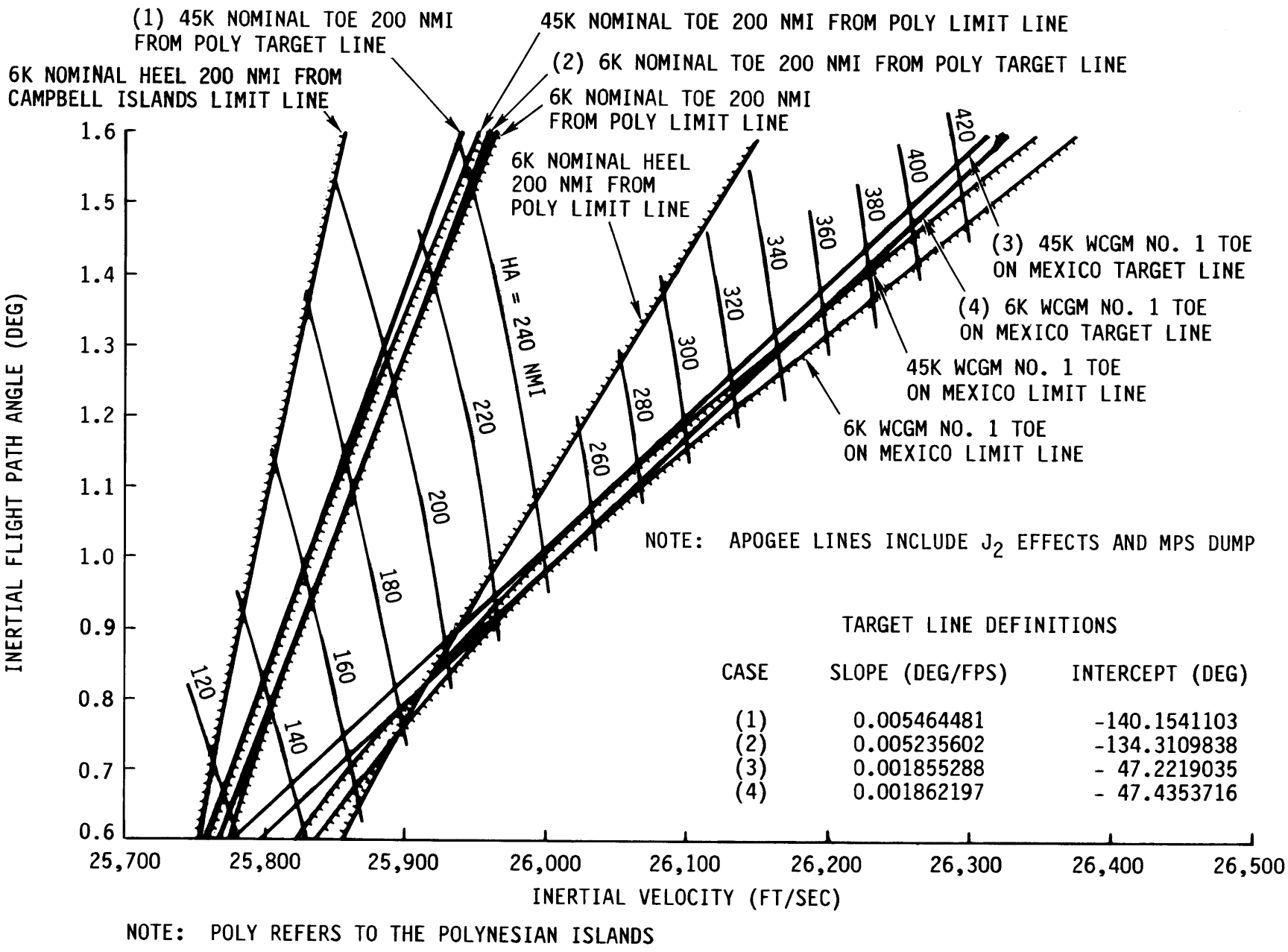

NOTE: APOGEE LINES INCLUDE J_2 EFFECTS AND MPS DUMP

TARGET LINE DEFINITIONS

CASE	SLOPE (DEG/FPS)	INTERCEPT (DEG)
(1)	0.005464481	-140.1541103
(2)	0.005235602	-134.3109838
(3)	0.001855288	- 47.2219035
(4)	0.001862197	- 47.4353716

NOTE: POLY REFERS TO THE POLYNESIAN ISLANDS

FIGURE 7-26

NOMINAL INTEGRATED DUMP TIMELINE

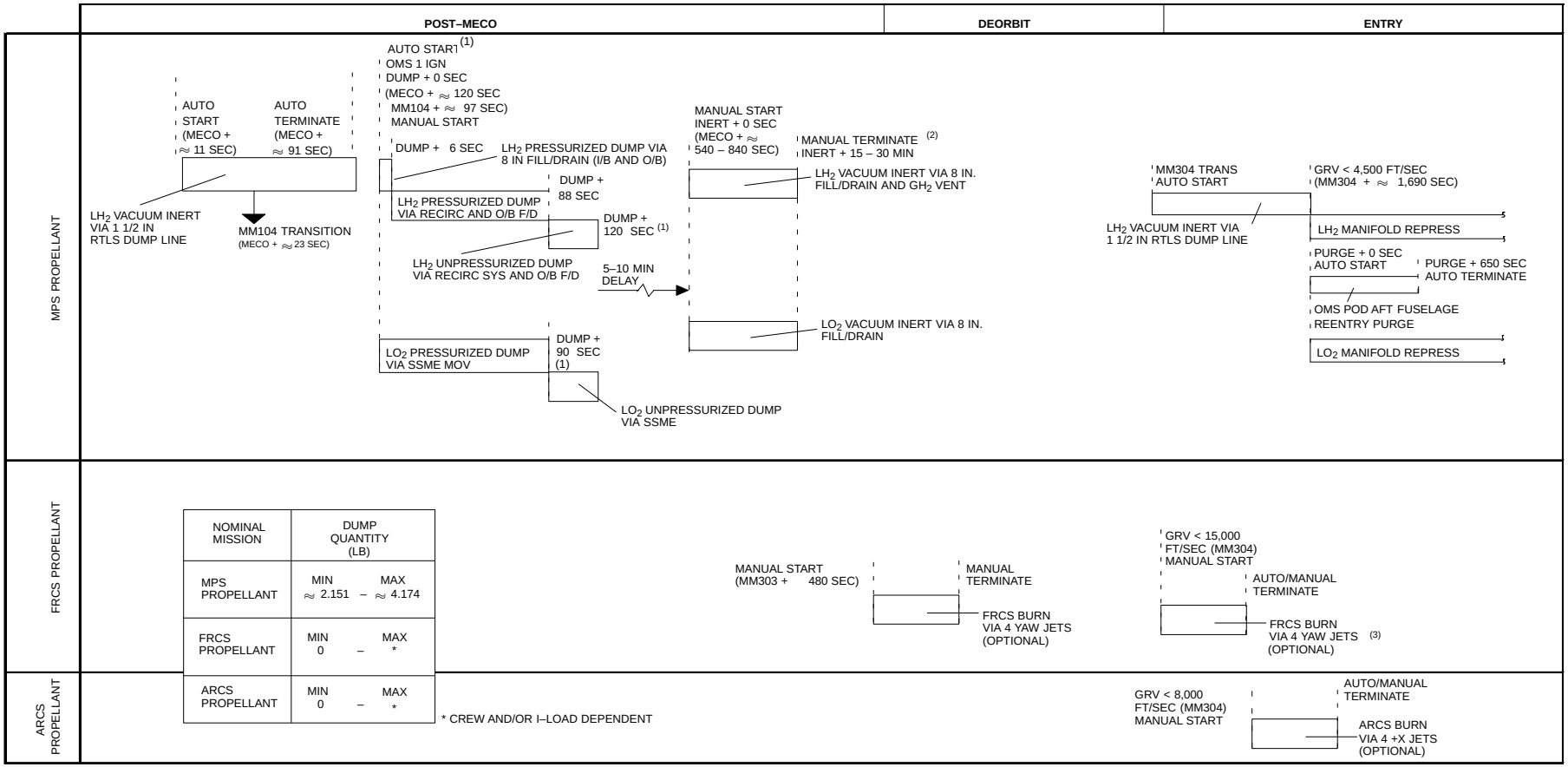

NOMINAL MISSION	DUMP QUANTITY (LB)
MPS PROPELLANT	MIN ≈ 2.151 – MAX ≈ 4.174
FRCS PROPELLANT	MIN 0 – MAX *
ARCS PROPELLANT	MIN 0 – MAX *

* CREW AND/OR I–LOAD DEPENDENT

NOTES:

(1) AUTO START AT OMS1 IGNITION FOR STANDARD INSERTION AND MANUAL START AFTER PROPELLANT SETTLING BURN FOR DIRECT INSERTION FOR MANUAL START. THE DUMP + 90 SEC EVENTS OCCUR AT DUMP + 120 SEC AND THE DUMP + 120 SEC EVENTS OCCUR AT DUMP + 140 SEC.

(2) AT THE END OF THE INERTING, THE O/B FILL/DRAIN VALVES ARE CLOSED AND THE I/B FILL/DRAIN VALVES ARE LEFT OPEN (BOTH LO_2 AND LH_2 WHEN THE LH_2 I/B FILL/DRAIN VALVE SWITCH IS RETURNED TO THE GND POSITION. THE TOPPING AND HI POINT BLEED VALVES RETURN TO THE CLOSED POSITION. THE PNEU He ISOLATION VALVES ARE SHUT TO POWER DOWN THE HELIUM SYSTEM AND COMPLETE THE MPS VACUUM INERTING.

(3) FRCS DUMP CAPABILITY EXISTS. FRCS PROPELLANT DUMP IS NOT CERTIFIED.

FIGURE 7-27

RTLS ABORT INTEGRATED DUMP TIMELINE

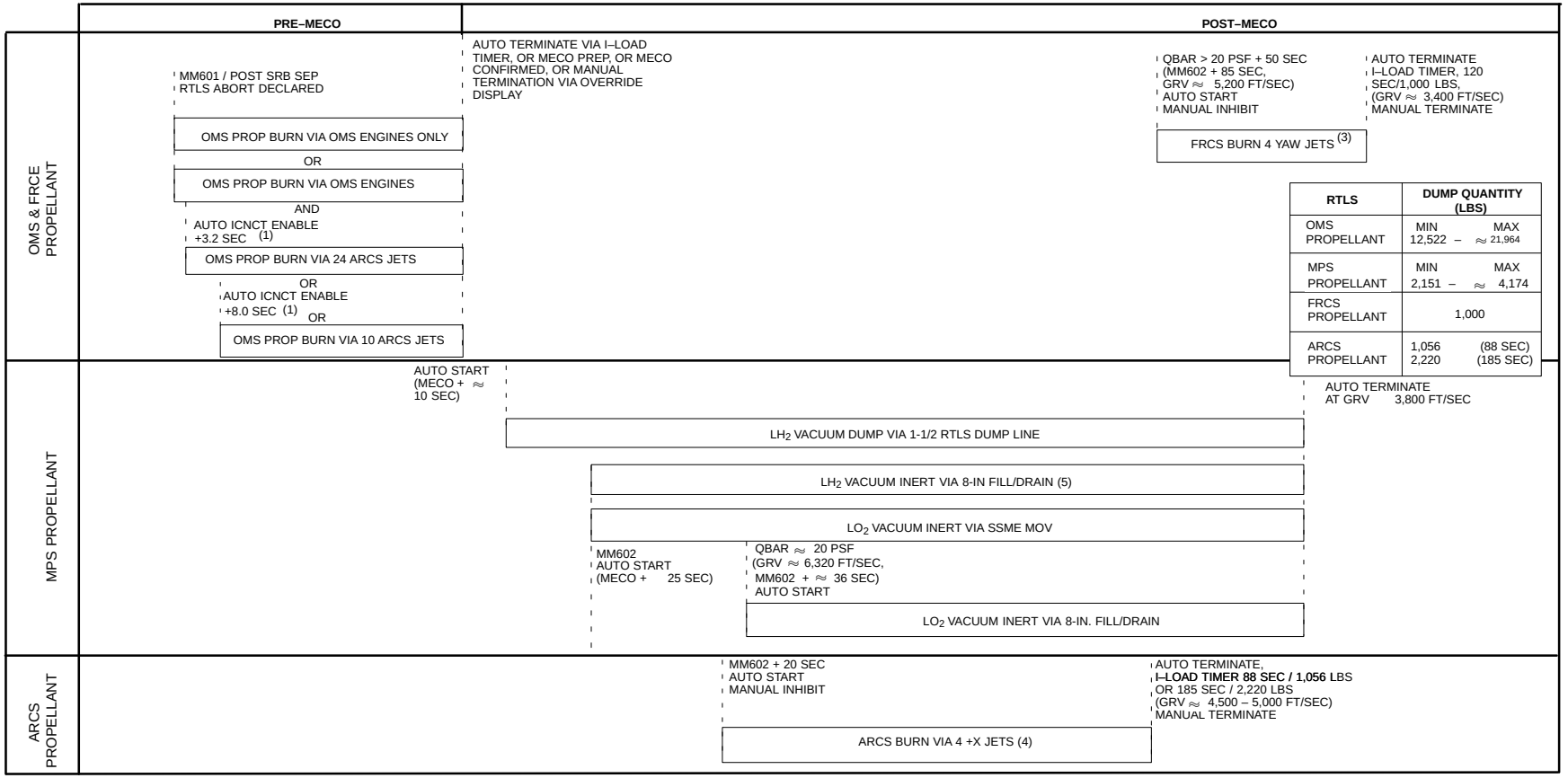

RTLS	DUMP QUANTITY (LBS)
OMS PROPELLANT	MIN 12,522 – MAX ≈ 21,964
MPS PROPELLANT	MIN 2,151 – MAX ≈ 4,174
FRCS PROPELLANT	1,000
ARCS PROPELLANT	1,056 (88 SEC) 2,220 (185 SEC)

(1) THIS DELAY IS DRIVEN BY AN I-LOAD VALUE AND THE TIME IT TAKES TO SUCCESSFULLY COMPLETE AN INTERCONNECT. THE I-LOAD WAS PREVIOUSLY SET TO 30 SECONDS. IT CURRENTLY HAS A VALUE OF 0 SECONDS. INTERCONNECT VALVE FAILURES CAN FORCE DELAY TO RANGE FROM 3.2 SECONDS TO 8.0 SECONDS.

(2) AT THE END OF THE INERTING, THE O/B FILL/DRAIN VALVES ARE CLOSED AND THE I/B FILL/DRAIN VALVES ARE LEFT OPEN (BOTH LO_2 AND LH_2 WHEN THE LH_2 I/B FILL/DRAIN VALVE SWITCH IS RETURNED TO THE GND POSITION. THE TOPPING AND HI POINT BLEED VALVES RETURN TO THE CLOSED POSITION. THE PNEU He ISOLATION VALVES ARE SHUT TO POWER DOWN THE HELIUM SYSTEM AND COMPLETE THE MPS VACUUM INERTING.

(3) FRCS DUMP IS NOT CERTIFIED FOR IMPLEMENTATION. SAME LOGIC AS ARCS DUMP EXCEPT FOUR OPPOSING SIDE FIRING JETS ARE FIRED. I-LOADED DUMP TIMER IS SIZED TO DUMP TO APPROXIMATELY 25% FRCS PROPELLANT REMAINING. SOFTWARE WILL ONLY FIRE TWO OR FOUR JETS. IF A SIDE FIRING JET IS REMOVED FROM THE JET AVAILABILITY TABLE, THE OPPOSING JET IS ALSO REMOVED.

(4) CURRENT CERTIFICATION FOR THIS DUMP CAPABILITY IS THE TIME IT TAKES TO DUMP DOWN TO 14% PVT. MOST MISSIONS ARE FLYING WITH THE I-LOAD SET TO 88 SEC. CURRENTLY THE MAXIMUM DUMP TIME IS 185 SECONDS.

(5) 8" FILL/DRAIN VALVE I-LOAD IS SET TO ZERO.

FIGURE 7–28

TAL ABORT INTEGRATED DUMP TIMELINE

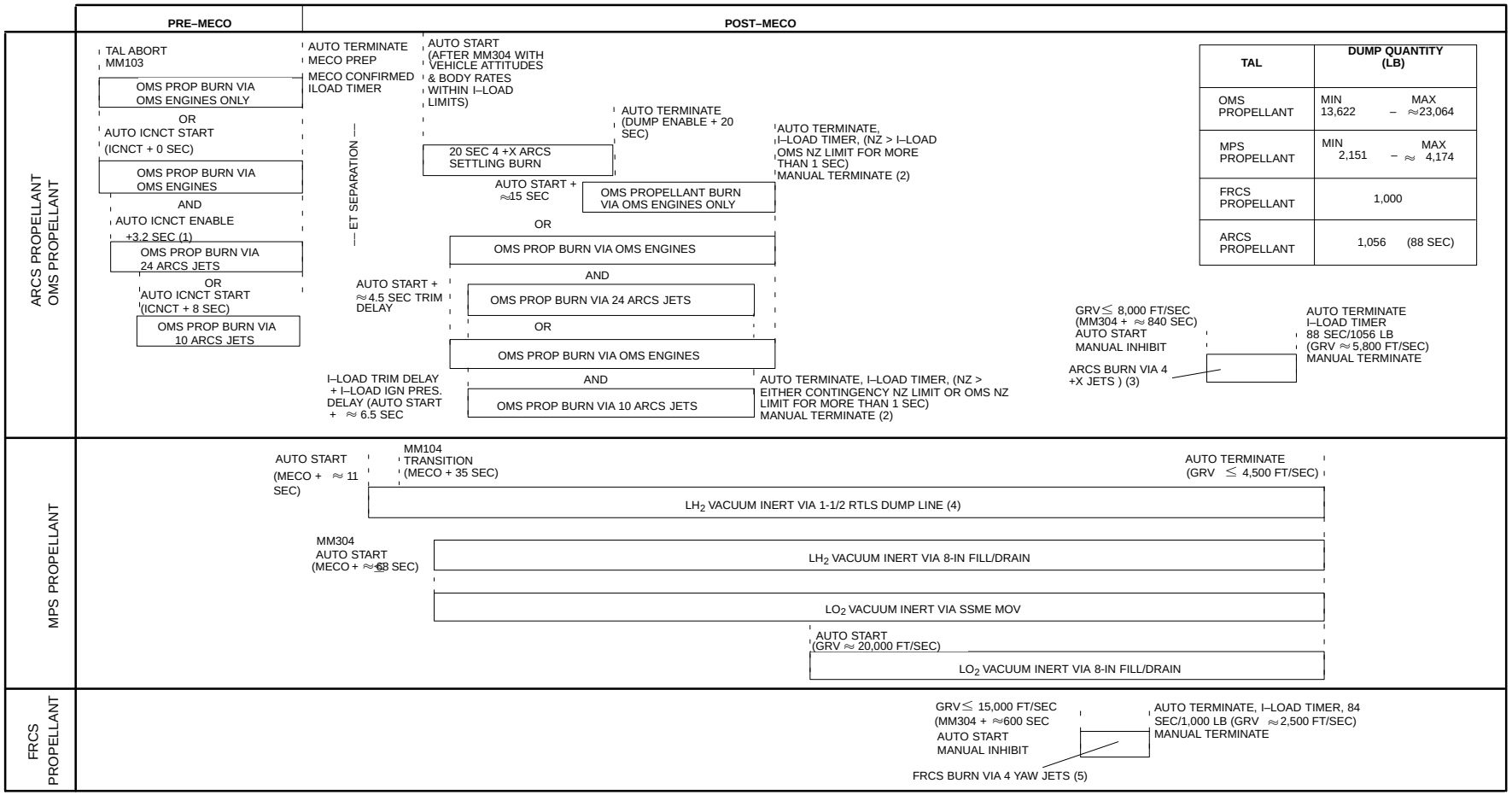

(1) THIS DELAY IS DRIVEN BY AN I-LOAD VALUE AND THE TIME IT TAKES TO SUCCESSFULLY COMPLETE AN INTERCONNECT. THE I-LOAD HAS HAD VALUES OF 30 SECONDS. IT CURRENTLY HAS A VALUE OF 0 SECONDS. INTERCONNECT VALVE FAILURES CAN FORCE DELAY TO RANGE FROM 3.2 SECONDS TO 8.0 SECONDS.

(2) OMS PROPELLANT BURN VIA 24 JETS OR 10 JETS IS MANUALLY TERMINATED WHEN OMS/RCS I/C INH/ENA COM = INH. WHEN ORBITER DUMP INHIBIT DISCRETE IS SET (EXECUTED ITEM 8 ON OVERRIDE DISPLAY), OMS PROPELLANT BURN VIA EITHER 24 OR 10 JETS AND OMS ENGINES WILL BE TERMINATED.

(3) CURRENT CERTIFICATION FOR THIS DUMP CAPABILITY IS THE TIME IT TAKES TO DUMP DOWN TO 14% PVT. MOST MISSIONS ARE FLYING WITH THE I-LOAD SET TO 88 SEC. A CURRENT PROPOSAL TO THE ABORT PANEL IS TO CAP THE DUMP TIME AT 185 SECONDS MAXIMUM.

(4) THE LH_2 VACUUM INERT VIA 1-1/2 IN RTLS DUMP LINE WILL BE CONTINUOUSLY DUMPED FROM MECO + APPROX. 10 SEC THROUGH GRV ≤ 4,500 FT/SEC.

(5) FRCS DUMP IS NOT CERTIFIED FOR IMPLEMENTATION. SAME LOGIC AS ARCS DUMP EXCEPT FOUR OPPOSING SIDE FIRING JETS ARE FIRED. I-LOADED DUMP TIMER IS SIZED TO DUMP TO APPROXIMATELY 25% FRCS PROPELLANT REMAINING. SOFTWARE WILL ONLY FIRE TWO OR FOUR JETS. IF A SIDE FIRING JET IS REMOVED FROM THE JET AVAILABILITY TABLE, THE OPPOSING JET IS ALSO REMOVED.

FIGURE 7–29

ATO ABORT INTEGRATED DUMP TIMELINE

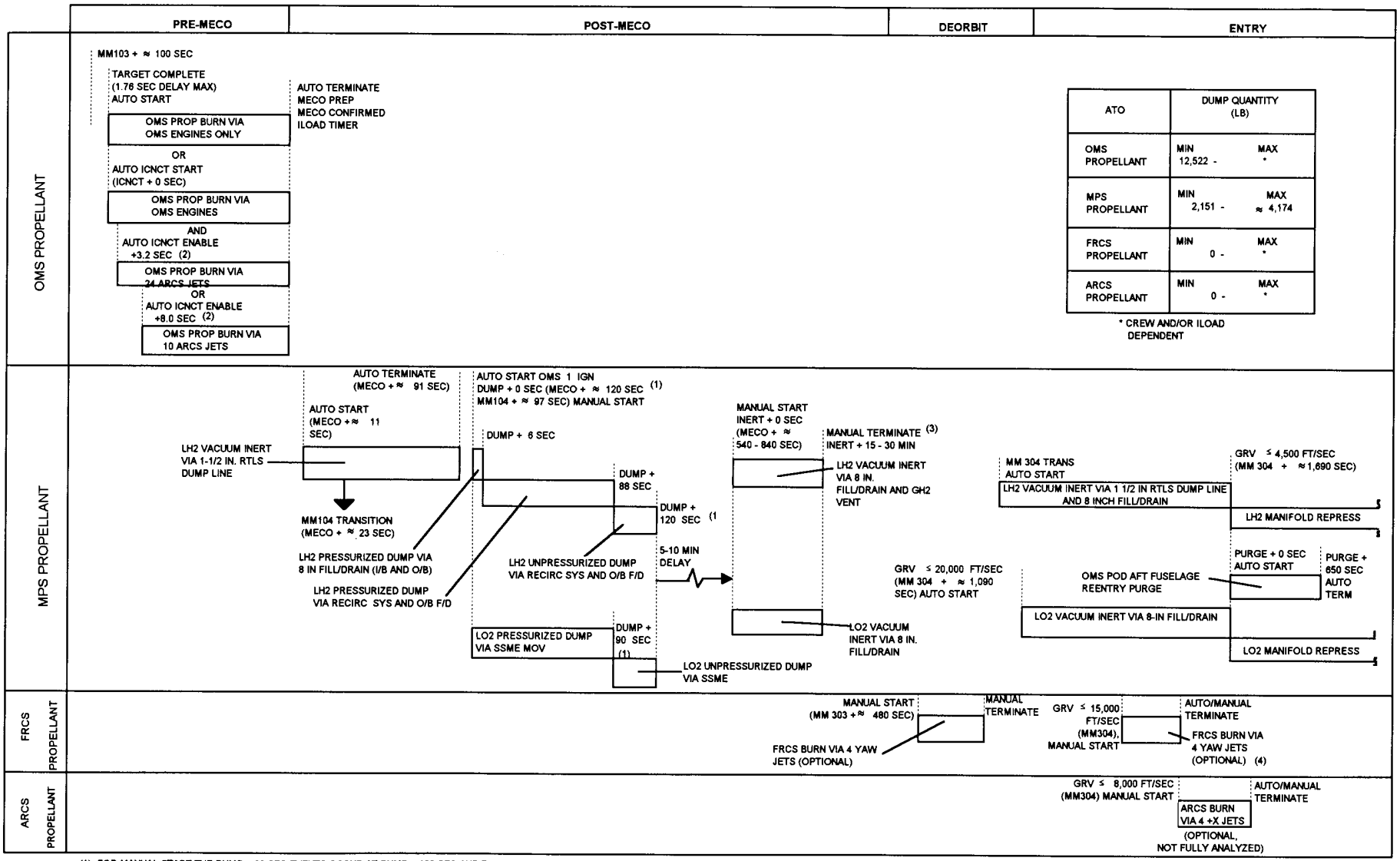

(1) FOR MANUAL START THE DUMP + 90 SEC EVENTS OCCUR AT DUMP + 120 SEC AND THE + 120 SEC EVENTS OCCUR AT DUMP + 140 SEC

(2) 30 SECONDS OF THIS DELAY IS I-LOADABLE, WITH INTERCONNECT FAILURES THIS DELAY CAN VARY FROM 34.5 SECONDS TO 37.4 SECONDS. SEE SECTION 6.2.3

(3) AT THE END OF INERTING THE OUTBOARD FILL/DRAIN VALVES ARE CLOSED AND THE I-B FILL/DRAIN VALVES ARE LEFT OPEN (BOTH O2 AND LH2) WHEN THE LH2 I/B DRAIN VALVE SWITCH IS RETURNED TO THE GND POSITION, THE TOPPING AND HI POINT BLEED VALVES RETURN TO THE CLOSED POSITION. THE PNEU He ISOLATION VALVES ARE SHUT TO POWER DOWN THE HELIUM SYSTEM AND COMPLETE THE MPS VACUUM INERTING.

(4) FRCS DUMP CAPABILITY EXISTS. FRCS PROPELLANT DUMP IS NOT CERTIFIED.

THIS PAGE INTENTIONALLY LEFT BLANK

8.0 FLIGHT PERFORMANCE RESERVE (FPR)

FPRs are the additional MPS propellants that are allocated to compensate for higher-than-nominal propellant consumption or lower-than-normal propellant loading. Their purpose is to assure with high probability that a controlled guidance MECO can be reached prior to depletion of either fuel or oxidizer. The amounts of each propellant to be reserved must be large enough to meet a specified probability requirement but must be as small as possible to maximize payload capability.

8.1 ANALYTICAL FPR

For the Space Shuttle ascent configuration, the FPR consists of propellant reserve and a fuel bias. The propellant reserve consists of LO_2 and LH_2 proportioned at the nominal MR while the fuel bias represents an additional amount of LH_2 included to reduce the chance of leaving a heavy LO_2 residual due to early fuel depletion. It is the objective of FPR analysis to determine the individual values of propellant reserve and bias which satisfy a controlled guidance MECO probability requirement and maximize useful weight at MECO. The FPR is minimized by optimizing the amount of fuel bias.

The FPR covers mean-plus-3σ ET propellant consumption (relative to propellant available) for a normal (nonabort) flight and RTLS intact abort as determined by statistically combining the individual effects of flight-to-flight vehicle systems dispersions. For TAL and ATO type intact aborts, the FPR covers 2σ high propellant consumption with one SSME failure at the worst time during ascent. The FPR is not intended to cover weight growth or any known changes in subsystems' performance. These effects must be treated as biases in the nominal performance assessments.

Assumptions related to dispersion statistics are:

a. All source dispersions are statistically independent.

b. Loading, MR, and vapor residual dispersions are assumed to be normally distributed.

c. ET propellant consumption caused by each dispersion may be linearly superimposed.

d. Dispersions affecting launch weight are subject to a fixed ratio of Δ propellant to Δ Gross Lift-off Weight (GLOW).

In terms of the usable residual propellant, R_u, defined as that propellant remaining at cutoff which could be burned at the nominal MR ϱ, the 3σ requirement for FPR is:

$$\mu_{R_u} - 3\sigma_{R_u} \geq 0$$

where μ_{R_u} is the mean for R_u and σ_{R_u} is the standard deviation for R_u

$$\text{and } \mu_{R_u} = \alpha - \mu_{X_c} - \mu_s$$

$$\sigma^2_{R_u} = \sigma^2_{X_c} + \sigma^2_s$$

where α = FPR at nominal mixture ratio

μ_{X_c}, σ_{X_c} = mean and std. deviation of X_c

μ_s, σ_s = mean and std. deviation of s

X_c = propellant consumption uncertainty due to all Class 1 dispersions

s = function containing Class 2 dispersions

NOTE: Class 1 dispersions are those which affect both ET propellants (LO_2 and LH_2) together at the nominal MR. Class 2 dispersions consist of ET loading errors, start transients, SSME MR error, and uncertainties in O_2 and H_2 vapor residuals.

The basic FPR equation for the maximum useful cutoff weight is therefore

$$\alpha = \mu_{X_c} + \mu_s + K_\sigma \left(\sigma^2_{X_c} + \sigma^2_s\right)^{\frac{1}{2}}$$

This is evaluated using the following relationships:

$$\sigma_1^2 = \frac{1}{\varrho^2}\,\sigma_{X^2_{LOX}} + \sigma^2_{X_{LH2}} + \nu^2\sigma^2_{X_\varrho} + \frac{1}{\varrho^2}\,\sigma^2_{Z_{O2}} + \sigma^2_{Z_{H2}}$$

$$\sigma_2^2 = \left(1 + \frac{1}{\varrho} - \gamma\right)^2 \sigma_{X^2_{LOX}} + \gamma^2\sigma^2_{X_{LH2}} + \nu^2\sigma^2_{X_\varrho} + \left(\frac{\varrho + 1}{\varrho}\right)^2 \sigma^2_{Z_{O2}}$$

$$\sigma_{12} = -\frac{1}{\varrho}\left(1 + \frac{1}{\varrho} - \gamma\right)\sigma^2_{X_{LOX}} - \gamma\sigma^2_{X_{LH2}} - \nu^2\sigma^2_{X_\varrho} - \left(\frac{\varrho + 1}{\varrho^2}\right)\sigma^2_{Z_{O2}}$$

$$\mu_s = (\varrho + 1)\left[\sigma_1 f_n\left(\frac{\beta}{\sigma_1}\right) - \beta\, F_n\left[\frac{-\beta}{\sigma_1}\right]\right]$$

$$\sigma_s^2 = (\varrho + 1)\left[(\varrho + 1)\,\sigma_1^2 + 2\sigma_{12}\right] F_n\left(\frac{-\beta}{\sigma_1}\right) + \sigma_2^2 - (\varrho + 1)\,\beta\mu_s - \mu_s^2$$

Here ϱ = Nominal combined engine mixture ratio $\frac{LOX}{LH_2}$

W_p = Total Usable Propellant

$$\nu = \frac{W_p}{\varrho(\varrho + 1)}$$

γ = Propellant sensitivity $\frac{\delta W_p}{\delta\ GLOW}$

β = Fuel bias $= R_{LH2} - \frac{R_{LOX}}{\varrho}$

$\sigma_{X_{LOX}}$, $\sigma_{X_{LH2}}$ = Std. deviations for LOX and LH_2 loading errors

σ_{X_ϱ} = Std. deviation for MR error

σ_{ZO2}, σ_{ZH_2} = Std. deviations for O_2, H_2 vapor residuals

$f_n(X) = \frac{1}{\sqrt{2\pi}}\, e^{-\frac{x^2}{2}}$, Std, normal PDF

$$F_n(X) = \int_{-\infty}^{x} f_n(x)\,dx, \text{ Std, normal CDF}$$

Liquid oxygen propellant is drained from the ET to the launch facility through the LO_2 overboard bleed system which is required to maintain the SSME prestart requirements. This occurs from termination of LO_2 replenish until SSME start which is nominally 4 minutes 55 seconds but may be extended up to 5 minutes more by a launch hold. The LO_2 drainback reduces usable propellant and increases the fuel bias and thus changes the guidance and LLCO probabilities. The following correction is therefore required for longer than nominal drainback or for loading updates which may be provided on the day of launch. Assuming excess LH_2 (β > o) and letting α_o represent the nominal usable residual propellant at cutoff, then

$$R_u = \alpha_o - x_c + \left(1 + \frac{1}{\varrho} - \gamma\right) x_{LOX} - \gamma\, x_{LH2} - \nu\, x_\varrho - \left(\frac{\varrho + 1}{\varrho}\right) Z_{O2}$$

$$\Delta R_u = \left(1 + \frac{1}{\varrho} - \gamma\right) \Delta L_{LOX} - \gamma\, \Delta L_{LH2}$$

where ΔL_{LOX}, ΔL_{LH2} are changes in the LO_2 and LH_2 loads, respectively.
For drainback, ΔL_{LOX} = –Rate $*$ Drainback Time.

Therefore,

$$\Delta\beta = \Delta L_{LH2} - \frac{1}{\rho}\, \Delta L_{LOX}$$

$$\Delta\alpha = \alpha\,(\beta_o + \Delta\beta) - \alpha\,(\beta)$$

The change in margin at fixed FPR σ - level is

$$\Delta M = \Delta R_u - \Delta\alpha$$

8.2 FPR COMPUTATION

The method used to calculate the FPR is diagrammed in Figure 8-1. It illustrates how dispersion effects are combined and an optimum fuel bias is determined. The propellant allocated to FPR consists of two parts: (1) the fuel bias and (2) an amount (the FPR) of fuel and oxidizer apportioned at the nominal MR to provide a given protection level against failing to reach desired MECO conditions. Both parts subtract from lift capability. As indicated in the figure, the total penalty can be minimized by proper selection of fuel bias. Reference is made in Figure 8-1 to the other tables and figures of this section and to the equations of Paragraph 8.1.

Prior to STS-26, FPR was computed from “specification” values of systems dispersions and was generally updated for each flight. For STS-27R and subsequent flights a generic (mission independent) FPR computation was baselined per PRCB Directive SR400, May 23, 1988. The systems dispersions data for this baseline were derived from reconstruction of flights STS-2 through STS-61C. The FPR database is updated periodically to reflect the best available dispersions statistics. Table 8.1 shows the currently approved dispersions and the flights on which they are based. The 3-sigma flight-derived values have been adjusted for sample size and 90% confidence level.

FPR is not necessarily based on the most current dispersion set. Planned changes to the vehicle and future expectations of changes to dispersions can be considered in

evaluating proposed FPR updates. The program can choose to retain an FPR curve if the situation warrants. In that case, the current flight-derived dispersions are documented in NSTS 08209, Volume III, Table 3.2.6-1. The tables in Volume III should be used for studies requiring dispersed trajectories. Tables 8.1 through 8.4 of this volume reflect the dispersions used to calculate the current FPR curve.

The effect of each Class 1 dispersion on the amount of MPS propellant required to achieve target MECO conditions is given in Table 8.2 for normal, earliest PTA, and latest RTLS trajectories. To select a baseline trajectory for simulation of the ± 3-sigma dispersions, 12 DOLILU II design nominal trajectories were assessed for maximum propellant consumption sensitivity to the flight derived, 6:1 dispersions. As a result, the Low Q/June/28.5° case was selected. Except for SRB burn rate and Isp, a parabolic fit to the Table 8.2 data is used to determine the mean (mu) and standard deviation (sigma) of delta-propellant-consumption due to each dispersion (see Figure 8-2). Due to the effect of adaptive guidance throttling a bi-linear fit is used for the SRB dispersions (see Figure 8-3). The resulting individual and combined delta-propellant-consumption statistics due to Class 1 dispersions (ET load, MR, and pressurant not included) are summarized in Table 8.3 for normal, PTA, and RTLS.

One item in Tables 8.2 and 8.3 is shown as applying to only one flight mode. The SSME thrust shape effect derives from comparison of reconstructions of normal three engine, 3G-limited flights against the corresponding performance using the baseline MPS model. There are no comparable data upon which to base a thrust shape allowance for engine-out flights, thus, this item is omitted for PTA and RTLS. Any effect on FPR would be minimal.

The RTLS consumption deltas are corrected for timing delay effects, which result from the high sensitivity of late RTLS propellant consumption to changes in downrange velocity at initiation of RTLS pitchback. During the 15 second abort decision delay after engine-out, a variable time elapses before PEG converges on a 2-engine, normal target solution. Convergence initiates an approximate 25° increase in thrust pitch attitude and significantly reduces the rate-of-increase of downrange velocity. Thus, more convergence delay means more propellant consumption, and conversely. In Table 8.2, the RTLS 3-sigma delta-propellant values for physical systems dispersions reflect guidance timing identical to the baseline (undispersed) trajectory. Separating the physical and timing effects yields an RTLS FPR which is independent of any particular baseline timing and thus properly generic.

A short discussion of mean dispersion effects is necessary at this point. An original spec dispersion consisted of a dispersion value (to be applied separately as a ± effect) with a mean value of zero. A flight derived dispersion, however, may have a significant non-zero mean value along with a ± dispersion value. Most of these non-zero means are now accounted for in the preflight performance predictions. In the few cases where

this is not done, it is necessary to add this separate effect into the FPR. Specifically, the mean effects (second last column of Table 8.1, excluding ET load, MR, and pressurant) of all the Class 1 flight-derived dispersions are simultaneously modeled in a single trajectory, with the propellant-consumption results identified as "effect of Class 1 means" in the second last line of Table 8.3. The ± dispersion effects (last column of Table 8.1, excluding ET load, MR, and pressurant) are then modeled individually, often resulting in small non-zero mean effects due to unsymmetrical trajectory modeling characteristics, and combined statistical mean and dispersed propellant-consumption values are calculated. This mean effect is shown as "combined ± effects" in the third last line of Table 8.3. The two sets of mean effects are summed in the last line of Table 8.3, and together with the 1-sigma dispersion effects from the ± dispersions, form the total Class 1 dispersion statistics results.

The effect of Class 2 dispersions is evaluated using the formulas given in Paragraph 8.1. Any small flight-derived mean values indicated in Table 8.1 for SSME MR or pressurant are ignored in FPR calculations because scheduled updates to the MPS inventory will eliminate them. Table 8.4 shows the 1-sigma dispersions and other necessary parameter values. Values for nominal usable propellant and OBMR are taken from the appropriate case from the Revision 00 series of MPS Propellant Inventories; the FPR calculation is quite insensitive to small changes in these nominal values. The MPS loading uncertainties derived by Martin Marietta Corporation (MMC) assume that the loading sequence is normal (i.e. not interrupted) and that a DOL propellant density update is available from the PLOAD processor. PLOAD uses LH_2 and LO_2 ullage pressure measurements for this purpose. If the measurements are not available or their accuracy is degraded in any way, the loading uncertainty increases. The case of no PLOAD update represents the maximum increase and covers any other case. The no PLOAD (also from MMC analysis) are given in Table 8.1 (percent) and at the bottom of Table 8.4 (pounds) and FPR calculations are provided for both sets of loading uncertainties.

The final resulting FPR, fuel bias plus FPR, and mean and standard deviation of the Class 2 dispersions effects are tabulated as functions of fuel bias in a series of tables. The key below has grouped these tables by ET type and whether or not the PLOAD program was used. Each group has three (3) tables, to cover the normal, PTA, and the RTLS cases. Each table contains the appropriate FPR sigma level and repeats the Class 1 mean and standard deviation from Table 8.3. On each table, scanning the FPR-Plus-Bias column for a minimum reveals the near-optimum fuel bias. For each ET/SSME combination, there is a plot of data from the normal mission, w/PLOAD table. In each case, this figure is labeled the Optimum FB Figure. It can be seen from any of these figures that the FPR-plus-bias performance penalty varies little within a couple of hundred pounds of the optimum bias.

ET Type	w/PLOAD	wo/PLOAD	Optimum FB Figure
LWT or SLWT	Table 8.5 to 8.7	Table 8.8 to 8.10	Figure 8-4

Additional information on FPR analysis methods and guidelines is provided in IL FSD&P/MAI-80-822, Deterministic Reserve; IL FSD&P/MAI-80-354, ARD FPR Briefing for the Ascent Flight Techniques Panel; IL FSD&P/MAI-80-351, Propellant Reserve for Inflight Margin Prediction by the ARD; IL FSD&P/MAI-80-350, Documentation of Ascent Flight Performance Reserve Methods; and IL FSD&P/MAI-80-157, FPR Probability Comparison.

8.3 (DELETED)

THIS PAGE INTENTIONALLY LEFT BLANK

TABLE 8.1

SYSTEM DISPERSIONS FOR FPR COMPUTATION

Dispersion	Units	Mean	Database[1] (N=)	3σ (90% Conf)	Class
SRB Burn Rate [2]	(mils)	0	STS-57 to STS-106 (N=43)[5]	3.767	I
SRB Isp [2]	(lb_f - sec/lb_m)	0.05	STS-67 to STS-106 (N=30)[6]	1.4400	I
Delta PMBT	(deg)	0.36	STS-26R to STS-106 (N=74)	4.52	I
SSME Thrust [3]	(lb_f)	0	STS-64 to STS-106 (N=34)[6]	4,691	I
SSME Isp [3]	(lb_f - sec/lb_m)	0	STS-64 to STS-106 (N=34)[6]	0.819	I
SSME Thrust Shape [3]	(lb_m)	–29	STS-64 to STS-106 (N=34)[6]	182	I
SSME Mixture Ratio	(MRUs)	0	STS-64 to STS-106 (N=34)[6]	0.023406	II
ORB/ET Inert Weight	(lb_m)	0	STS-79 to STS-106 (N=20)[7]	1,925	I
LO_2 Load, with/ without PLOAD	(%) LWT SLWT	 0 0	Lockheed-Martin Analysis	 0.29/0.37 0.30/0.38	II
LH_2 Load, with/ without PLOAD	(%) LWT SLWT	 0 0	STS-26R to STS-106 (Excludes DoD Flts) (N=68)	 0.40/0.40 0.40/0.40	II
LO_2 Start Transient [4]	(lb_m)	0	STS-26R to STS-106 (N=72)[6]	94.63	II
LH_2 Start Transient [4]	(lb_m)	0	STS-26R to STS-106 (N=73)[7]	43.10	II
GO_2 Pressurant	(lb_m)	0	STS-40 to STS-106 (N=59)	148.17	II
GH_2 Pressurant	(lb_m)	0	STS-26R to STS-106 (N=73)[8]	64.31	II
Collectors	-	F(t)	STS-67 to STS-106 (N=30)[6]	F(t)	I
Timing Delay [9]	–	N/A	–	N/A	I

[1] Flight derived, reconstructed minus predicted values. Flights in chronological order.
[2] Average of left and right SRM.
[3] Cluster of three engines
[4] Start transient dispersion is RSS'd with loading dispersion to obtain dispersion in load at T_o
[5] Database excludes STS-61 only
[6] Database excludes STS-78 and STS-93
[7] Database excludes STS-93 only
[8] Database excludes STS-30R only
[9] Timing delay applicable to RTLS mode only

TABLE 8.2

EFFECT OF 3σ CLASS 1 (6:1) DISPERSIONS ON PROPELLANT (lb_m) REQUIRED TO REACH MECO

Dispersion	+NOR	−NOR	+PTA	−PTA	+RTLS	−RTLS
SRB Burn Rate LWT and SLWT	−561	1,076	−491	708	413	170
SRB Isp LWT and SLWT	−892	958	−849	747	−572	598
PMBT LWT and SLWT	−344	400	−282	318	−11	102
SSME Thrust LWT and SLWT	−348	370	−914	854	−1,219	1,219
SSME Isp LWT and SLWT	−956	962	−945	943	−624	730
SSME Thrust Shape LWT and SLWT	182	−182	182	−182	182	−182
ORB/ET Inert Weight LWT and SLWT	1,792	−1,775	1,953	−1,921	2,034	−1,912
Six Collectors LWT and SLWT	666	−666	434	−434	654	−654

TABLE 8.3

PROCESSED CLASS 1 (6:1) PROPELLANT CONSUMPTION DISPERSIONS (lb_m)

	NOR		PTA		RTLS	
	μ	σ	μ	σ	μ	σ
SRB Burn Rate LWT and SLWT	68.5	277.7	28.9	201.0	77.5	71.2
SRB Isp LWT and SLWT	8.8	308.4	−13.6	266.2	3.5	195.0
Delta PMBT LWT and SLWT	7.5	124.1	4.8	100.1	12.1	20.9
SSME Thrust LWT and SLWT	1.2	119.7	−3.3	294.7	0.0	406.3
SSME Isp LWT and SLWT	0.4	319.7	−0.1	314.7	5.9	225.8
SSME Thrust Shape LWT and SLWT	0.0	60.7	0.0	60.7	0.0	60.7
ORB/ET Inert Weight LWT and SLWT	1.0	594.5	1.8	645.7	6.8	657.7
Six Collectors LWT and SLWT	39.6	222.0	239.0	144.7	34.0	218.0
Combined ± Effects LWT and SLWT	127.0	843.0	257.5	865.3	139.8	862.2
Effect of Class 1 Means LWT and SLWT	−58.0		−49.0		−2.0	
Total μ_{xc}, σ_{xc} LWT and SLWT	69.0	843.0	208.5	865.3	137.8	862.2

Numbers reflect reference fuel biases of: 876 lb_m, NOR; 833 lb_m, PTA; 912 lb_m, RTLS

TABLE 8.4

CLASS 2 (NON 6:1) DISPERSIONS AND AUXILIARY DATA FOR FPR COMPUTATION

	NOR	PTA	RTLS
LO_2 Load at T_0, 1σ (lb_m) [4] (LWT, w PLOAD/wo PLOAD) (SLWT, w PLOAD/wo PLOAD)	 1,376/1,742 1,376/1,742	 1,376/1,742 1,376/1,742	 1,376/1,742 1,376/1,742
LH_2 Load at T_0, 1σ (lb_m) [4] (LWT, w PLOAD/wo PLOAD) (SLWT, w PLOAD/wo PLOAD)	 309/309 309/309	 309/309 309/309	 309/309 309/309
OBMR 1σ (MRU)	0.0078	0.008819	0.008714
GO_2 Pressurant 1σ (lb_m)	49.4	49.4	49.4
GH_2 Pressurant 1σ (lb_m)	21.4	21.4	21.4
Nom. MPS Usable at OBMR (lb_m) [5]	1,590,516	1,589,340	1,587,832
Nom. OBMR (MRU) [5]	6.0543	6.0551	6.0545
Gamma	0.926	1.006	1.02
FPR σ Level	3	2	3

[4] Includes start transient uncertainty

[5] Revision 0004S Propellant Inventories

TABLE 8.5

NORMAL TRAJECTORY FPR FOR NOMINAL DOL (LWT AND SLWT)

3σ FPR

Weights in pounds-mass

Mean X_c = 69 Sigma X_c = 843

Fuel Bias	FPR	FPR + Bias	Mean S	Sigma S
0	6770	6770	1356	1570
50	6323	6373	1187	1464
100	5899	5999	1032	1359
150	5500	5650	892	1257
200	5131	5331	766	1158
250	4793	5043	653	1064
300	4488	4788	552	975
350	4218	4568	464	893
400	3982	4382	387	819
450	3781	4231	320	753
500	3612	4112	263	696
550	3473	4023	215	648
600	3361	3961	174	608
650	3273	3923	139	578
700	3206	3906	111	554
750	3155	3905	87	537
800	3118	3918	68	526
850	3092	3942	53	519
900	3074	3974	41	516
950	3062	4012	31	514
1000	3054	4054	23	514
1050	3050	4100	18	515
1100	3047	4147	13	516
1150	3046	4196	10	518
1200	3046	4246	7	519
1250	3047	4297	5	521
1300	3047	4347	4	522
1350	3048	4398	3	523
1400	3049	4449	2	524
1450	3049	4499	1	525
1500	3050	4550	1	526
1550	3050	4600	1	526
1600	3051	4651	0	526
1650	3051	4701	0	527
1700	3051	4751	0	527
1750	3051	4801	0	527
1800	3051	4851	0	527
1850	3051	4901	0	527
1900	3051	4951	0	527
1950	3051	5001	0	527
2000	3051	5051	0	527

TABLE 8.6

PTA TRAJECTORY FPR FOR NOMINAL DOL (LWT AND SLWT)

2σ FPR

Weights in pounds-mass

Mean X_c = 208 Sigma X_c = 865

Fuel Bias	FPR	FPR + Bias	Mean S	Sigma S
0	5396	5396	1422	1672
50	5036	5086	1253	1564
100	4695	4795	1097	1457
150	4375	4525	955	1353
200	4076	4276	827	1251
250	3802	4052	711	1153
300	3552	3852	607	1059
350	3327	3677	516	972
400	3128	3528	435	891
450	2954	3404	364	818
500	2804	3304	303	752
550	2678	3228	250	695
600	2573	3173	205	646
650	2487	3137	167	605
700	2418	3118	135	572
750	2364	3114	108	547
800	2322	3122	86	528
850	2290	3140	68	515
900	2266	3166	53	506
950	2248	3198	41	500
1000	2236	3236	32	497
1050	2227	3277	24	495
1100	2221	3321	19	495
1150	2217	3367	14	496
1200	2215	3415	10	497
1250	2213	3463	8	498
1300	2212	3512	6	499
1350	2212	3562	4	501
1400	2212	3612	3	502
1450	2212	3662	2	502
1500	2212	3712	2	503
1550	2212	3762	1	504
1600	2212	3812	1	504
1650	2212	3862	1	505
1700	2212	3912	0	505
1750	2212	3962	0	505
1800	2212	4012	0	505
1850	2212	4062	0	505
1900	2212	4112	0	505
1950	2213	4163	0	505
2000	2213	4213	0	505

TABLE 8.7

RTLS TRAJECTORY FPR FOR NOMINAL DOL (LWT AND SLWT)

3σ FPR

Weights in pounds-mass

Mean X_c = 138 Sigma X_c = 862

Fuel Bias	FPR	FPR + Bias	Mean S	Sigma S
0	7185	7185	1414	1668
50	6730	6780	1245	1560
100	6296	6396	1090	1453
150	5886	6036	948	1348
200	5502	5702	820	1246
250	5147	5397	704	1147
300	4824	5124	601	1054
350	4533	4883	510	966
400	4275	4675	429	885
450	4050	4500	359	812
500	3857	4357	298	746
550	3694	4244	246	688
600	3559	4159	201	639
650	3450	4100	164	599
700	3364	4064	132	566
750	3296	4046	106	540
800	3244	4044	84	521
850	3206	4056	66	508
900	3177	4077	52	498
950	3157	4107	40	493
1000	3143	4143	31	490
1050	3134	4184	24	488
1100	3128	4228	18	488
1150	3124	4274	13	488
1200	3122	4322	10	489
1250	3121	4371	7	491
1300	3121	4421	5	492
1350	3121	4471	4	493
1400	3121	4521	3	494
1450	3122	4572	2	495
1500	3122	4622	1	495
1550	3123	4673	1	496
1600	3123	4723	1	496
1650	3123	4773	0	497
1700	3123	4823	0	497
1750	3124	4874	0	497
1800	3124	4924	0	497
1850	3124	4974	0	497
1900	3124	5024	0	497
1950	3124	5074	0	497
2000	3124	5124	0	497

TABLE 8.8

NORMAL TRAJECTORY FPR WITHOUT PLOAD (LWT AND SLWT)

3σ FPR

Weights in pounds-mass

Mean X_c= 69 Sigma X_c = 843

Fuel Bias	FPR	FPR + Bias	Mean S	Sigma S
0	7085	7085	1444	1655
50	6637	6687	1274	1550
100	6209	6309	1118	1446
150	5806	5956	976	1345
200	5429	5629	847	1246
250	5082	5332	730	1152
300	4766	5066	626	1063
350	4482	4832	533	981
400	4231	4631	451	905
450	4012	4462	379	837
500	3826	4326	316	778
550	3669	4219	262	726
600	3541	4141	216	684
650	3437	4087	177	649
700	3355	4055	143	622
750	3292	4042	116	602
800	3244	4044	93	588
850	3209	4059	73	578
900	3184	4084	58	573
950	3166	4116	45	570
1000	3155	4155	35	569
1050	3147	4197	27	569
1100	3143	4243	21	571
1150	3141	4291	16	572
1200	3140	4340	12	574
1250	3141	4391	9	576
1300	3141	4441	7	578
1350	3142	4492	5	579
1400	3143	4543	3	581
1450	3144	4594	3	582
1500	3145	4645	2	583
1550	3146	4696	1	583
1600	3146	4746	1	584
1650	3147	4797	1	585
1700	3147	4847	0	585
1750	3147	4897	0	585
1800	3148	4948	0	585
1850	3148	4998	0	585
1900	3148	5048	0	586
1950	3148	5098	0	586
2000	3148	5148	0	586

TABLE 8.9

PTA TRAJECTORY FPR WITHOUT PLOAD (LWT AND SLWT)

2σ FPR

Weights in pounds-mass

Mean X_c = 208 Sigma X_c = 865

Fuel Bias	FPR	FPR + Bias	Mean S	Sigma S
0	5659	5659	1506	1772
50	5297	5347	1337	1664
100	4952	5052	1180	1557
150	4625	4775	1036	1452
200	4319	4519	905	1349
250	4035	4285	786	1250
300	3774	4074	679	1155
350	3537	3887	583	1066
400	3323	3723	497	982
450	3134	3584	422	905
500	2969	3469	356	835
550	2826	3376	298	772
600	2705	3305	248	718
650	2604	3254	206	671
700	2520	3220	169	632
750	2453	3203	138	601
800	2399	3199	112	576
850	2357	3207	90	557
900	2324	3224	72	544
950	2300	3250	57	534
1000	2281	3281	45	528
1050	2268	3318	35	525
1100	2258	3358	28	523
1150	2251	3401	21	523
1200	2247	3447	16	523
1250	2244	3494	12	524
1300	2242	3542	9	525
1350	2241	3591	7	526
1400	2240	3640	5	527
1450	2240	3690	4	528
1500	2240	3740	3	529
1550	2240	3790	2	530
1600	2240	3840	1	531
1650	2240	3890	1	531
1700	2241	3941	1	532
1750	2241	3991	1	532
1800	2241	4041	0	533
1850	2241	4091	0	533
1900	2241	4141	0	533
1950	2241	4191	0	533
2000	2241	4241	0	533

TABLE 8.10

RTLS TRAJECTORY FPR WITHOUT PLOAD (LWT AND SLWT)

3σ FPR

Weights in pounds-mass

Mean X_c = 138 Sigma X_c = 862

Fuel Bias	FPR	FPR + Bias	Mean S	Sigma S
0	7549	7549	1499	1772
50	7090	7140	1329	1664
100	6649	6749	1173	1557
150	6230	6380	1029	1451
200	5836	6036	898	1348
250	5468	5718	779	1248
300	5129	5429	673	1153
350	4820	5170	577	1063
400	4542	4942	492	978
450	4295	4745	417	900
500	4079	4579	351	830
550	3893	4443	294	767
600	3736	4336	245	711
650	3605	4255	202	664
700	3498	4198	166	625
750	3412	4162	135	593
800	3344	4144	110	567
850	3291	4141	88	548
900	3251	4151	70	534
950	3221	4171	56	524
1000	3199	4199	44	518
1050	3184	4234	34	514
1100	3173	4273	27	512
1150	3166	4316	21	512
1200	3161	4362	16	512
1250	3159	4409	12	512
1300	3157	4457	9	513
1350	3157	4507	7	514
1400	3157	4557	5	516
1450	3157	4607	4	517
1500	3157	4657	3	517
1550	3158	4708	2	518
1600	3158	4758	1	519
1650	3159	4809	1	519
1700	3159	4859	1	520
1750	3159	4909	1	520
1800	3159	4959	0	520
1850	3160	5010	0	521
1900	3160	5060	0	521
1950	3160	5110	0	521
2000	3160	5160	0	521

TABLE 8.11 (DELETED)

TABLE 8.12 (DELETED)

TABLE 8.13 (DELETED)

TABLE 8.14 (DELETED)

TABLE 8.15 (DELETED)

TABLE 8.16 (DELETED)

TABLE 8.17 (DELETED)

TABLE 8.18 (DELETED)

TABLE 8.19 (DELETED)

TABLE 8.20 (DELETED)

TABLE 8.21 (DELETED)

TABLE 8.22 (DELETED)

TABLE 8.23 (DELETED)

TABLE 8.24 (DELETED)

TABLE 8.25 (DELETED)

TABLE 8.26 (DELETED)

TABLE 8.27 (DELETED)

TABLE 8.28 (DELETED)

THIS PAGE INTENTIONALLY LEFT BLANK

FIGURE 8-1

STEPS IN FPR CALCULATION

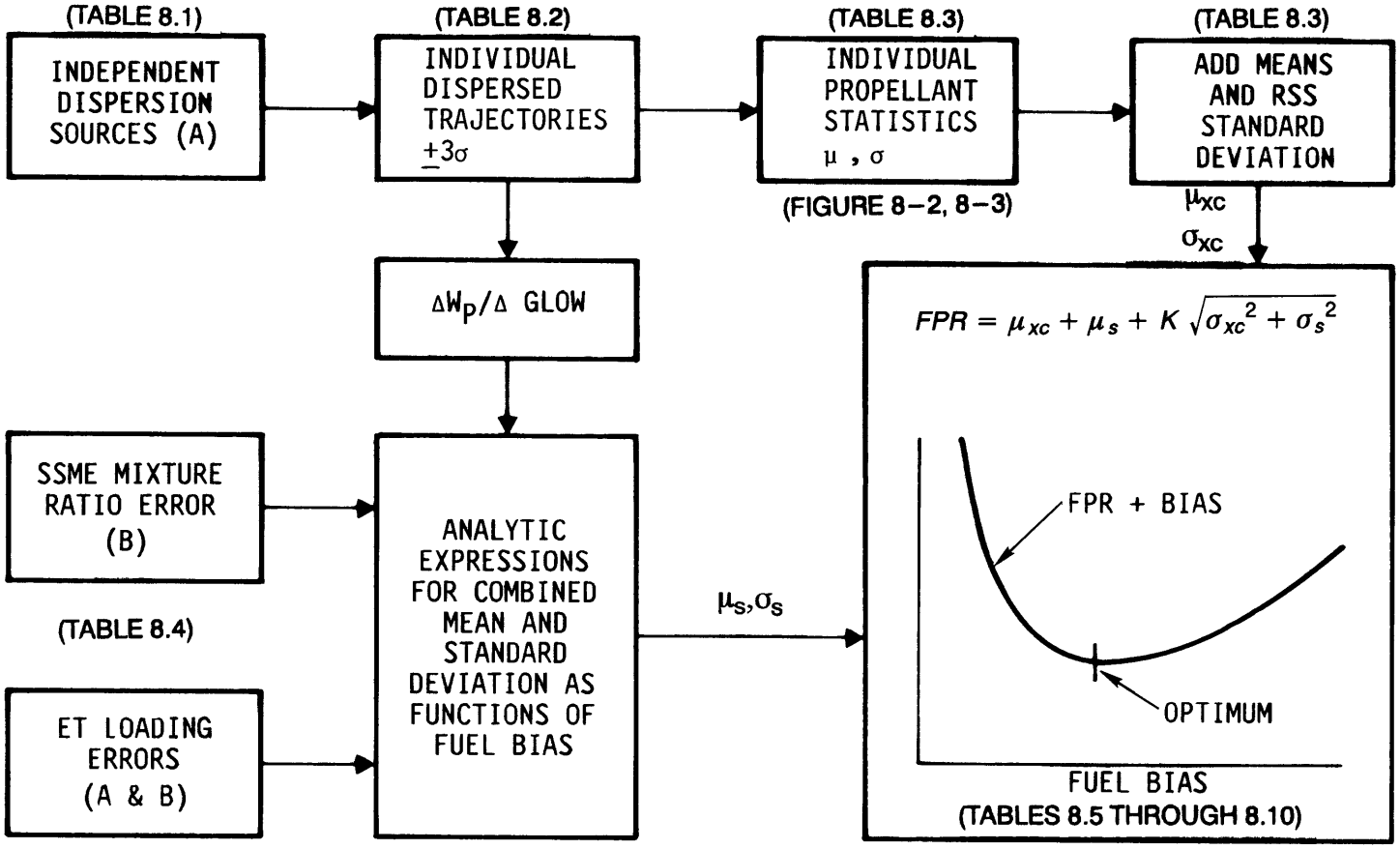

A. AFFECTS PROPELLANT CONSUMPTION AT NOMINAL RATIO OF 6:1 (CLASS 1)

B. UNBALANCED LO_2/LH_2 CONSUMPTION OR LOADS (CLASS 2)

FIGURE 8-2

PROCESSING UNSYMMETRICAL PARAMETERS BY A PARABOLIC FIT

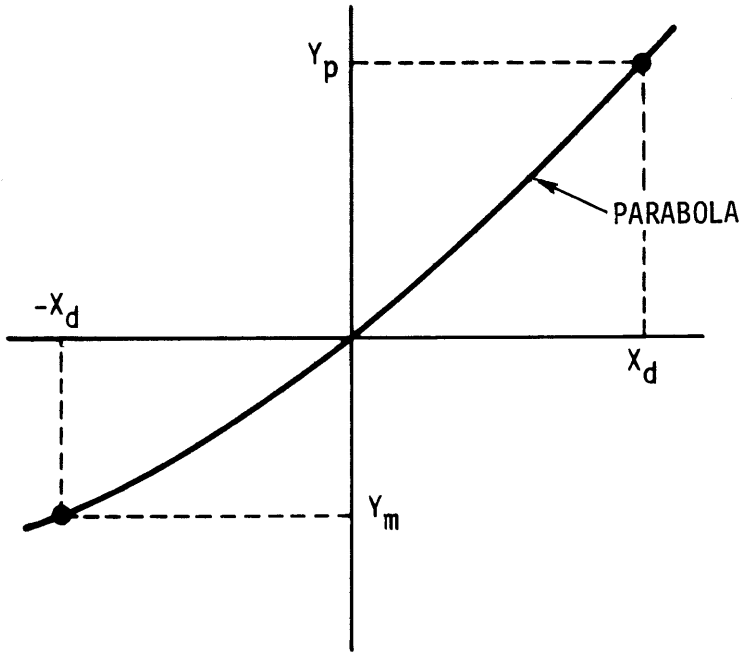

ASSUMPTIONS

- SOURCE DISPERSION NORMALLY DISTRIBUTED WITH A MEAN OF ZERO
- PARAMETER DISPERSIONS LIE ON A PARABOLA

X_d ~ SOURCE DISPERSION

Y ~ PARAMETER DISPERSION

$$\mu = 1/2\ (Y_p + Y_m)\ \frac{\sigma_x^2}{x_d^2} \text{ where } X_d = k\sigma_x$$

$$\sigma_y^2 = \left(\frac{\sigma_x^2}{x_d^2}\right)\left[1/2\ (Y_p + y_m)^2\ \frac{\sigma_x^2}{x_d^2} + 1/4\ (Y_p - Y_m)^2\right]$$

FIGURE 8-3

PROCESSING UNSYMMETRICAL PARAMETERS BY A BILINEAR FIT

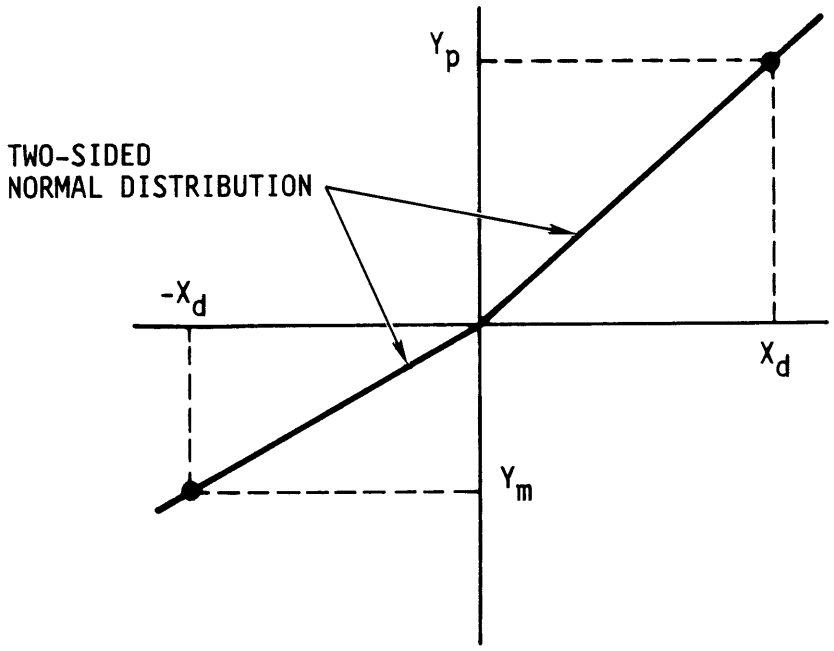

ASSUMPTIONS

- SOURCE DISPERSION NORMALLY DISTRIBUTED WITH A MEAN OF ZERO
- PARAMETER DISPERSIONS LIE ON LEFT AND RIGHT STRAIGHT LINES OF DIFFERENT SLOPE

X_d - SOURCE DISPERSION

Y - PARAMETER DISPERSION

$$\mu = \frac{1}{\sqrt{2\pi}} (Y_p + Y_m) \frac{\sigma_x}{X_d} \text{ where } X_d = K\sigma_x$$

$$\sigma_y^2 = \left(\frac{\sigma_x^2}{X_d^2}\right) \left[1/2\ (Y_p^2 + Y_m^2) - \frac{1}{2\pi} (Y_p + Y_m)^2\right]$$

FIGURE 8-4

FPR AND FPR + BIAS FOR NO FAIL TRAJECTORY (3σ)
(LWT AND SLWT)

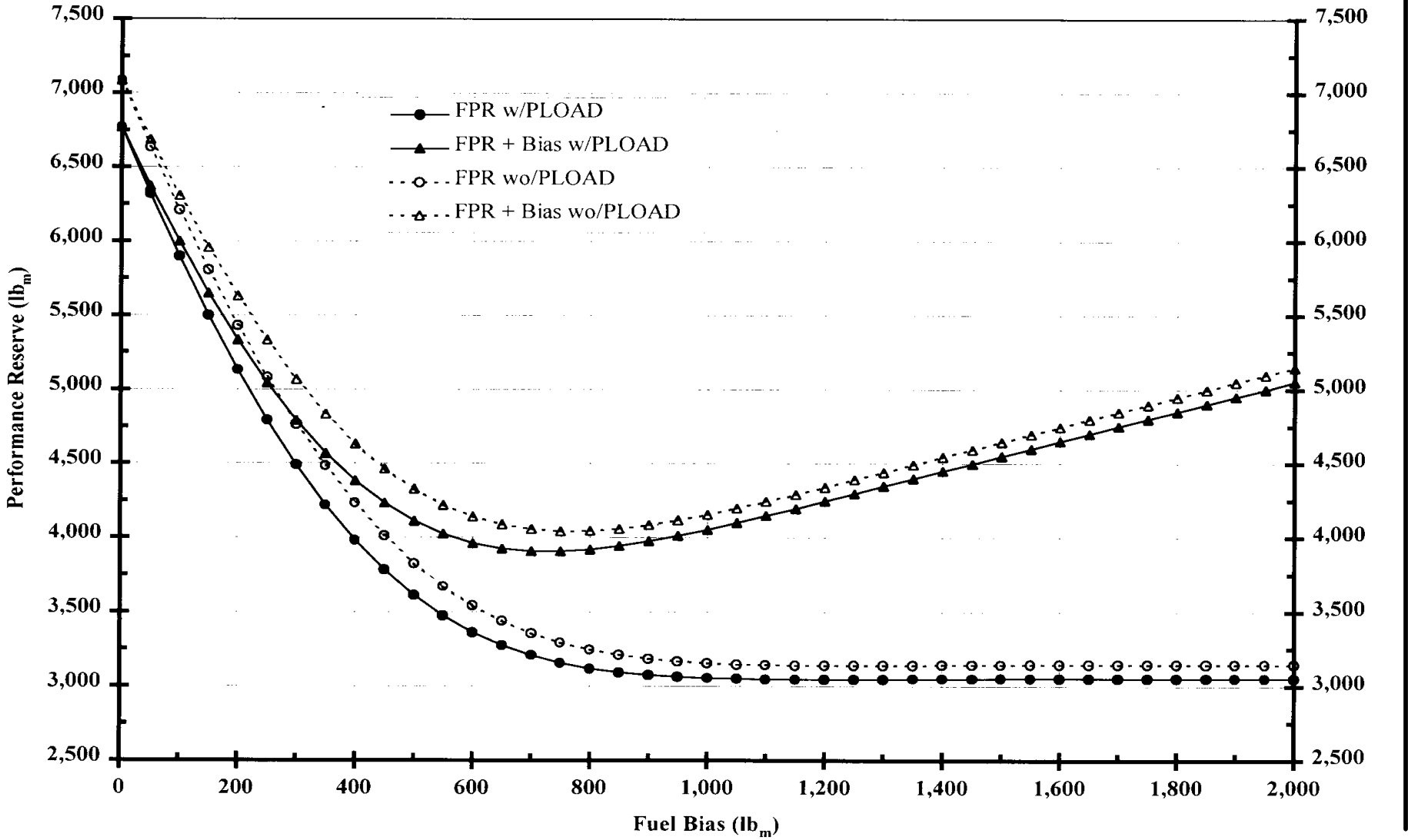

FIGURE 8-5 (DELETED)

FIGURE 8-6 (DELETED)

FIGURE 8-7 (DELETED)

THIS PAGE INTENTIONALLY LEFT BLANK

9.0 SOFTWARE

The purpose of this section is to provide details of several flight software functions which are important to the assessment of ascent performance. These are Orbiter elevon schedules and load relief, Adaptive Guidance Throttling (AGT), and sequencing. Some of the important flight control phases and major GN&C events occurring during first stage of ascent are shown in relation to the high dynamic pressure region of flight in Figure 9-1. Details of the flight software requirements are documented in the Functional Subsystem Software Requirements Documents: STS83-0002 for Guidance, STS83-0005 for Navigation, STS83-0008 for Flight Control, STS83-0010 for Redundancy Management, STS83-0016 for Effector Interface, and STS83-0026 for Sequencing.

9.1 ELEVON LOAD RELIEF

During ascent, the Orbiter elevon structure is protected from excessive loads by (1) a scheduled elevon position profile based on the design flight trajectory with environmental and system dispersions and (2) a function within the ascent digital autopilot, called elevon load relief, which provides elevon position commands as necessary to deviate from the scheduled profile in a direction to reduce elevon hinge moments whenever the elevon structural capability may be exceeded based on elevon actuator differential pressure measurements. The inboard elevons are slaved together as are the outboard elevons.

As shown in Figure 9-2, if the inboard and outboard elevon actuator differential pressures stay between the positive and negative drive limits (DRVLIB, DRVLOB), the elevons follow the I-Loaded deflection profile. If the actuator differential pressures exceed either of the limits, elevon load relief will cause the elevons to move in the direction of the applied hinge moment to reduce the elevon load. After the actuator differential pressures drop below the I-Loaded drive limit values, the elevons maintain their positions until the differential pressures fall below the I-Loaded return limits (RETLIB and RETLOB). The gap between the drive and return limits is the dead zone.

When the actuator differential pressures fall below the return limits, elevon load relief starts the elevons moving back to the scheduled elevon deflection profile. Thus, elevon load relief alters the elevon schedule when the elevon actuator differential pressures exceed the drive and return limits; otherwise the nominal elevon schedule is followed. The drive and return limits are based on elevon structural capabilities. They are not symmetric about zero although there is only one drive limit and one return limit for each pair of inboard and outboard elevons. Therefore, an I-Loaded bias (BIASIB, BIASOB) is added to the differential pressures to make the elevon load relief limits compatible with asymmetric structural capability limits. There are thus six I-Loads which are required by elevon load relief: DRVLIB, DRVLOB, RETLIB, RETLOB, BIASIB, BIASOB.

Details of elevon actuators, hinge moments, and elevon load relief I-Loads and logic are provided in Tables 9.1 through 9.5.

9.2 ADAPTIVE GUIDANCE THROTTLING (AGT)

Aerodynamic loading of the Space Shuttle launch vehicle during ascent is directly related to the dynamic pressure. To avoid exceeding the maximum allowable dynamic pressure, the SSMEs are throttled down during the maximum dynamic pressure region of ascent. Close control of vehicle dynamic pressure is difficult due to variations in SRB propellant burn characteristics which have a significant effect on vehicle performance. Allowances for RSRM propulsion dispersions result in performance degradation due to (1) trajectory shaping to decrease maximum dynamic pressure and (2) the increase in FPR.

A technique known as AGT has been devised to minimize these dispersion allowances. AGT makes it possible to change the baseline throttle profile during flight. The RSRM thrust over the first 20 seconds of flight is evaluated. If it appears that the thrust is off-nominal, AGT software is utilized to compute adjustments to either the SSME throttle or pitch attitude I-Loads (or both) to compensate for the off-nominal condition. This ability to control SSME throttle settings in response to SRB-induced acceleration dispersions allows greater control of dynamic pressure during ascent, ascent trajectories which are more optimal for performance can be designed, and allowance in the FPR for RSRM thrust dispersions can be reduced.

SSME throttle command (KCMD)is a function of navigation-sensed vehicle relative velocity (VRHOMAG) and is determined from throttle command I-Loads (THROT[I]) and velocity I-Loads (QPOLY[I]). The calculation to determine KCMD is

$$\text{If } QPOLY(I) \leq VRHOMAG < QPOLY\,(I+1)$$
$$\text{then } KCMD = THROT\,(I)$$
$$\text{where } I = 1, 2, 3, 4$$

The throttling rate is 10%/sec with all engines throttled simultaneously.

The AGT logic modifies the baseline throttle schedule. Based on preflight predictions, an estimate of the mission elapsed time, TREF-ADJUST, required to achieve a reference velocity, VREF-ADJUST, is made and both are stored in the flight software as I-Loads. The value of VREF-ADJUST is chosen to be less than the first throttle-down velocity. The values of both I-Loads are dependent on SRB performance predictions and payload weight. After lift-off, guidance monitors VRHOMAG and when it exceeds VREF-ADJUST with no SSME failures, a one-time computation of the MET required (TREQD) to attain VREF-ADJUST and TREF-ADJUST is made:

$$TDEL\text{-}ADJUST = TREQD - TREF\text{-}ADJUST$$

The sign and magnitude of TDEL-ADJUST indicate the relative performance of the SRBs. If TDEL-ADJUST < 0, the SRB performance is higher than predicted and if TDEL-ADJUST > 0, then SRB performance is lower than predicted.

The computer algorithm determining the required change to the throttle schedule is:

$$\text{THROT (J)} = \text{THROT (J)} + \text{ROUND}\left[\left(\frac{\text{FACTOR}}{\text{QPOLY (J + 1)} - \text{QPOLY (J)}}\right) * \text{TDEL–ADJUST}\right]$$

If TDEL - ADJUST < 0,
Then J = LTHRT, “HOT” SRB throttle index
FACTOR = THRT - FAC, “HOT” SRB throttle factor

If TDEL-ADJUST > 0,
Then J = LTHRTL, “COLD” SRB throttle index
FACTOR = THRT-FACL, “COLD” SRB throttle factor

All the variables are I-Loads except for TDEL-ADJUST which is computed by guidance.

The SSME throttle command is not the only parameter modified by guidance to compensate for SRB performance dispersions. Using TDEL-ADJUST as a relative SRB performance indicator, the commanded pitch profile is also modified and is known as adaptive guidance pitch biasing. Its purpose is also to help control vehicle dynamic pressure during first stage. Adaptive pitch biasing is first computed and included in the guidance pitch command when TDEL-ADJUST is computed. The sign of TDEL-ADJUST determines which I-Loaded pitch factor is to be used by guidance in its pitch biasing computation:

If TDEL-ADJUST < 0, the “HOT” SRB pitch factor (PT-FAC) is selected and guidance will pitch the vehicle towards vertical slightly resulting in a less positive pitch rate.

If TDEL-ADJUST > 0, the “COLD” SRB pitch factor (PT-FACL) is selected and the vehicle will pitch towards horizontal slightly resulting in a more positive pitch rate.

The pitch bias algorithm is

THETAC = THETAC - (PTFAC * TDEL - ADJUST) * (KRAMP - (KRAMP - PTPCT) * KLOAD) * (1 - THETAC **2)

The pitch bias is not a constant - it is ramped out with vehicle load relief gains between Velocity Gain Tabs 3 and 4. If an SSME fails before Velocity Gain Tab 3 is achieved, the pitch bias is set to zero.

9.3 SEQUENCING

The in-flight computer programs are written so they can be executed by a single computer or by all computers executing an identical program in the same time frame. The multicomputer mode is used for critical mission phases such as launch, ascent, entry and abort.

The Orbiter software for a major mission phase must fit into the 106, 496-word central memory of each computer. However, to accomplish all of the computing functions for all mission phases, more words of memory are required than available. To fit the software needed into the computer memory space available, the computer programs have been subdivided into nine memory groups corresponding to functions executed during specific flight and check-out phases.

The software is divided into two major groups - the system software group and the applications processing software. The system software group consists of the following three sets of programs: The flight computer operating program, the user interface programs, and the system control program. These tell the computers how to perform and how to communicate with other equipment. The applications processing software contains, among things, specific software programs for GN&C which are required for launch, ascent flight to orbit, maneuvering on-orbit, and landing on a runway.

The two software groups are grouped by function and partitioned into memory configurations for specific mission phases. When requested, memory is reconfigured from mass memory so operating sequences for the needed function can be overlaid into the main computer memory.

The highest level of the applications software is the Operational Sequences (OPS) which is required to perform part of a mission phase. Each OPS is a set of unique software required to perform phase-oriented tasks. An OPS can be further subdivided into groups called MMs, each representing a portion of the OPS mission phase. The OPS and MM designations for all mission phases are illustrated in Figure 9-3. The MM transitions are diagrammed in Figure 9-4.

The DAP reconfiguration logic is the bookkeeper of the flight control software. In response to control mode changes, changes in failure status, and the occurrence of events, the reconfiguration logic generates the indicators that are needed by the DAP and guidance/steering for moding, sequencing, and initialization. Subphases useful for the software description of the DAP and guidance/steering are shown in Figure 9-5 for a nominal mission and in Figure 9-6 for an RTLS abort. These subphases are defined in terms of externally and locally derived events described in Table 9.6.

During the ascent phase of a Space Shuttle mission there are two separations of Space Shuttle elements marking the transition between the stages of ascent. These are SRB

separation and ET separation. Prior to and during these separation events, there is a sequence of functions performed by the flight software which is necessary for proper GN&C moding and for the safe execution of the separation of either the SRBs or ET. Listings of the functions performed by the flight software during SRB and ET separation are provided in Tables 9.7 and 9.8, respectively.

The flight software was designed to allow for SRB separation inhibits should either the roll rate, pitch rate, yaw rate, or dynamic pressure be at values that would exceed limits set by NSTS 07700, Volume X. This capability, however, is not currently utilized. The decision to make this function non-operational was based on sensitivity studies which showed that the separation inhibit logic did not provide consistent positive benefits to the SRB separation system. Furthermore, a trigger of the separation inhibit requires highly dispersed conditions and/or multiple failures, increasing the probability that the vehicle state vector will degrade further after the inhibit.

Also, it was felt that with the decreasing separation envelopes the probability of a single parameter causing an inhibit was greater than the probability of two or more parameters exceeding their limits. An inhibit caused by a single parameter would put the vehicle at more risk than if the SRB separation sequence was allowed to continue. Finally, within the generic groundrules for no-fail and intact aborts, no condition which would result in a separation inhibit was identified.

Separation of the Orbiter from the ET is also inhibited by the software when conditions which could cause recontact occur. Exceeding the following range of values will cause separation to be inhibited:

a. Nominal/AOA/ATO

   1. Roll rate: $-.7$ deg/sec to $+.7$ deg/sec
   2. Pitch rate: $-.7$ deg/sec to $+.7$ deg/sec
   3. Yaw rate: $-.7$ deg/sec to $+.7$ deg/sec

b. RTLS

   1. Roll rate: -20 deg/sec to $+20$ deg/sec
   2. Pitch rate: -20 deg/sec to $+.25$ deg/sec
   3. Yaw rate: -20 deg/sec to $+20.5$ deg/sec
   4. Angle of Attack: -1.5 deg to $+89$ deg
   5. Angle of Sideslip: -20 deg to $+20$ deg

The capability to inhibit ET separation for RTLS has been made non-operational for most situations. A sensitivity study performed during Generic Heavyweight RTLS ET

Separation Certification showed that inhibiting separation tended to further degrade the mated vehicle's control authority. This is due to the increase in dynamic pressure (Qbar), which builds rapidly following MECO during RTLS. In addition, the building Qbar increases the risk of Orbiter/ET recontact following structural release. However, it is even more unacceptable to allow the AOA or pitch rate to exceed the maximum values specified above; the risk of recontact is too great. Therefore, the maximum pitch rate and AOA inhibit limits remain operational.

The post-MECO MPS, OMS, and RCS propellant dump sequence timelines and rationale for nominal missions and RTLS, ATO and TAL aborts are provided in NSTS 08934, Volume VI.

TABLE 9.1

ELEVON ACTUATOR GEOMETRY

	Position (deg)	Inboard (in)	Outboard (in)
Effective arm length (L)	−10.0	15.098	8.800
	−7.709	15.095	8.793 ←Zero stroke (outboard)
	−7.585	15.094	
	−5.0	15.061	8.792 ←Zero stroke (inboard)
	0.0	14.915*	8.767*
	5.0	14.669	8.671
	10.0	14.331	8.517
			8.307
		Inboard (in^2)	Outboard (in^2)
RAM area (A)		21.82	18.04
		Inboard (in^3)	Outboard (in^3)
A * L used in ΔP calculations for elevon load relief		325.445	158.157
*Values used in determining ΔP for drive and return settings			

TABLE 9.2

ELEVON HINGE MOMENT DATA

		OV–102	OV–103 and Subs
Minimum guaranteed structural capability (MGSC)*	Inboard elevon	1.03×10^6 in–lb	1.025×10^6 in–lb
		-0.844×10^6 in–lb	-0.844×10^6 in–lb
	Outboard elevon	0.513×10^6 in–lb	0.346×10^6 in–lb
		-0.437×10^6 in–lb	-0.437×10^6 in–lb
Dynamic friction (F)		Inboard	Outboard
	Actuator	1,500 in–lb	880 in–lb
	Elevon	3,600 in–lb	3,600 in–lb
	Total	5,100 in–lb	4,480 in–lb
Total elevon actuator hinge moment	ACTHM – ELHM + F where ACTHM = Actuator hinge moment ELHM = Elevon aerodynamic hinge moment		
*Limits are based on larger of hot/cold values in IL 280–403–83–103 and 380–103–80–106			

TABLE 9.3

ELEVON LOAD RELIEF DRIVE AND RETURN SETTINGS

Hinge Moments					
		DS (10^6 in–lb)		RS (10^6 in–lb)	
		OV–102	OV–103 and Subs	OV–102	OV–103 and Subs
Inboard	Negative	−0.825	−0.825	−0.718	−0.715
	Positive	+0.511	+0.644	+0.403	+0.534
Outboard	Negative	−0.423	−0.246	−0.377	−0.191
	Positive	+0.281	+0.337	+0.235	+0.282
Actuator $\Delta P = \frac{\text{Hinge Moment}}{A * L}$					
		DS (psi)		RS (psi)	
		OV–102	OV–103 and Subs	OV–102	OV–103 and Subs
Inboard	Negative	−2,535.490	−2,534.988	−2,206.160	−2,196.990
	Positive	+1,569.100	+1,978.827	+1,239.750	+1,640.829
Outboard	Negative	−2,674.975	−1,555.420	−2,383.020	−1,207.663
	Positive	+1,777.025	+2,130.798	+1,485.070	+1,783.042

- Drive setting (DS) to initiate load relief
  - Inboard: DS (1) = −MGSC ± (200,000 in–lb)* OV–103/4/5
    + 333,000/−205,000 OV–102
  - Outboard: DS (0) = −MGSC ± (100,000 in–lb)* OV–103/4/5
    + 156,000/−90,000 OV–102
- Return setting (RS) to terminate load relief
  - Inboard: RS (1) = DS (1) ± (110,000 in–lb) +
  - Outboard: RS (0) = DS (0) ± (55,000 in–lb) +

* Reductions to allow for ΔP transducer uncertainty and wind shear/gust transients − use + for MGSC > 0; use − for MGSC < 0

\+ Use + for DS < 0; use – for DS > 0

TABLE 9.4

ELEVON LOAD RELIEF I-LOADS

	Inboard Elevons			Outboard Elevons		
		Value (psi)*			Value (psi)*	
	MSID	OV-102	OV-103 and Subs	MSID	OV-102	OV-103 and Subs
BIAS	V97U1413C	−483.195	−278.0	V97U1416C	−448.975	+288.0
DRVLIM	V97U1776C	+2,052.295	+2,257.0	V97U1777C	+2,226.000	+1,843.0
RETLIM	V97U2232C	+1,722.965	+1,919.0	V97U2233C	+1,934.045	+1,495.0

BIAS = 1/2 [positive DS (psi) + negative DS (psi)] or 1/2 [positive RS (psi) + negative RS (psi)]
DRVLIM = Positive DS (psi) − BIAS or − [negative DS (psi)] + BIAS
RETLIM = Positive RS (psi) − BIAS or − [negative RS (psi)] + BIAS

*Values shown are subject to change - for specific mission values, see the appropriate mission I-Load definition CR

TABLE 9.5

ELEVON LOAD RELIEF LOGIC

Elevon load relief is initiated when

$$\Delta P_{min} - BIAS - DRVLIM$$

or

$$\Delta P_{max} \quad BIAS + DRVLIM$$

where ΔP_{min} is the lowest elevon actuator ΔP measurement, left or right

ΔP_{max} is the highest elevon actuator ΔP measurement, left or right

The elevons remain off–schedule if

$$BIAS - RETLIM \quad \Delta P_{min} \quad BIAS + DRVLIM$$

and

$$BIAS + RETLIM - \Delta P_{max} - BIAS + DRVLIM$$

The elevons return to schedule if

$$\Delta P_{min} \quad BIAS - RETLIM$$

or

$$\Delta P_{max} - BIAS + RETLIM$$

TABLE 9.6

OVERVIEW OF DAP EVENTS/SEQUENCING

Event	Event Name	Local Variable	Forcing Function*	Action*
19	SRB_IGN_CMD		SRB ignition command	
19A	(LIFT-OFF)	• S1C, PRELO	MET ≥ MET_LIFT-OFF (worst case lift-off)	• Control loops closed
		• LIFT-OFF		• Initiate fader on holddown bias
		• INTERPS_S1		• Stage 1 gain scheduling initiated
		• S1G		• Stage 1 guidance commands initiated
		• ATTFILT	(19A) ≥ • (S_QUAT)	• Accept guidance cmds
19B	(LO_PLUS_T2)	• LO_PLUS_T2	MET = MET_LIM_LCH	
		• SRBLIM_ACTV		• Normal SRB component limits engaged
		• AUTOTRIM_QR		• Pitch & yaw trim integrator turned ON
		• ELEV_LR		• Elevon load relief turned ON
19C	(RL_NOM)	• PRL_S1, PRL_LCH	(18A) + MET_90THRUST	• Normal SSME fixed rate limits engaged
21A	(AUTOTRIM_ DISABLE)	• AUTOTRIM_QR	VREL ≥ VREL_AUTOTRIM_ INHIBIT	• Pitch & yaw trim integrators turned OFF
21B	(FILTSW)	• FILTSW	VREL ≥ VREL_FILTSW	• Roll bending filter switched to B
21C	(YFILTSW)	• YFILTSW	VREL ≥ VREL_FILTSW	• Switched yaw bending filter gain

*Numbers in this column change when I-Loads are changed

TABLE 9.6

OVERVIEW OF DAP EVENTS/SEQUENCING - Continued

Event	Event Name	Local Variable	Forcing Function*	Action*
25A	(PRE_SEP)	• FAIL_MIX_ENABLE	MET ≥≤ MET_25A	• Enable roll mixing logic change if SSME failure has occurred
				• Roll lead-lag switched
		• PRE_SEP		• Enable fader on KL_MPS & KN_NY gains
		• NYSEP_FB_ENABLE		• Enable N_y feedback for SRB separation control
		• PC_FILTER		• P_c monitoring/filtering initiated
		• ELEV_LR		• Disable elevon load relief
25B	(AUTOTRIM RESET)	• AUTOTRIM RESET	E25A ≥ • (PC4F < PC_TRIM_RESET • PC5F < PC_TRIM_RESET) + MET ≥ MET_25B	• Enable fader on trim integrators
				• Enable fader on KN_MPS, KL_SRB, KL_DELPSI, KM_MPS, & KM_SRB GAINS
				• Enable Stage 2 roll mixing logic change for no SSME failure
				• Enable fader to DQMPST pitch trim
		• UNPAR_YAW_ ENABLE		• Lateral attitude gain switched
		• SNGL_ME_CNTL_ ENABLE		• Enable RCS jet cmds at two SSME out
25C	(COMLIM4)	• COMLIM4	E25B • PC4F < PC_ COMLIM	• Engage V97U2427C component limiting on both SRBs

*Numbers in this column change when I-Loads are changed

TABLE 9.6

OVERVIEW OF DAP EVENTS/SEQUENCING - Continued

Event	Event Name	Local Variable	Forcing Function*	Action*
25D	(COMLIM5)	• COMLIM5	E25B • PC5F < PC_ COMLIM	• Engage V97U2427C component limiting on both SRBs
25E	(NYSEP_ DISABLE)	• NYSEP_FB_ENABLE	(COMLIM4 • COMLIM5) + MET ≥ MET_25E	• Disengage N_y feedback through 4-sec fader
27	SRB_NULL_CMD	• PC_FILTER	SRB_MODING_SEP = ON	• Terminate P_c monitoring filtering
		• SRB_NULL_CMD		• Null SRB actuators
				• Employ Orbiter pitch and yaw RGAs
28	(SRB_SEP_CMD) (SRB separation command issued)	• S2C, S1C		• Stage 2 control; selected SOPs and FDIR disabled (separate CR)
				• Enable *1.2-deg pitch trim
		• ATTCMD		• Roll bending filter switches to C
				• Pitch and yaw trim integrator limits changed to second stage values
		• SRBSEP		• 4-sec SRB separation period initiated
		• INTERPS S2, $\overline{\text{INTERPS S1}}$		• Stage 2 gain scheduling initiated
		• FRZ_CMD		• Three-axis attitude hold engaged; guidance initiated for convergence

*Numbers in this column change when I-Loads are changed

TABLE 9.6

OVERVIEW OF DAP EVENTS/SEQUENCING - Continued

Event	Event Name	Local Variable	Forcing Function*	Action*
		• PRL_S2, PRL_S1		• Engage PRL
29	STG2_STEER_ INIT (Stage 2 guidance ready)	• SRBSEP	GUIDANCE_INITIATE = ON	• 4-sec SRB separation period complete
		• S2G, S1G		• Stage 2 guidance engaged for control
29A	(AUTOTRIM_ ENABLE	• AUTOTRIM_QR		• Roll, pitch, and yaw trim turned ON
		• AUTOTRIM_P • PAR_PITCH_ENABLE	SEC_ME_FL_CNFM] + [$t \geq (t_{E28}$ + 60 SEC) • SEC_ME_FL_CNFM]	• Lateral attitude gain switched
30A	ME_RETRIM	• PAR_PITCH_ENABLE	S_SSME_TRIM = ON	• Initiate trim and bias limit for pitch parallel
32	MECO_CMD	• AUTOTRIM_QR, • AUTOTRIM_P	MECO_CMD	• Trim integrators disabled
		• UNPAR_YAW_ENABLE		• Unparallel MEs in yaw

*Numbers in this column change when I-Loads are changed

TABLE 9.6

OVERVIEW OF DAP EVENTS/SEQUENCING - Concluded

Event	Event Name	Local Variable	Forcing Function*	Action*
		• PRL_S2, PRL_MECO • FRZCMD, PEGCMD • S2G		• PRL limits reduced
33	ME_ZERO_ THRUST		ZERO_THRUST	• ASC_DAP deactivated (except body flap) and TRANS_DAP activated

*Numbers in this column change when I-Loads are changed

TABLE 9.7

SRB SEPARATION SEQUENCE EVENTS

Event	Name	Primary Que	Backup Que	Actions
25	SRB Separation Monitor	MET ≥ SRB_SEP_Monitor, V97U9750C, and no MECO confirmed	- -	Monitor for SRB SEP sequence initiation
25A	PRE_SEP	MET ≥ MET_25A, V97U2435C	- -	Enable N_y feedback Disable elevon load relief
25B	Auto Trim Reset	Event 25A and both SRBs $P_c \leq$ PC_Trim_Reset, V97U2202C	MET ≥ MET_25B, V97U2436C	Fade TVC gains, trim integrators Fade MPS pitch trim Enable RCS roll control
25E	NY_SEP_Disable	Event 25B and both SRBs $P_c \leq$ PC COMLIM, V97U2203C	MET ≥ MET_25E, V97U2437C	Disengage N_y feedback through 4-sec fader
26	SRB SEP Sequence Initiation	Both SRBs $P_c \leq$ 50 psi for four passes and within MAX_SRB_SEP_CUE_DIFRNTL, V97U9761C, of each other	MET ≥ SRB_SEP_B/U_QUE, V97U9751C	Set LH/RH P_c 50 psi flag Start SRB SEP INIT timers (Δt) • Function moding for separation • SRB separation command SRB RSS safe, power off
27	Function Moding for Separation	Δt ≥ SRB_SEP_MODING_T_DELAY, V97U9752C, minus 480 ms	- -	Null SRB actuators Arm SRB separation PICs Monitor SSMEs status
28	SRB Separation Cmd	Δt ≥ SRB_SEP_CMD_T_DLY, V97U9753C, minus 480 ms or Δt ≥ SRB_SEP_CMD_T_DLY_ABT, V99U7589C, minus 480 ms if one SSME failed or Δt ≥ SRB_SEP_CMD_T_D_CONT_ABT, V99U7676C, minus 480 ms if two SSMEs failed	- -	Switch from SRB to Orbiter RGAs Initiate three axis hold Initiate MPS pitch trim Issue SRB SEP Fire 1 and Fire 2/3 commands Initiate second stage software functions Start SRB separation sequence termination timer

TABLE 9.7

SRB SEPARATION SEQUENCE EVENTS - Concluded

Event	Name	Primary Que	Backup Que	Actions
- -	SRB Separation Sequence Termination	Event 28 + 4.0 seconds	- -	Terminate attitude hold SRB power off MEC master reset (one pass later) Deschedule sequence

TABLE 9.8

ET SEPARATION SEQUENCE OF EVENTS

Time (sec)	Events**	Sequence of Events for Nominal Separation
0	32	MECO command declared by SSME OPS
0.8 to 1.3	33	MECO confirm (SSME OPS) and ET separation sequence initiated
		Start Zero Thrust Timer
4.45 to 5.05	33B	Zero thrust: terminate ascent DAP, initiate TRANS DAP
5.800		All prevalves commanded close and detected true by ET separation sequencer computed prevalve close time
		Issue MPS 17-in feedline disconnect valve close cmds
9.160		ARM ET/Orbiter unlatch PIC start 1.5 sec timer
10.760		Deadface electrical connector
11.880		Unlatch and retract ET/Orbiter umbilical
		Start Sep PICs ARM timer
17.480		ET/Orbiter structural separation PIC arm flag set true
19.080		Check inhibits
		Separation minus “Z” command flag set true
19.240 (Min)		Thrusters ON
19.320 (Nom)	34	Set ET separation command flag true
19.400 (Max)		ET/Orbiter structural separation Fire 1 and 2 flags set true
~26.00*	36	MM104 transition
Time (sec)	**Events**	**Sequence of Events for RTLS Separation**
0	A35	MECO command
		Initiate GRTLS DAP
0.8 to 1.3	A36	MECO confirm, ET separation sequence initiated
		Start Zero Thrust Timer
4.45 to 5.05	A36A	Zero thrust: terminate ascent DAP

NOTE: All times shown are typical only.
*Variable time, all other times are a fixed delta time from MECO command.
**See SS-P-002-510, Space Shuttle Computer Programs Development Specifications (CPDS), for event description.

TABLE 9.8

ET SEPARATION SEQUENCE OF EVENTS - Continued

Time (sec)	Events**	Sequence of Events for RTLS Separation - Concluded
5.800		All prevalves commanded close indicator detected true by ET separation sequencer
		Issue MPS 17-in feedline disconnect valve close commands
9.160		Set ET umbilical unlatch PIC arm flag true
10.760		Deadface electrical connector
10.920		Unlatch and retract ET/Orbiter umbilical
		Start Sep PICs ARM timer
12.120		Set ET/Orbiter structural separation PIC arm flag true
13.720 (Min)	A37	Check inhibits
13.800 (Nom)		Set ET separation command flag true
13.880 (Max)		Set ET/Orbiter structural separation Fire 1 and 2 flags true
		Signal Flight Control that RTLS separation command is issued
		Thrusters ON
~23.8*	A39	MM602 transition
Time (sec)	**Events**	**Sequence of Events for Fast Separation Timeline - MM103 with 2 SSMEs Failed**
0		ET separation pushbutton depressed
		ET separation initiate flag set
	A35, 36	MECO command and MECO confirm
0.04		ET separation sequencer initiated
		Fast separation flag set true
		Set RTLS abort flag true if in MM102

NOTE: All times shown are typical only.
*Variable time, all other times are a fixed delta time from MECO command.
**See SS-P-002-510 for event description.

TABLE 9.8

ET SEPARATION SEQUENCE OF EVENTS - Concluded

Time (sec)	Events**	Sequence of Events for Fast Separation Timeline - Concluded
		ET/Orbiter structural separation PIC arm flag set true
		ET umbilical unlatch PIC arm flag set true
3.56		All prevalves command close indicator detected true by ET separation sequence
4.68		Deadface electrical connector
	27	SRB separation function moding flag set true
4.84		Issue ET umbilical unlatch Fire 1 and 2 flags
		Set −Z command flag
5.00		Issue ET umbilical retract Fire 1 and 2 flags
		Set ET/Orbiter structural Fire 1 and 2 flags
	A37	Set ET separation command flag true
5.16	28	Set SRB separation command flag true if in MM102

NOTE: All times shown are typical only.
*Variable time, all other times are a fixed delta time from MECO command.
**See SS-P-002-510 for event description.

TABLE 9.9 (DELETED)

TABLE 9.10 (DELETED)

TABLE 9.11 (DELETED)

FIGURE 9-1

FLIGHT CONTROL PHASES AND MAJOR EVENTS DURING FIRST-STAGE ASCENT

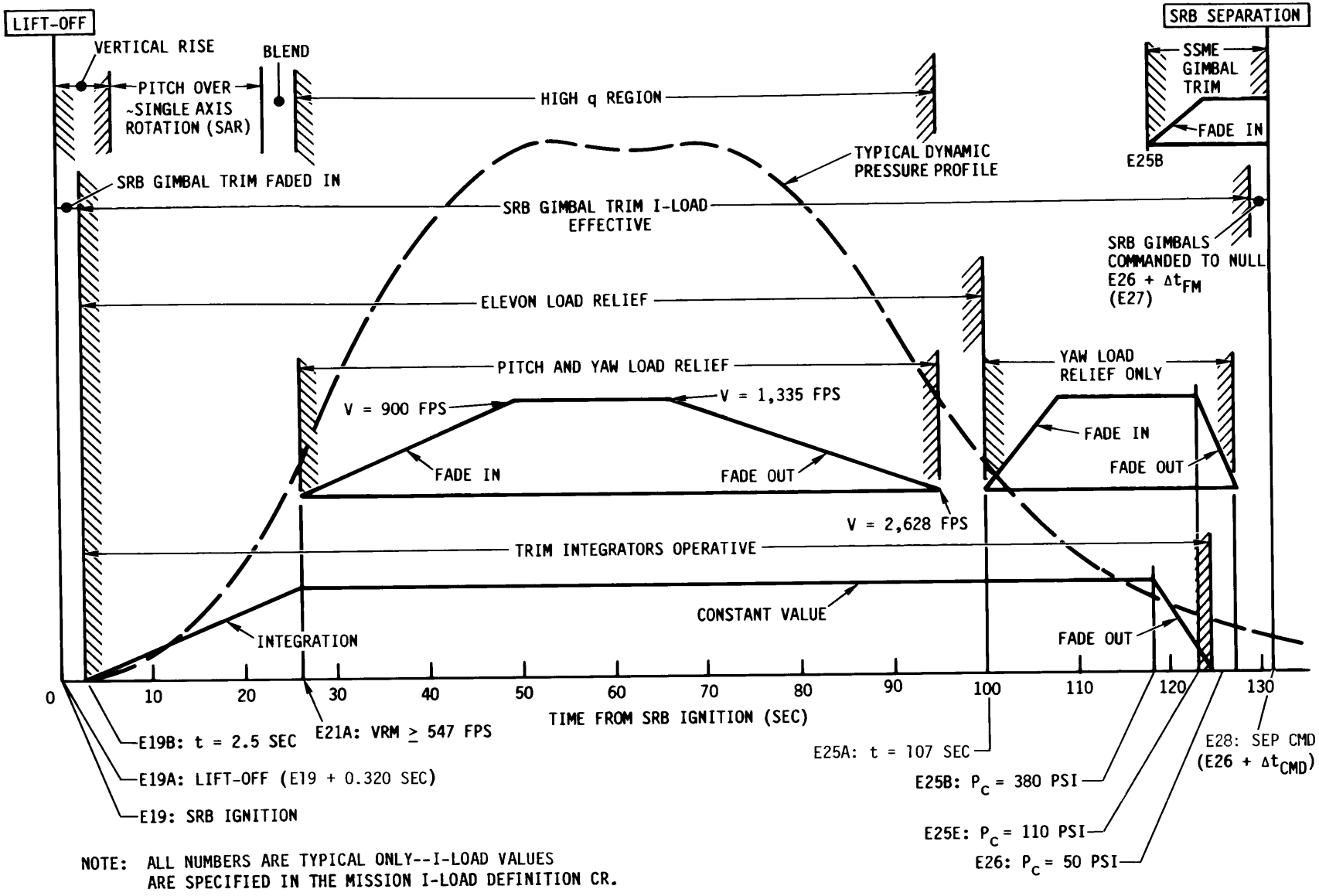

NOTE: ALL NUMBERS ARE TYPICAL ONLY--I-LOAD VALUES ARE SPECIFIED IN THE MISSION I-LOAD DEFINITION CR.

FIGURE 9-2

ACTIVE ELEVON HINGE MOMENT LOAD RELIEF

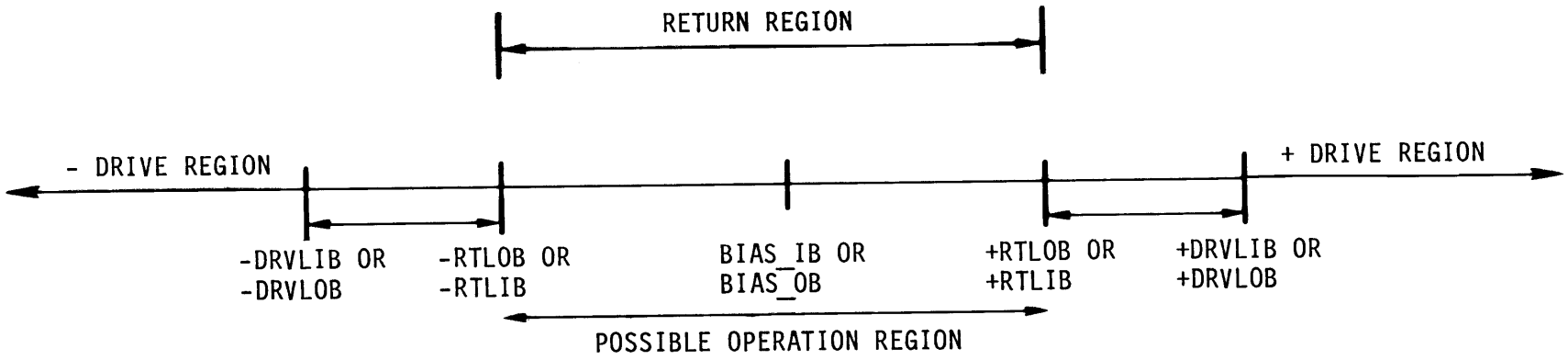

FIGURE 9-3

PROFILE OF MISSION PHASE, FLIGHT CONTROL DESIGNATION, AND MM PROGRAM NUMBERS

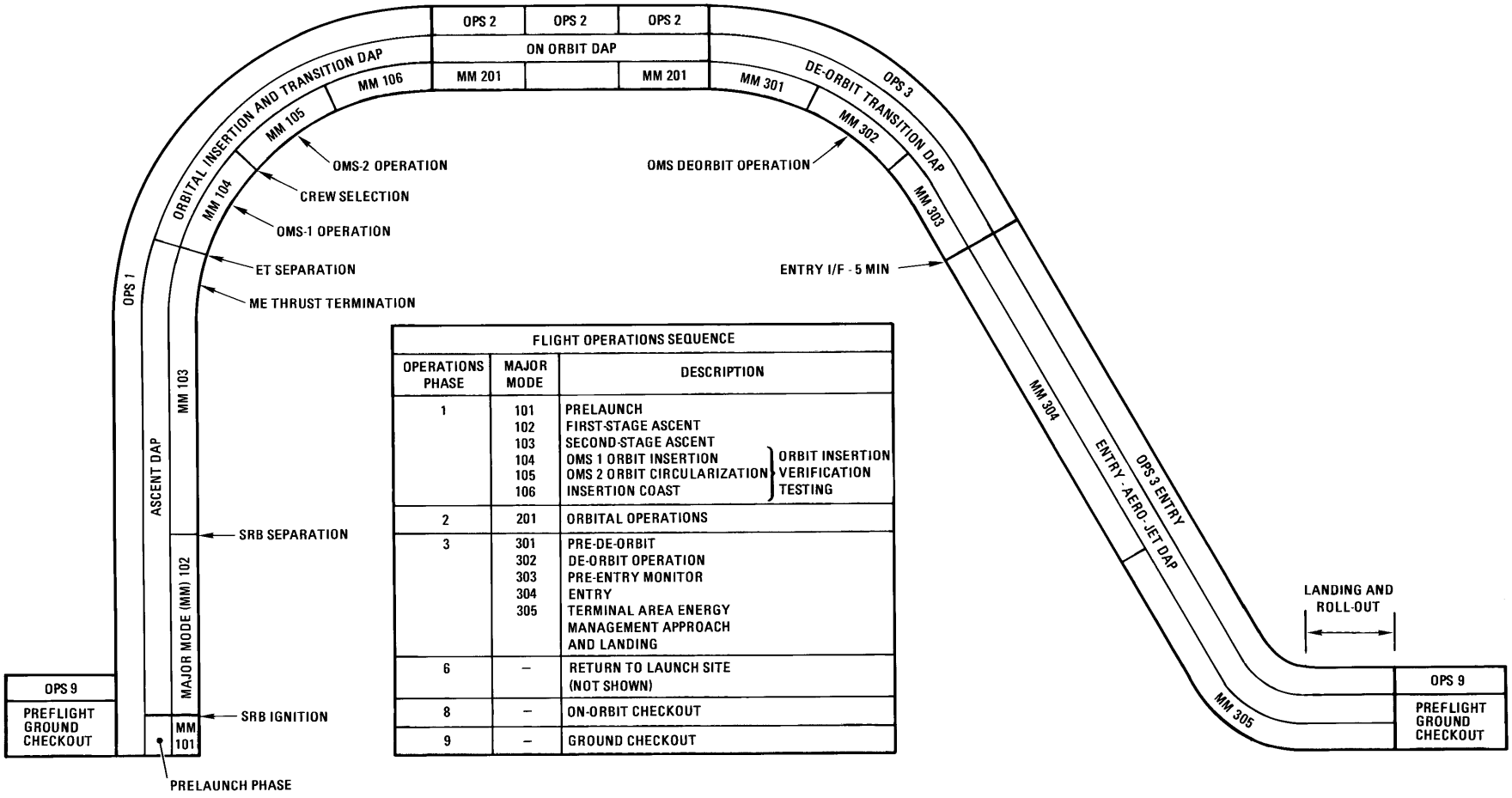

FLIGHT OPERATIONS SEQUENCE			
OPERATIONS PHASE	MAJOR MODE	DESCRIPTION	
1	101	PRELAUNCH	
	102	FIRST-STAGE ASCENT	
	103	SECOND-STAGE ASCENT	
	104	OMS 1 ORBIT INSERTION	ORBIT INSERTION VERIFICATION TESTING
	105	OMS 2 ORBIT CIRCULARIZATION	
	106	INSERTION COAST	
2	201	ORBITAL OPERATIONS	
3	301	PRE-DE-ORBIT	
	302	DE-ORBIT OPERATION	
	303	PRE-ENTRY MONITOR	
	304	ENTRY	
	305	TERMINAL AREA ENERGY MANAGEMENT APPROACH AND LANDING	
6	–	RETURN TO LAUNCH SITE (NOT SHOWN)	
8	–	ON-ORBIT CHECKOUT	
9	–	GROUND CHECKOUT	

FIGURE 9-4

MM TRANSITIONS

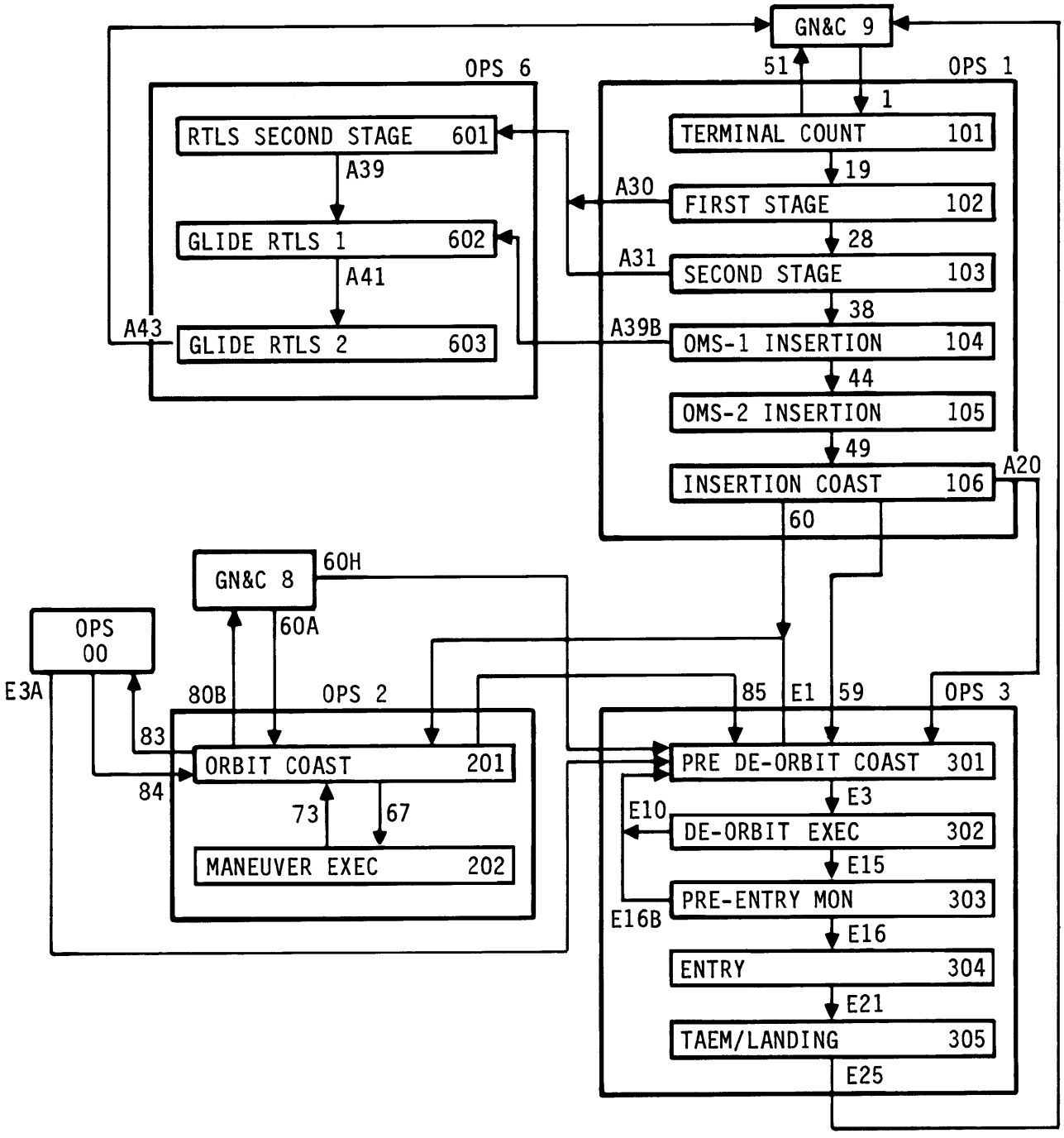

NOTES: 1. TRANSITIONS ARE NOTED VIA EVENT NUMBERS

2. IF THE ATO SWITCH IS INITIATED DURING SECOND-STAGE MAJOR MODE OR OMS-1 INSERTION MAJOR MODE, THE GUIDANCE TARGETS ARE RECOMPUTED BUT NO MAJOR MODE TRANSITIONS TAKE PLACE.

FIGURE 9-5

ASC_DAP AND GC_STEER SUBPHASES, NOMINAL MISSION

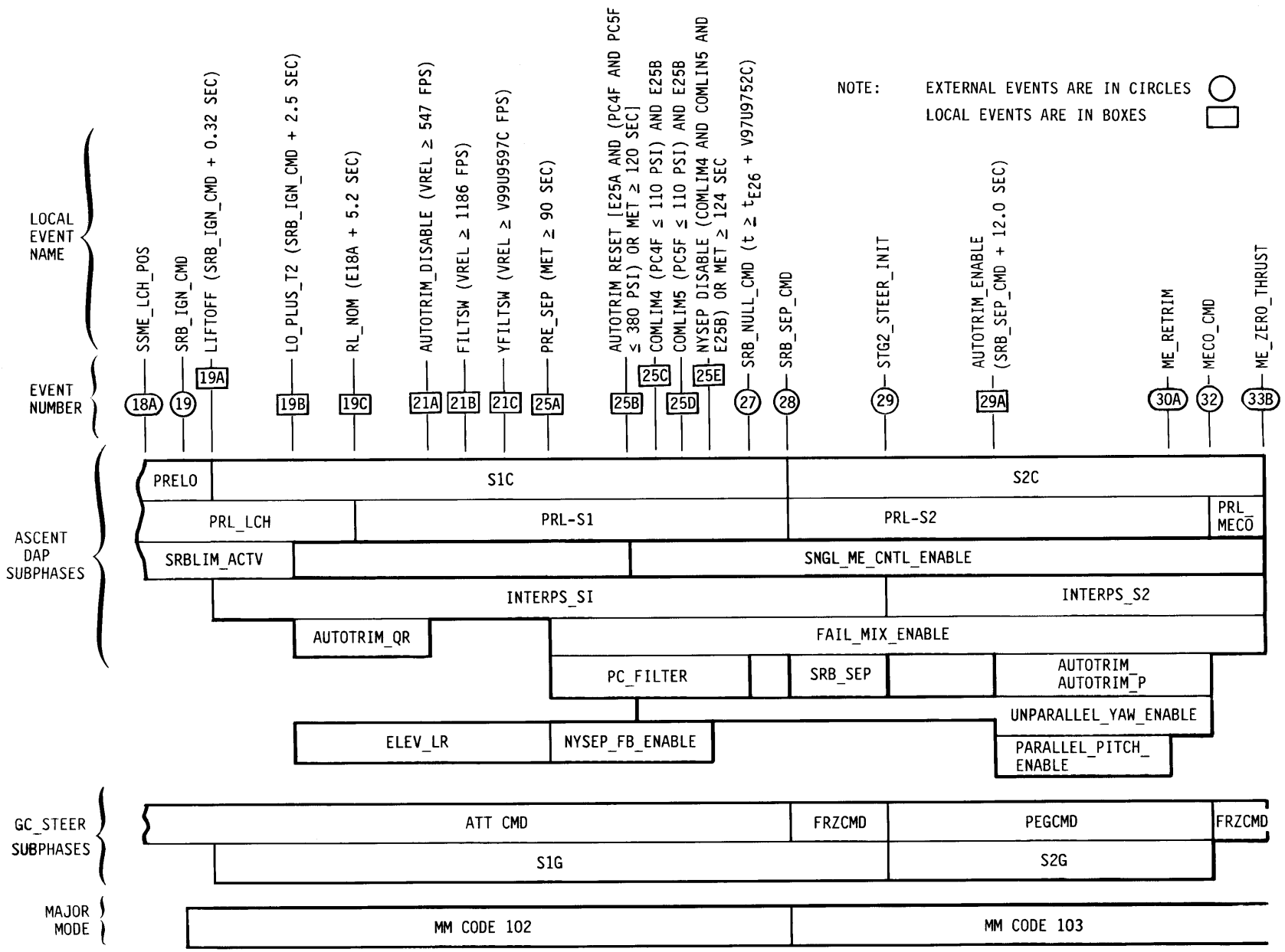

FIGURE 9-6

ASC_DAP AND GC_STEER SUBPHASES, RTLS ABORT

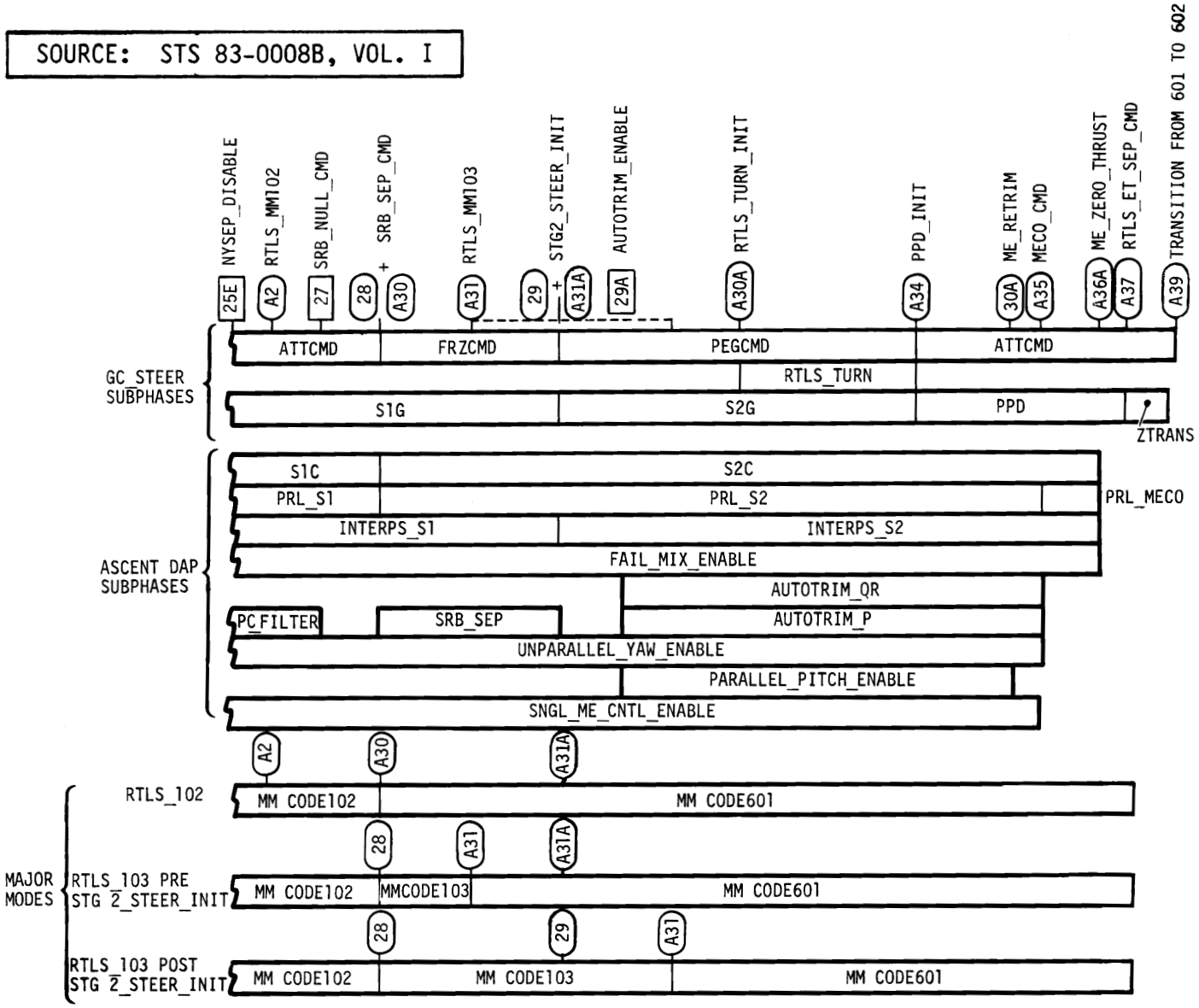

10.0 ASCENT SIMULATION MATH MODELS

Math models of the Earth's environment and the Space Shuttle's onboard systems and induced environment form the basis for the predicted trajectory, dynamics, and performance of the integrated trajectory, dynamics, and performance of the integrated Shuttle Vehicle. The math models to be used for simulation of the ascent flight phase (lift-off to orbit insertion) of a Space Shuttle mission are generally documented in the CMMD. However, prior to the existence of the CMMD, selected math model references and data were documented in this section to establish a baseline among ascent simulations. Data in this section is considered a requirement and has precedence over data in the CMMD in the case of a conflict.

10.1 ATMOSPHERE

The reference atmospheres used for launches from KSC are the Revised Range Reference Atmosphere (RRRA) and the 1963 Patrick Reference Atmosphere (PRA-63). The extreme atmosphere models are the 1971 Kennedy Cold and Hot atmospheres. Normally, simulations of launches from KSC use the RRRA to an altitude of 70 kilometers, then the atmosphere data is transitioned to the PRA-63 over 20 kilometers (70-90) km).

10.2 WINDS

The design winds for the boost phase and for entry (in the case of an abort) are those specified in NSTS 07700, Volume X - Book 2 (Appendix 10.10). These consist of steady-state vector winds, vector wind shear, and synthetic vector wind profiles with discrete and spectral gusts.

When measured (Jimsphere or MET) winds are used, they are transitioned from the last measured data point to the appropriate monthly synthetic mean winds over an interval of five kilometers.

10.3 EARTH GEOMETRY

The Earth's mean sea level surface, an equipotential surface known as the geoid, can be approximated very accurately (to within 1 part in 10^5) by an ellipsoid of revolution about the Earth's rotation axis. The primary parameters specifying an ellipsoid are its equatorial radius, *Re* (the semi-major axis) and its flattening given by:

$$f = (\mathrm{Re} - Rp) / \mathrm{Re}$$

where Rp is the polar radius (the semi-minor axis). For numerical convenience, inverse flattening, 1/f, is usually given. Secondary parameters Rp and eccentricity e are often used in calculations and are given by:

$$Rp = \mathrm{Re}(1 - f)$$

$$e = \sqrt{\mathrm{Re}^2 - Rp^2} \;/\; \mathrm{Re} = \sqrt{2f - f^2}$$

The ellipsoid provides a suitable reference system for locating points of interest by latitude, longitude and altitude.

The 1960 Fischer Ellipsoid was adopted by NASA for locating launch sites, landing sites, and tracking stations. It is used in Shuttle onboard navigation and generally in ascent trajectory calculations. Its parameters are given in Table 10.2 along with those of the World Geodetic Survey (WGS) 1984 ellipsoid, another widely used reference, e.g., by Global Positioning Satellite (GPS). The difference between these two systems, and also other more recent systems, is negligible for Shuttle ascent performance calculations but not for tracking and navigation.

Trajectory simulation and GN&C calculations require models of the Earth's rotation axis and rate of rotation. The mission dependent transformation from Mean Aires of 1950 (M50) to Earth-centered inertial true-of-date coordinates provides the current Earth pole unit vector in M50 coordinates; it is the third row of the transformation matrix. The rotation rate varies slightly with time by amounts negligible for Shuttle analysis. Table 10.2 gives the value used in Shuttle onboard navigation (first column) and a mean value for the J2000 epoch (second column).

10.4 LAUNCH AND LANDING SITES

The launch site locations for the Space Shuttle are provided in Paragraph 7.2. At KSC, the Fischer Ellipsoid is 207.81 feet above mean sea.

The SSP landing sites are listed in Tables 10.3 and 10.4 which show the type of landing for which each site is used. Runway data for each landing site giving the location, elevation, orientation, and length of each runway are listed in Table 10.6.

10.5 EARTH GRAVITY

Since the Earth's internal mass distribution is not homogeneous and its shape is not spherical, the geopotential is commonly expressed as a series of spherical harmonics.

For the geocentric equatorial inertial reference frame, the generalized form of the geopotential function, Φ, for a mass point, m < < M, exterior to the Earth is represented by:

$$\Phi_{\oplus} = \frac{\mu_{\oplus}}{r}\left[1 + \sum_{n=1}^{\infty}\sum_{m=0}^{n}\left(\frac{R_{eq}}{r}\right)^{n} \varrho_{nm}(\sin\phi)\,(C_{nm}\cos m\lambda + S_{nm}\sin m\lambda)\right] \quad (1)$$

Where:
- $\mu_{\oplus}$ = $GM_{\oplus}$
- G = Newtonian Gravitational Constant
- $M_{\oplus}$ = Mass of the Earth
- r = Distance of mass point from Earth's center of mass = $\left(x^2 + y^2 + z^2\right)^{\frac{1}{2}}$
- $\varrho_{nm}(\sin\phi)$ = associated Legendre functions (degree n, order m)
- ϕ = geocentric latitude of mass point = $\sin^{-1}\left(\frac{z}{r}\right)$
- R_{eq} = Earth's Equatorial Radius
- C_{nm}, S_{nm} = Tesseral Harmonic Coefficients ($n \neq m$) = Sectorial Harmonic Coefficients ($n = m$)
- λ = longitude of the mass point

Zonal harmonics correspond to m = o. If the zonal harmonic coefficients are defined as $J_n = -C_{no}$, then equation (1) can be separated to account for the zonal and tesseral effects as follows:

$$\Phi_{\oplus} = \frac{\mu_{\oplus}}{r}\left[1 - \sum_{n=2}^{\infty}\left(\frac{R_{eq}}{r}\right)^{n} J_n\varrho_n(\sin\phi) + \sum_{n=2}^{\infty}\sum_{m=1}^{n}\left(\frac{R_{eq}}{r}\right)^{n}(C_{nm}\cos m\lambda + S_{nm}\sin m\lambda)\,\varrho_{nm}(\sin\phi)\right] \quad (2)$$

Where : $\varrho_n(\sin\phi) = \varrho_{no}(\sin\phi)$ are Legendre polynomials

The n=1 term is absent due to the origin of the reference frame being the Earth's center of mass.

The Legendre polynomials may be computed from Rodrigues' formula

$$\varrho_n(u) = \frac{1}{2^n n!}\,\frac{d^n\left(u^2 - 1\right)^n}{du^n}\;;\; u = \sin\phi$$

or a recursion formula

$$\varrho_{n+1}(u) = 2u\,\varrho_n(u) - \varrho_{n-1}(u) - \frac{\left[u\varrho_n(u) - \varrho_{n-1}(u)\right]}{(n+1)}$$

The first 7 terms are:

$$\varrho_0(u) = 1$$
$$\varrho_1(u) = \sin\emptyset$$
$$\varrho_2(u) = \frac{1}{2}\left(3\sin^2\emptyset - 1\right)$$
$$\varrho_3(u) = \frac{1}{2}\left(5\sin^3\emptyset - 3\sin\emptyset\right)$$
$$\varrho_4(u) = \frac{1}{8}\left(35\sin^4\emptyset - 30\sin^2\emptyset + 3\right)$$
$$\varrho_5(u) = \frac{1}{8}\left(63\sin^5\emptyset - 70\sin^3\emptyset + 15\sin\emptyset\right)$$
$$\varrho_6(u) = \frac{1}{16}\left(231\sin^6\emptyset - 315\sin^4\emptyset + 105\sin^2\emptyset - 5\right)$$

The associated Legendre functions may be computed by:

$$\varrho_{nm}(u) = \frac{\left(1-u^2\right)^{\frac{m}{2}}}{2^n n!}\,\frac{d^{n+m}\left(u^2-1\right)^m}{du^{n+m}}$$
$$\therefore \varrho_{nm}(u) = \left(1-u^2\right)^{\frac{m}{2}}\,\frac{d^m\varrho_n(u)}{du^m}$$

or by

$$\varrho_{nm}(u) = 2^{-n}\left(1-u^2\right)^{\frac{m}{2}}\sum_{k=0}^{\ell}(-1)^k\frac{(2n-2k)!}{k!(n-k)!(n-m-2k)!}u^{n-m-2k}$$

where ℓ is either $\frac{n-m}{2}$ or $\frac{n-m-1}{2}$, whichever is an integer.

Note that since $u = \sin\emptyset$, then $\left(1-u^2\right)^{\frac{m}{2}} = \cos^m\emptyset$. These functions through degree $n = 4$ and order $m = 4$ are :

$$\varrho_{11}(u) = \cos\emptyset \qquad \varrho_{41}(u) = \frac{1}{2}\cos\emptyset\left(35\sin^3\emptyset - 15\sin\emptyset\right)$$

$$\varrho_{21}(u) = 3\cos\emptyset\sin\emptyset \qquad \varrho_{42}(u) = \frac{1}{2}\cos^2\emptyset\left(105\sin^2\emptyset - 15\right)$$

$$\varrho_{22}(u) = 3\cos^2\emptyset \qquad \varrho_{43}(u) = 105\cos^3\emptyset\sin\emptyset$$

$$\varrho_{31}(u) = \frac{1}{2}\cos\emptyset\left(15\sin^2\emptyset - 3\right) \qquad \varrho_{44}(u) = 105\cos^4\emptyset$$

$$\varrho_{32}(u) = 15\cos^2\emptyset\sin\emptyset$$

$$\varrho_{33}(u) = 15\cos^2\emptyset \qquad \varrho_{no}(u) \equiv \varrho_n(u)$$

Zonal harmonics depend only on latitude and are a consequence of oblateness. They are therefore dependent only on that mass distribution which is symmetric about the Earth's north-south axis. Since the Earth closely approximates an oblate spheroid, the geopotential function can be expressed by considering only the zonal harmonic corrections:

$$\Phi_\oplus \approx \frac{\mu_\oplus}{r}\left[1 - \sum_{n=2}^{\infty}\left(\frac{R_{eq}}{r}\right)^n J_n\varrho_n(\sin\emptyset)\right] \quad (3)$$

or,

$$\Phi_\oplus \approx \frac{\mu_\oplus}{r}\left[1 - \emptyset_2 - \emptyset_3 - \emptyset_4 - \emptyset_5 - \emptyset_6 - \epsilon\right] \quad (4)$$

Where :

$$\emptyset_2 = \left(\frac{R_{eq}}{r}\right)^2\frac{J_2}{2}\left(3\sin^2\emptyset - 1\right)$$

$$\emptyset_3 = \left(\frac{R_{eq}}{r}\right)^3\frac{J_3}{2}\left(5\sin^3\emptyset - 3\sin\emptyset\right)$$

$$\emptyset_4 = \left(\frac{R_{eq}}{r}\right)^4\frac{J_4}{8}\left(35\sin^4\emptyset - 30\sin^2\emptyset + 3\right)$$

$$\emptyset_5 = \left(\frac{R_{eq}}{r}\right)^5\frac{J_5}{8}\left(63\sin^5\emptyset - 70\sin^3\emptyset + 15\sin\emptyset\right)$$

$$\emptyset_6 = \left(\frac{R_{eq}}{r}\right)^6\frac{J_6}{16}\left(231\sin^6\emptyset - 315\sin^4\emptyset + 105\sin^2\emptyset - 5\right)$$

$$\epsilon = \text{Higher Order Terms}$$

For ascent trajectory analysis, usually equation (4) is used with only the first four terms. Sometimes, the second, third, and fourth zonal harmonic coefficients are designated by J, H, K which are related to J_2, J_3, J_4 as follows:

$$J = \frac{3}{2} J_2$$

$$H = + \frac{5}{2} J_3$$

$$K = - \frac{30}{8} J_4$$

The gravitational acceleration vector in the Earth-Centered Inertial (ECI) frame is given by:

$$\bar{g} = \ddot{\bar{r}}_G = \nabla \Phi_\oplus = \frac{d\Phi_\oplus}{dx} \bar{I} + \frac{d\Phi_\oplus}{dy} \bar{J} + \frac{d\Phi_\oplus}{dz} \bar{K}$$

where $\bar{I}$, $\bar{J}$, $\bar{K}$ are unit vectors along the x_I, y_I, z_I axes of the ECI frame.

This can be written as:

$$\begin{bmatrix} \ddot{x}_G \\ \ddot{y}_G \\ \ddot{z}_G \end{bmatrix} = \begin{bmatrix} \frac{d\Phi_\oplus}{dx} \\ \frac{d\Phi_\oplus}{dy} \\ \frac{d\Phi_\oplus}{dz} \end{bmatrix} \quad (5)$$

Therefore, based on eq. (4) for Φ,

$$\ddot{x}_G = -\frac{\mu_\oplus x}{r^3}\left[1 + \frac{3}{2}\left(\frac{R_{eq}}{r}\right)^2 J_2\left(1 - 5\sin^2\phi\right) + \frac{5}{2}\left(\frac{R_{eq}}{r}\right)^3 J_3\left(3\sin\phi - 7\sin^3\phi\right)\right.$$
$$- \frac{5}{8}\left(\frac{R_{eq}}{r}\right)^4 J_4\left(3 - 42\sin^2\phi + 63\sin^4\phi\right) - \frac{3}{8}\left(\frac{R_{eq}}{r}\right)^5 J_5\left(35\sin\phi -\right.$$
$$\left.210\sin^3\phi + 231\sin^5\phi\right) + \frac{1}{16}\left(\frac{R_{eq}}{r}\right)^6 J_6\left(35 - 945\sin^2\phi + 3465\sin^4\phi -\right.$$
$$\left.\left.3003\sin^6\phi\right)\right]$$

$$\ddot{y}_G = \frac{y}{x}\ddot{x}_G$$

$$\ddot{z}_G = -\frac{\mu_+ z}{r^3}\left[1 + \frac{3}{2}\left(\frac{R_{eq}}{r}\right)^2 J_2\left(3 - 5\sin^2\phi\right) + \frac{5}{2}\left(\frac{R_{eq}}{r}\right)^3 J_3\left(6\sin\phi - 7\sin^3\phi\right)\right.$$
$$- \frac{5}{8}\left(\frac{R_{eq}}{r}\right)^4 J_4\left(15 - 70\sin^2\phi + 63\sin^4\phi\right) - \frac{3}{8}\left(\frac{R_{eq}}{r}\right)^5 J_5\left(105\sin\phi -\right.$$
$$\left.315\sin^3\phi + 231\sin^5\phi\right) + \frac{1}{16}\left(\frac{R_{eq}}{r}\right)^6 J_6\left(245 - 2205\sin^2\phi + 4851\sin^4\phi -\right.$$
$$\left.\left.3003\sin^6\phi\right)\right] + \frac{\mu_\oplus}{r^2}\left[\frac{3}{2}\left(\frac{R_{eq}}{r}\right)^3 J_3 - \frac{15}{8}\left(\frac{R_{eq}}{r}\right)^5 J_5\right]$$

The recommended values of the Earth gravity constants to be used with this model are tabulated in Table 10.7. They are the values currently specified for Shuttle onboard GN&C calculations (STS83-0005. Functional Subsystem Software Requirements, Navigation Ascent/RTLS, September 19, 1996) with the exceptional that J_5 through J_{10} are not used. Note that the gravitational reference radius, Rg, is denoted by Req in the above equations, but the value is not the same (intentionally) as the equatorial radius, Re, given in Table 10.2.

10.6 AERODYNAMICS

Aerodynamic data are available for the Shuttle Vehicle in its various flight configurations.

For the Orbiter Vehicle entry aerodynamic data, refer to STS85-0118, Operational Aerodynamic Design Data Book, Volume III, Orbiter Vehicle. For aerodynamic data on the Orbiter Vehicle mated with the ET and SRB, refer to STS85-0118, Volumes II and V, Launch Vehicle. STS85-0118, Volume 1, documents the equations for correct aerodynamic data usage.

To ease computational usage, Orbiter data are stored in the standard GEMASS format in card image files on the EFCA1 system. The files are accessible per the ECFA1 secured files shown below:

Description	Format	Absolute UNIX Path Name
Orbiter Rigid	GEMASS ASCII	/pa/carvajal/alpha/shuttle/entry/oadb96rigid
Orbiter RCS	GEMASS ASCII	/pa/carvajal/alpha/shuttle/entry/oadb96rcs
Orbiter Flexible	GEMASS ASCII	/pa/carvajal/alpha/shuttle/entry/oadb96flex
Orbiter Uncertainty	GEMASS ASCII	/pa/carvajal/alpha/shuttle/entry/oadb96unc

Ascent vehicle aerodynamics and airloads for the Orbiter, ET, and SRB components are provided in STS85-0118, Volumes I, II, IV, and V. These data are available electronically in controlled access data files at Boeing Reusable Space Systems (B-RSS)/ Huntington Beach. Database file names and formats are available in the CMMD.

A review of the data books should be made prior to using the listed files so that the user will be aware of the data limits of the various parameters. In addition, the format of the data files should be reviewed with aerodynamic personnel at NASA/Applied Aeroscience and CFD Branch and/or B-RSS/Huntington Beach to make optimal use of each file. There may exist a number of data files constructed for use in flight simulation analyses or airloads data files not mentioned above. Prior to the usage of any Shuttle aerodynamic or airloads data files not mentioned above, the user should consult with the Aerodynamics Subsystem managers at NASA/Applied Aeroscience and CFD Branch or B-RSS/Huntington Beach Aerodynamics to assure that the files are based on the current database.

10.7 MASS PROPERTIES

The primary sources of SSP mass properties data are the current issues of NSTS 09095 and NSTS 08934, Volume II.

The Space Shuttle Launch Vehicle (SRBs + Orbiter + ET) envelopes a total volume of 148,200 ft^3 (V_{bouy}) so that there is a buoyancy force by the air which acts opposite to that of the vehicle's weight vector. This force is given by:

$F_{bouy} = V_{bouy} * \varrho\ air * g$

Where: ϱ air - ambient air density
g - acceleration due to gravity

Some of the volume enclosed by the Shuttle Vehicle is vented to the ambient atmosphere. This volume, V_{vent}, amounts to 39,217 ft^3 and contains a mass of air which is accelerated along with the rest of the vehicle mass by the Shuttle's propulsion system. This mass must therefore be added to the mass of the vehicle hardware for the equations of motion and is determined as follows:

$M_{vent} = V_{vent} * \varrho\ air$

Typical effects of buoyancy and vented volume on trajectory parameters for nominal ascent are summarized in Table 10.8.

There are certain non-propulsive consumables which are depleted and should be accounted for in the determination of vehicle mass during ascent. This includes ice and frost, liquid air, liquid nitrogen and water in the TPS, SSME helium purge, APU propellant, flash evaporator water, and ET ice/ablation. These are combined to provide an average mass depletion rate of these items as follows:

ET-1 through ET-50
Lift-off to SRB separation: 1.64 lb/sec
SRB separation to MECO: 0.759 lb/sec

The total integrated Shuttle Systems losses to MECO is 503 pounds. If this total is found to be expended prior to MECO, then the rate is to be set to zero.

ET-51 through ET-90
Lift-off to SRB separation: 1.72 lb/sec
SRB separation to MECO: 0.836 lb/sec

The total integrated Shuttle Systems losses to MECO is 543 pounds. If this total is found to be expended prior to MECO, then the rate is to be set to zero.

ET-91 through ET-999
Lift-off to SRB separation: 3.584 lb/sec
SRB separation to MECO: 0.787 lb/sec

The total integrated Shuttle Systems losses to MECO is 743 pounds. If this total is found to be expended prior to MECO, then the rate is to be set to zero.

10.7.1 Mass Properties - MECO Command Through MPS Dump

From MECO Command through the end of the MPS Dump sequence, the mass properties of the Shuttle/Orbiter are affected by the Thrust Tail-off profiles, the Initial Shutdown

Throttle level, a Helium POGO injection, valve closure leakage, venting, the pressurized MPS Dump, and vacuum inerting.

MECO Command through MECO Command + 8 Seconds:

Table 5.4.1 of NSTS 08209, Volume I provides the shutdown characteristics from 65% and 67% throttle levels. The 67% thrust is the throttle level for no fail and RTLS aborts. The data in Table 5.4.1 is for each SSME.

In order to model the shutdown consumption correctly, the simulation must multiply the Total shutdown flow amount by the columns in Table 5.4.1 labeled Total LH_2 flow and Total LO_2 flow, respectively, as time increases following MECO Command. The shutdown consumption amounts are then subtracted from the total liquid LH_2 and LO_2 quantities that were present at MECO Command. There is no integration to be performed. The columns labeled LH_2 flow rate and LO_2 flow rate are for information only and should not be integrated to obtain shutdown consumptions, since the shutdown consumption profile is non-linear.

Table 5.4.2 of NSTS 08209, Volume I provides the shutdown characteristics from 91% throttle. The 91% thrust is the throttle level for TAL, PTA and PTM aborts, with one SSME failed. The same procedure of multiplying the Total shutdown flow amounts by the columns labeled Total LH_2 flow and Total LO_2 flow, as time increases, is to be followed.

Depending on whether MECO is a guided MECO or a low level shutdown, the amount of propellant remaining in the ET lines and the Orbiter lines will vary. If the propellant in the ET lines at MECO Command is more than the Total shutdown consumption, then the propellant in the Orbiter lines will be replenished. If the propellant in the ET lines is not enough to replenish the shutdown consumption, then the propellant in the Orbiter lines will decrease during tail-off.

Total propellant in Orbiter lines at MECO Command + 8 seconds = Orbiter lines propellant at MECO Command - Shutdown Consumption + Propellant in ET lines. If Total propellant in Orbiter lines at MECO Command + 8 seconds > Orbiter lines propellant at MECO Command, then Total propellant in Orbiter lines at MECO Command + 8 seconds = Orbiter lines propellant at MECO Command.

MECO Command + 8 seconds through ET Separation Period:

NSTS 08209, Volume I provides MPS Propellant Dump Performance Summaries for no fail, AOA/ATO, TAL, and RTLS Abort. Table Numbers are 4.1.10 through 4.1.13. Propellant quantities lost during MECO Command + 8 seconds through ET separation are provided in the top half of the summaries. Table 4.1.10, the no-fail trajectory data, can be used as an example.

Propellant mass at MECO, is the propellant in the Orbiter lines + SSME x 3. A value of 4802 lb_m is provided for the guided MECO case, where there is enough propellant in the ET lines to replenish the Orbiter lines during shutdown. Footnote a of the table provides a value of 4052 lb_m for the LLCO case. The actual value of propellant mass at MECO can be anywhere in between, depending on how much propellant was remaining in the ET lines, when the guided MECO was commanded.

For the LLCO case, the minimum amount of propellant mass remains in the Orbiter lines, because the propellant at MECO Command is reduced by the amount of the shutdown consumption during the MECO Command + 8 seconds time period. Therefore, the 4,052 lb_m of LO_2 at MECO Command is reduced by the appropriate mass in Table 5.3 to give a lower mass at MECO + 8 seconds. The LH_2 system has a Fuel Bias added to the ET propellant, therefore the Orbiter lines LH_2 propellant for the Guided MECO case and the low level case can be assumed to be full at all times.

Vented after SSME Valve Closure, is the propellant lost from the SSMEs following tail-off. This reduces the propellant remaining in the SSME x 3. The quantity in the SSME x 3 is provided in the MPS Propellant Inventory Load Sheets in NSTS 08209, Volume I. For example, in the R9702L inventory, the 1498 lb_m of LO_2 reduces to 1326 lb_m; and the 116 lb_m of LH_2 reduces to 58 lb_m. The quantities for the one SSME out Abort case are reduced, since one of the three SSMEs is closed off prior to MECO Command + 8 seconds. For the one SSME out Abort cases, the quantities are equivalent to 2/3 of the no-fail (three SSME shutdown) values. For a Single Engine Abort case, the quantities would be 1/3 of the no-fail values.

Helium POGO Injection (10 ft^3), is the quantity of LO_2 displaced from the Orbiter lines back into the ET (LO_2 line), at MECO + 8 seconds, for the Guided MECO case, assuming there was enough propellant in the ET (LO_2 line) to replenish the shutdown consumption. The value is 710 lb_m. If the Orbiter line is not full at MECO + 8 seconds, then a reduced amount of LO_2 is displaced back into the ET. If the propellant mass at MECO + 8 seconds = 4802 lb_m (LO_2), then 710 lb_m is displaced. For less propellant remaining at MECO + 8 seconds, the 710 lb_m is reduced by the same amount. For the one SSME out Abort cases, the quantity is reduced to 2/3 of the no-fail quantity (473 lb_m). For a Single Engine Abort case, the quantity would be 1/3 of the no-fail quantity (236 lb_m). Helium POGO Injection reduces the propellant remaining in the SSME x 3 and increases the propellant remaining in the Orbiter lines and/or ET.

Disconnect Closure (0.7 ft^3), is the propellant lost between the ET valves and Orbiter valves at the ET/Orbiter interface. Volume of the space between the valves, on the Orbiter side = 0.7 cu. ft. The value is 50 lb_m and assumes that enough propellant was in the ET lines to replenish the Orbiter lines during shutdown. If the Orbiter lines are

not completely full at MECO Command + 8 seconds, then the Disconnect Closure value is reduced accordingly. A low level shutdown case will therefore have no Disconnect Closure value on the LO_2 side. Disconnect Closure reduces the propellant remaining in the Orbiter lines.

Propellant mass at ET separation, is the propellant at MECO Command + 8 seconds, minus the quantities vented after SSME valve closure, minus the Helium POGO injection displacement quantities, minus the Disconnect Closure amount.

ET separation through MPS Dump Complete Period:

High Pressure Oxidizer Turbopump (HPOTP) seal leakage (120 seconds), is the amount of LO_2 that leaks over the 120 second period from ET separation to the start of the MPS Dump. The 270 lb_m of LO_2 for the no-fail case can be modeled as a leak with a flow rate of 270 lb_m per 120 seconds, starting at ET separation. HPOTP seal leakage reduces the propellant remaining in the SSME x 3.

LH_2 Feedline Venting (110 seconds), is the amount of LH_2 vented from ET separation to the start of the MPS dump. The 157 lb_m of LH_2 for the no-fail case can be modeled as a leak with a flow rate of 157 lb_m per 110 seconds, starting after Tail-off. LH_2 Feedline Venting reduces the propellant remaining in the LH_2 Orbiter lines.

Propellant mass at start of dump, is the propellant mass at ET separation minus the HPOTP seal leakage and the LH_2 Feedline Venting. The HPOTP and LH_2 Feedline Venting should be considered non-propulsive. The propellant quantities at the start of the dump are used to look up the starting total value of the propellant, to be used by the MPS Dump force and flowrate model, documented in the CMMD, CMM-00067, MPS dump and Vacuum Inerting (MPS-17).

Propellant mass at end of dump, is the propellant remaining at the end of the pressurized MPS dump. Less than 200 lb_m of LO_2 remains and less than 4 lb_m of LH_2 remains, at the completion of the dump.

Fill/Drain line vacuum inerting performed after the pressurized MPS dump, vents the remaining propellant to space. Following the vacuum inerting, no propellant remains.

10.8 PROPULSION

The basic data for the Space Shuttle propulsion systems, consisting of the MPS, RSRM, OMS, and RCS, are provided in Section 5.0.

A nonlinear model is used to adjust the SSME thrust, propellant flow rates, specific impulse, and propellant MR whenever the SSME power level is other than the RPL. The adjusted value, y_i, of the parameter is the sum of the tag value, $\bar{y}_i$, of the parameter at 100% RPL and the computed adjustment, Δy_i, of the parameter:

$$y_i = \bar{y}_i + \Delta y_i$$

The value of Δy_i is computed from the following polynomial:

$$\Delta y_i = A_{i1}(\rho - 1) + A_{i2}\left(\rho^2 - 1\right) + A_{i3}\left(\rho^3 - 1\right)$$

Where : i = parameter index

A_{i1}, A_{i2}, A_{i3} = influence cofficients (Table 10.9.1)

ρ = power level $\left(\frac{\% \text{ RPL}}{100}\right)$

The influence coefficients for the Block II/IIA SSMEs are listed in Table 10.9.1.

Based on these equations, the final adjusted values of the following individual SSME performance parameters are computed:

Thrust : $F = \overline{F} + \Delta F$

Liquid propellant flow rate : $\dot{W}_O = \dot{W}_O + \Delta\dot{W}_O$, $\dot{W}_H = \overline{\dot{W}}_H + \Delta\dot{W}_H$

Gaseous propellant flow rate : $\dot{W}_{GO_2} = \overline{\dot{W}}_{GO_2} + \Delta\dot{W}_{GO_2}$, $\dot{W}_{GH_2} = \overline{\dot{W}}_{GH_2} + \dot{W}_{GH_2}$

Overboard flow rate : $\left(\dot{W}_O\right)_{O/B} = \dot{W}_O - \dot{W}_{GO_2}$, $\left(\dot{W}_H\right)_{O/B} = \dot{W}_H - \dot{W}_{GH_2}$

Specific impulse : $Isp = \dfrac{F}{\left[\left(\dot{W}_O\right)_{O/B} + \left(\dot{W}_H\right)_{O/B}\right]}$

Mixture ratio : $MR = \dfrac{\left(\dot{W}_O\right)_{O/B}}{\left(\dot{W}_H\right)_{O/B}}$

Chamber Pressure : $P_c = \overline{P}_c + \Delta P_c$

Nozzle Exit Area : $A_{EX} = \overline{A}_{EX} + \Delta A_{EX}$

10.9 ASCENT GN&C

The sources for the modeling of the Ascent GN&C software and hardware are the following Flight Subsystem Software Requirements (FSSR) documents: STS83-0002 (Guidance), STS83-0005 (Navigation), STS83-0008 (Flight Control), STS83-0010 (Redundancy Management), STS83-0015 (Sensor/Controller SOPs), STS83-0016 (Effector SOPs), and STS83-0026 (Sequencing), as well as Sections 6.0 and 9.0 of this volume. Additional sources include the CMMD and SSD92D0673A, GN&C Databook.

10.10 NONRIGID BODY EFFECTS

During ascent, the Orbiter structure deflects under the combined effect of thrust, inertia forces, aerodynamic forces, and differential pressures. As a result, some Orbiter hardware elements change their alignments relative to the ET centerline in ways which can affect the trajectory. These elements include the elevons, the SSME nozzles, the Inertial Measurement Unit (IMUs), and the Accelerometer Assemblies (AAs). This section discusses some of the details of the math models developed to account for these nonrigid body effects.

10.10.1 Elevon Aeroelastic Deformation

Aerodynamic force and moment coefficients and elevon hinge moments are dependent on Orbiter elevon position. Conversely, the elevon deflections depend on elevon hinge moments because elevons behave elastically under load. This interdependence between hinge moments and elevon deflections is resolved by using commanded elevon positions to compute the rigid body part of the hinge moment coefficient and the sensitivity of hinge moment coefficient to changes in elevon position. The final flexed elevon positions are used in calculating the aerodynamic force and moment coefficients.

The total inboard/outboard elevon hinge moment is computed from the following equation:

$$HM_{e_{TOTAL_{I(0)}}} = C_{h_{e_{TOTAL_{I(0)}}}} q S_e C_e \quad (1)$$

Where : q is the dynamic pressure $\left(\frac{1}{2} \varrho \text{ air } V_{00}{}^2\right)$

S_e is the reference area $\left(210 \text{ ft}^2\right)$

C_e is the reference length (90.7 in.)

The total inboard/outboard elevon hinge moment coefficient is given by:

$$C_{h_{e_{TOTAL_{I(0)}}}} = C_{h_{e_{I(0)}}} + \Delta C_{h_{e_{I(0)}}} + \Delta C_{h_{e_{FLEX_{I(0)}}}} \quad (2)$$

Where :

$C_{h_{e_{I(0)}}}$ is the rigid body inboard/outboard elevon hinge moment coefficient tabulated in STS85-0118, Volume 2.

$\Delta C_{h_{e_{I(0)}}}$ is the change in elevon hinge moment coefficient due to rigid body deflection of the inboard/outboard panel.

$\Delta C_{h_{e_{FLEX_{I(0)}}}}$ is the change in elevon hinge moment coefficient due to elevon aeroelastic deformation.

The second term in eq. (2) is determined from the following polynomial:

$$\Delta C_{he_{I(0)}} = Bx + Cx^2 + Dy + Exy + Fy^2 \quad (3)$$

Where: B, C, D, E, F are tabulated for both inboard and outboard elevons in STS85-0118, Volume II.

$$x = \delta_{e_{I\,OFF\,NOM}} - \delta_{e_{I\,NOM}}$$
$$y = \delta_{e_{o\,OFF\,NOM}} - \delta_{e_{o\,NOM}}$$

$\delta_{e_{I\,OFF\,NOM}}$, $\delta_{e_{o\,OFF\,NOM}}$ are the current values of the inboard and outboard elevons.

$\delta_{e_{I\,NOM}}$, $\delta_{e_{o\,NOM}}$ are the reference values of the inboard and outboard elevons obtained from wind tunnel tests.

The sensitivities of hinge moment coefficients to inboard and outboard elevon deflection changes are:

$$C_{he_{I\delta_{eo}}} = D + Ex + 2\,Fy \quad (4)$$
$$C_{he_{I\delta_{ei}}} = B + 2\,Cx + Ey \quad (5)$$
$$C_{he_{o\delta_{eo}}} = D + Ex + 2\,Fy \quad (6)$$
$$C_{he_{o\delta_{ei}}} = B + 2\,Cx + Ey \quad (7)$$

Where: B, C, D, E, F, x, y are as defined above.

The total inboard/outboard flexible elevon hinge moment coefficient is given by:

$$C_{he_{TOTAL\ FLEX_{I(0)}}} = \frac{G_{I(0)}}{H} \quad (8)$$

$$\text{Where : } G_I = -\left(C_{he_o} + \Delta C_{he_o}\right) I - \left(C_{he_i} + \Delta C_{he_i}\right)(1 - J)$$

$$G_O = -\left(C_{he_i} + \Delta C_{he_i}\right) L - \left(C_{he_o} + \Delta C_{he_o}\right)(1 - M)$$

$$H = I * L - (1 - M)(1 - J)$$

$$I = C_{he_I \delta_{e_o}} K_o q S_e C_e$$

$$J = C_{he_o \delta_{e_o}} K_o q S_e C_e$$

$$L = C_{he_o \delta_{e_I}} K_I q S_e C_e$$

$$M = C_{he_I \delta_{e_I}} K_I q S_e C_e$$

K_I – inboard elevon spring constant $\left(1.547 \times 10^{-6} \text{ deg/in.lb}\right)$

K_o – outboard elevon spring constant $\left(3.323 \times 10^{-6} \text{ deg/in.lb}\right)$

The change in elevon deflection due to aeroelastic deformation is then determined from the following:

$$\Delta \delta_{e_{FLEX_{I(0)}}} = K_{I(0)} q S_e C_e C_{he_{TOTAL}}{}_{FLEX_{I(0)}} \qquad (9)$$

The total flexed elevon deflection is obtained by summing the rigid body deflection and the change in deflection due to aeroelastic deformation:

$$\delta_{e_I}^{F}{}_{(0)} = \delta_{e_{I(0)}} + \delta_{e_{FLEX_{I(0)}}} \qquad (10)$$

These total elevon deflections are to be used in computing elevon position corrections for the six longitudinal and lateral-directional aero coefficients.

10.10.2 Thrust Structure Deformation Effects on SSME Gimbal Angles

A model was developed to calculate SSME nozzle deflections due to elastic deformation of the MPS thrust structure cause by thrust and inertial loads during ascent. The model is based on structural analysis results with the following assumptions:

a. OV-102 structure.

b. No engine failures.

c. All three engines at same power level and angular displacement with respect to null.

d. Deflections due to inertial loads are directly proportional to acceleration.

e. The effect of lateral acceleration is insignificant.

f. Gimbal deflection rage is within five degrees of null.

The differences in the elasticity of the thrust structures of the various Orbiter Vehicles are considered to have an insignificant effect (in the order of ± .02 degree) on the predicted changes in SSME gimbal angles. The model consists of a second order equation as detailed in Table 10.10. This model is to be used in all SSP ascent analyses.

10.10.3 Effect of Crew Module Deformation on AAs and IMU

The Orbiter AAs and IMU acquire pitch misalignments during ascent due to bending of the crew module structure to which they are attached. Longitudinal pitch plane bending of the Orbiter, relative to its ideal alignment with the ET, has been calculated using post-flight loads data. The resulting rotation, or slope (Θ_{bend}), of the crew module is shown in Figure 10-1. These data have been modelled by a series of straight-line segments expressed by the following table:

MET (sec)	0	50	70	≥120
Θ_{Bend} (deg)	.25	-.04	.11	.25

A positive Θ_{bend} is a positive rotation about the + y body axis.

The pitch plane alignment of the AAs is influenced not only by the longitudinal bending but also to bulkhead deflection caused by the differential pressure between the crew module and surrounding Orbiter compartments. The effect due to this pressure differential, $\Delta \varrho$, is given by:

$$\theta_{press} = 0.0211 \text{ deg/psi} * \Delta \varrho \text{ (psi)}$$

The sense of rotation is the same as for Θ_{bend}. The pressure differential can be computed from:

$$\Delta \varrho = 15 \text{ psi} + \Delta \varrho_A$$

Where: $\Delta \varrho_A$ is the difference between the pressure in the adjacent forward RCS compartment and the ambient pressure. This correction can reduce errors to about 0.2 psi and 0.004 degree and is given by:

MET (sec)	0	45	60	70	100	≥120
ϱ_A (psi)	0	.35	1.6	1.8	.3	0

During first stage, guidance commands a predetermined attitude history so that any error in the IMU information induces an error in vehicle attitude. This manifests itself in the body axis Attitude Error Vector (EBFB) computed by GC_STEER as actual minus desired. Thus, to simulate IMU pitch misalignment, the angle $\Delta\,\Theta_{bend}$ should be added to the second component of EBFB. IMU misalignment in second stage has no significant effect.

Pitch misalignment of the AAs affects the ascent trajectory only during load relief (approximately 25 to 90 seconds MET) by causing the z-accelerometer to pick up a component of x-acceleration. This effect is simulated by adding the following increment to the z-accelerometer output prior to quantization:

$$\Delta N_z = -N_x \sin\left(\Delta\Theta_{bend} + \Delta\Theta_{press}\right)$$

10.10.4 Second Stage Crew Vibration Analysis

This section describes second stage crewseat vibration predictions. Crewseat vibrations during second stage are caused by fluctuations in SSME thrust. A prediction of this vibration was made by applying SSME thrust oscillation forces to a coupled Shuttle math model with the Orbiter having a detailed crew cabin and mission specific payload. The responses of the crew cabin floor and crewseats were computed and compared to the human sensitivity range (reference Shock and Vibration Handbook).

All preflight predictions for STS-26 through STS-41, and STS-43 have been grouped into two categories. All IUS payloads “which are mounted” in a cradle in the payload bay, produce low vibration predictions which are imperceptible to humans. All other payloads produce higher vibration predictions which are within the range of human perception. For these payloads, the predicted responses decrease as the Payload CG moves aft. ICD limits restricting Payload CG preclude the possibility of reaching levels of vibration which are unpleasant to humans (as shown in Figure 10-3 entitled Predicted Crew Vibration as a Function of Payload CG). Furthermore, crewseat vibrations of the magnitude and duration predicted in these analyses do not affect astronaut work proficiency, nor do they compromise crew health and safety. The vibrations do not present any systems stability or loads concerns.

10.11 SRB TAIL-OFF PITCH MOMENT

This section describes a flight derived model of a pitch moment present in the region of SRB tail-off. It has been observed consistently since the start of the Shuttle Program. The phenomena is suspected to be due in part to interaction between the SRB and Main Engine thrust plumes and has been verified in part by analysis of wind tunnel data. For a complete discussion of the aerodynamics, see Rockwell Letter 90MA2300.

The model was derived by reconstruction of flight response using data from STS-11 through STS-61C. The effect appears to be relatively independent of variations in trajectory conditions (altitude or dynamic pressure). The magnitude and shape of the observed moment varies slightly from flight-to-flight but generally by no more than 10%.

The tail-off pitch moment model is intended for use in simulations for flight design, preflight prediction and design verification, and for post-flight reconstruction activities. It is implemented as a table of incremental pitch moment as a function of the total SRB thrust level (sum of the left and right motors) and should be activated as the tail-off region is approached.

Data for this model are given in Table 10.11 and shown graphically in Figure 10-2.

THIS PAGE INTENTIONALLY LEFT BLANK

TABLE 10.1 (DELETED)

TABLE 10.2
EARTH GEOMETRY AND ROTATION CONSTANTS

	Fischer 1960[1]	WGS–84[2]
– Equatorial radius, Re	6,378,166. m	6.378,137. m
	20,925,741.47 ft	20,925,646.33 ft
– Polar radius, Rp	20,855,591.48 ft	20,855,486.59 ft
– Flattening, 1/f	298.3	298.2572236
– Eccentricity, e	0.0818133340	0.0818191908
– Rotation rate, ω_I wrt. inertial equinox	$7.29211514646 \times 10^{-5}$ rad/sec	$7.29211514671 \times 10^{-5}$ rad/sec

[1] Fischer Ellipsoid is also denoted by Mercury 1960. The values in this column are used for Shuttle onboard navigation calculations.

[2] WGS 1984. Used by GPS. Rotation rate for J2000 epoch.

TABLE 10.3

RUNWAY SUMMARY FOR ETR LAUNCHES TO 28.45-DEGREE INCLINATION (a) OPS-3 AREAS

Land Site	Name	Location	RW ID	Function
1	KSC	Florida	KSC 15 KSC 33	EOM, AOA, ATO, ELS EOM, AOA, ATO, ELS
2	Dakar Amilcar Cabral	Senegal Cape Verde	YOF 01 AML 02	TAL, ELS ELS
3	Moron	Spain	MRN 21 MRN 03	TAL, ELS TAL, ELS
4	Las Palmas Kinshasa	Canary Islands Zaire	GDV 03 KIN 25	ELS ELS
5	Casablanca	Morocco	CAS 35 CAS 17	TAL, ELS TAL, ELS
6	Edwards AFB	California	EDW 22 EDW 17	EOM, AOA, ATO, ELS EOM, AOA, ATO, ELS
7	Honolulu	Hawaii	HNL 08 HNL 26	ELS ELS
8	Northrup	New Mexico	NOR 17 NOR 23	EOM, AOA, ATO, ELS EOM, AOA, ATO, ELS
9	Edwards AFB	California	EDW 23 EDW 15	EOM, AOA, ATO, ELS EOM, AOA, ATO, ELS
10	Edwards AFB Northrup	California New Mexico	EDW 04 NOR 05	EOM, AOA, ATO, ELS EOM, AOA, ATO, ELS
11	Diego Garcia	Chagos Islands	JDG 31 JDG 13	ELS ELS
12	King Khalid Int'l	Saudi Arabia	KKI 15 KKI 33	ELS ELS
13	Anderson AFB	Guam	GUA 06 GUA 24	ELS ELS
14	Darwin Hao Atoll	Australia French Polynesia	DDN 29 HAO 12	ELS ELS
15	Hoedspruit	South Africa	HDS 18 HDS 36	ELS ELS

TABLE 10.3

RUNWAY SUMMARY FOR ETR LAUNCHES TO 28.45-DEGREE INCLINATION - Concluded
(b) OPS-1/6 AREAS

RTLS/TAL Site	Name	Location	RW ID	Function
1	KSC	Florida	KSC 15 KSC 33	RTLS RTLS
2	Dakar Amilcar Cabral	Senegal Cape Verde	YOF 01 AML 02	TAL ELS
3	Moron	Spain	MRN 21 MRN 03	TAL TAL
4	Las Palmas Kinshasa	Canary Islands Zaire	GDV 03 KIN 25	ELS ELS
5	Casablanca	Morocco	CAS 35 CAS 17	TAL, ELS TAL, ELS

TABLE 10.4

RUNWAY SUMMARY FOR ETR LAUNCHES TO 57-DEGREE INCLINATION (a) OPS-3 AREAS

Land Site	Name	Location	RW ID	Function
1	KSC	Florida	KSC 15 KSC 33	EOM, ELS EOM, ELS
2	Zaragoza Diyarbakir	Spain Turkey	ZZA 31 DIY 34	TAL, ELS ELS
3	Moron	Spain	MRN 21 MRN 03	TAL, ELS TAL, ELS
4	Koln/Bonn Brize Norton	West Germany United Kingdom	KBO 32 BZN 26	TAL, ELS TAL, ELS
5	Casablanca	Morocco	CAS 35 CAS 17	ELS ELS
6	Edwards AFB	California	EDW 22 EDW 17	EOM, ATO, ELS EOM, ATO, ELS
7	Honolulu	Hawaii	HNL 08 HNL 26	TAL, ELS TAL, ELS
8	Northrup	New Mexico	NOR 17 NOR 23	EOM, AOA, ELS EOM, AOA, ELS
9	Edwards AFB	California	EDW 23 EDW 15	EOM, ATO, ELS EOM, ATO, ELS
10	Moses Lake	Washington	MWH 14 MWH 32	ELS ELS
11	Diego Garcia	Chagos Islands	JDG 31 JDG 13	ELS ELS
12	King Khalid Int'l	Saudi Arabia	KKI 15 KKI 33	ELS ELS
13	Anderson AFB	Guam	GUA 08 GUA 24	ELS ELS
14	Darwin Sydney	Australia Australia	DDN 29 SSY 16	ELS ELS
15	Hao Atoll Hoedspruit	French Polynesia South Africa	HAO 12 HDS 18	ELS ELS

TABLE 10.4

RUNWAY SUMMARY FOR ETR LAUNCHES TO 57-DEGREE INCLINATION - Concluded

(b) OPS-1/6 AREAS

RTLS/TAL Site	Name	Location	RW ID	Function
1	KSC	Florida	KSC 15 KSC 33	RTLS RTLS
2	Zaragoza Diyarbakir	Spain Turkey	ZZA 31 DIY 34	TAL ELS
3	Moron	Spain	MRN 21 MRN 03	TAL TAL
4	Koln/Bonn Brize Norton	West Germany United Kingdom	KBO 32 BZN 26	ELS ELS
5	Casablanca	Morocco	CAS 35 CAS 17	TAL, ELS TAL, ELS

TABLE 10.5 (DELETED)

TABLE 10.6

RUNWAY DATA

Runway	Latitude (deg)	Longitude (deg)	Altitude Above Ellipsoid (ft)	Geodetic Altitude (ft)	Azimuth (deg N)	Magnetic Variance (deg)	Length (ft)
Edwards (EDW)	04 34.894590	−117.90493	2,118	−186	58.216838	14.18333	26,500
	*05 34.948730	−117.864438	2,086	−184	64.387971	14.18333	26,600
	*15 34.959172	−117.866397	2,085	−184	167.545132	14.8333	31,200
	*17 34.930885	−117.836884	2,087	−185	190.072211	14.8333	39,200
	22 34.916280	−117.862415	2,097	−184	238.241163	14.8333	26,500
	*23 34.966397	−117.819643	2,085	−185	244.413631	14.8333	26,600
	*33 34.917862	−117.855320	2,085	−184	347.551218	14.8333	31,200
	*35 34.847938	−117.854758	2,084	−184	10.06197	14.8333	39,200
Northrup (NOR) (WSMR)	*05 32.932953	−106.447440	3,766	−139	64.448012	11.21667	15,000
	*17 32.960354	−106.417382	3,771	−139	187.242292	11.21667	15,000
	*23 32.950724	−106.403333	3,772	−139	244.471998	11.21667	15,000
	*35 32.919467	−106.423541	3,766	−139	7.238021	11.21667	15,000
Kennedy (KSC)	15 28.632910	−80.706033	−199	−208	149.988296	−2.25000	15,000
	33 28.597180	−80.682650	−199	−208	329.999488	−2.25000	15,000
Dakar (YOF)	01 14.726284	−17.476758	16	−59	352.571055	−12.696667	11,450
	19 14.757563	−17.480949	4	−59	172.571141	−12.696667	11,450

* Lakebed runways; all others concrete with crown.

TABLE 10.6

RUNWAY DATA – Concluded

Runway	Latitude (deg)	Longitude (deg)	Altitude Above Ellipsoid (ft)	Geodetic Altitude (ft)	Azimuth (deg N)	Magnetic Variance (deg)	Length (ft)
Rota	10 36.647088	– 6.369589	102	39	96.727377	– 7.00	12,100
(AOG)	28 36.643200	– 6.328755	100	39	276.751749	– 7.00	12,100
Kadena	05 26.346304	127.751718	48	– 14	51.049134	– 4.00	12,000
(KAD)	23 26.367224	127.780452	114	– 14	231.061887	– 4.00	12,000
Hawaii	08 21.306779	– 157.945832	16	6	89.989777	12.00	12,000
(HNL)	26 21.306781	– 157.910589	17	7	270.002585	12.00	12,000
Zaragoza	13R 41.682295	– 1.079446	893	58	119.502981	– 4.578333	12,196
(ZZA)	31L 41.665906	– 1.040835	921	58	299.528653	– 4.578333	12,196
Koln/Bonn	32 50.855345	7.165009	356	56	318.120130	– 2.44333	12,467
(KBO)	14 50.380623	7.129175	284	56	138.092335	– 2.44333	12,467
Moron	03 37.161269	– 5.622641	318	31	19.982474	– 6.178333	11,800
(MRN)	21 37.191825	– 5.608753	302	31	199.990867	– 6.178333	11,800

* Lakebed runways; all others concrete with crown.

TABLE 10.7

EARTH GRAVITY CONSTANTS

Gravitational constant	μ	$1.40764487566 \times 10^{16}$ ft^3/sec^2
Gravitational reference radius	Rg	6,378,140. m 20,925,656.1680 ft
Reference acceleration of gravity for force/mass conversion	g_0	32.174049 ft/sec^2
Zonal harmonic coefficients		
• 2nd zonal harmonic coefficient	J_2	1082.6271×10^{-6}
• 3rd zonal harmonic coefficient	J_3	$-2.5358868 \times 10^{-6}$
• 4th zonal harmonic coefficient	J_4	$-1.6246180 \times 10^{-6}$
• 5th zonal harmonic coefficient	J_5	-0.210×10^{-6}
• 6th zonal harmonic coefficient	J_6	0.646×10^{-6}
• 7th zonal harmonic coefficient	J_7	-0.333×10^{-6}
• 8th zonal harmonic coefficient	J_8	-0.270×10^{-6}
• 9th zonal harmonic coefficient	J_9	-0.053×10^{-6}
• 10th zonal harmonic coefficient	J_{10}	-0.054×10^{-6}

Tesseral harmonic coefficients

• $C_{21} = -0.00027635957 \times 10^{-6}$	• $S_{21} = -0.0052357454 \times 10^{-6}$
• $C_{22} = 1.5711423 \times 10^{-6}$	• $S_{22} = -0.90231337 \times 10^{-6}$
• $C_{31} = 2.1907694 \times 10^{-6}$	• $S_{31} = 0.27267074 \times 10^{-6}$
• $C_{32} = 0.30466825 \times 10^{-6}$	• $S_{32} = -0.21259298 \times 10^{-6}$
• $C_{33} = 0.097966803 \times 10^{-6}$	• $S_{33} = 0.19681077 \times 10^{-6}$
• $C_{41} = -0.50552749 \times 10^{-6}$	• $S_{41} = -0.44125015 \times 10^{-6}$
• $C_{42} = 0.078842515 \times 10^{-6}$	• $S_{42} = 0.14818958 \times 10^{-6}$
• $C_{43} = 0.059073749 \times 10^{-6}$	• $S_{43} = -0.012140873 \times 10^{-6}$
• $C_{44} = -0.0041542493 \times 10^{-6}$	• $S_{44} = 0.0063163541 \times 10^{-6}$

TABLE 10.8

TYPICAL BUOYANCY AND VENTED VOLUME EFFECTS

	Buoyancy (108,983 ft^3)	Vented Vol (39,217 ft^3)	Both
Δ MAXQ(psf)	+0.1	−0.3	−0.2
Staging			
Δ Q (pfs)	−0.3	+0.1	−0.3
Δ ALT (ft)	+317	−40	+256
Δ VEL (fps)	+2.3	−1.4	+1.1
$\Delta \gamma$ (deg)	+0.04	−0.00	+0.04
Δ MECO wt (lb)	+109	−44	+66
Δ MECO time (sec)	−0.06	+0.03	−0.04

TABLE 10.9 (DELETED)

TABLE 10.9.1

BLOCK II/IIA SSMEs INFLUENCE COEFFICIENTS

Parameter (Y)	A_{ij}		
	j = 1	j = 2	j = 3
F	462,014.433	6,544.29988	0.0
$\dot{W}_{O_2}$	857.653171	36.2920961	− 10.5142105
$\dot{W}_{H_2}$	142.184188	6.01627715	− 1.74296417
$\dot{W}_{GO2}$	2.57731942	− 1.16788141	0.434694338
$\dot{W}_{GH2}$	0.699999967	0.0	0.0
P_c	2,746.99991	0.0	0.0
A_{ex}	5.80781835	0.0	0.0
*Per SSEIG briefing Revision 00-03L and 00-04S Annual Propellant Inventory Update, M. C. R. Evans, B-RSS, March 2000			

TABLE 10.9.2 (DELETED)

TABLE 10.9.3 (DELETED)

TABLE 10.10

SSME DEFLECTIONS DUE TO ELASTIC STRUCTURAL DEFLECTION

$$\Delta\beta_{y,z_i} = -\left(A + B\beta_{y_i} + C\beta^2{}_{y_i} + D\beta_{z_i} + E\beta^2{}_{z_i}\right)\frac{Ti}{470,000\ lb} + Fn_x + Gn_z$$

Where:

$\Delta\beta_{y_iz_i}$ = total SSME-i nozzle pitch, yaw rotation due to elastic structural deflection (deg)

β_{y_i} = SSME-i nozzle pitch angle respect to null for rigid structure (deg)

β_{z_i} = SSME-i nozzle yaw angle with respect to null for rigid structure (deg)

T_i = thrust produced by SSME = i (lb)

n_x = longitudinal acceleration (G_S) – positive forward

n_z = normal accelerations (G_S) – positive upward

	SSME – 1		SSME – 2		SSME – 3	
	Pitch	Yaw	Pitch	Yaw	Pitch	Yaw
A	0.566	– 0.3802	0.5052	0.0831	1.4776	– 0.4265
B	0.03537	– 0.00134	0.02995	– 0.000261	0.09415	– 0.00102
C	0.000206	– 0.000408	– 0.000382	– 0.000276	– 0.00007	– 0.000192
D	0.00049	0.00863	– 0.00563	– 0.000349	– 0.00413	0.00313
E	– 0.000278	0.000238	0.000066	0.000158	– 0.00043	0.000142
F	0.1054	– 0.0104	0.1143	0.0102	0.1645	– 0.0108
G	– 0.0368	0.0069	– 0.0331	0.0069	– 0.1580	– 0.0082

NOTES :
1. $\Delta\beta_{y_i}$, β_{y_i} are positive deflections down (deg)
2. $\Delta\beta_{z_i}$, β_{z_i} are positive deflections left (deg)
3. Values for A, B, C, D, E, F, G, based on OV-102 with three engines running

TABLE 10.11

SRB TAIL-OFF PITCH MOMENT

Total SRB Thrust (LBF)	Pitching Moment (FT – LB)
4000000.0	0.0
3325478.0	– 518000.0
3188119.0	– 567000.0
3017023.0	– 640000.0
2703750.0	– 780000.0
2181134.0	– 1010000.0
1686420.0	– 1170000.0
1335401.0	– 1400000.0
1094964.0	– 1700000.0
910284.0	– 2300000.0
718708.0	– 2650000.0
572050.0	– 2900000.0
442715.0	– 2950000.0
335404.0	– 2700000.0
251291.0	– 2240000.0
185136.0	– 1200000.0
133048.0	– 750000.0
93898.0	– 500000.0
64510.0	– 100000.0
0.0	0.0

FIGURE 10-1

CREW MODULE SLOPE MODEL

SOURCE: RI/STSD IL FSD&P/AFS-84-068

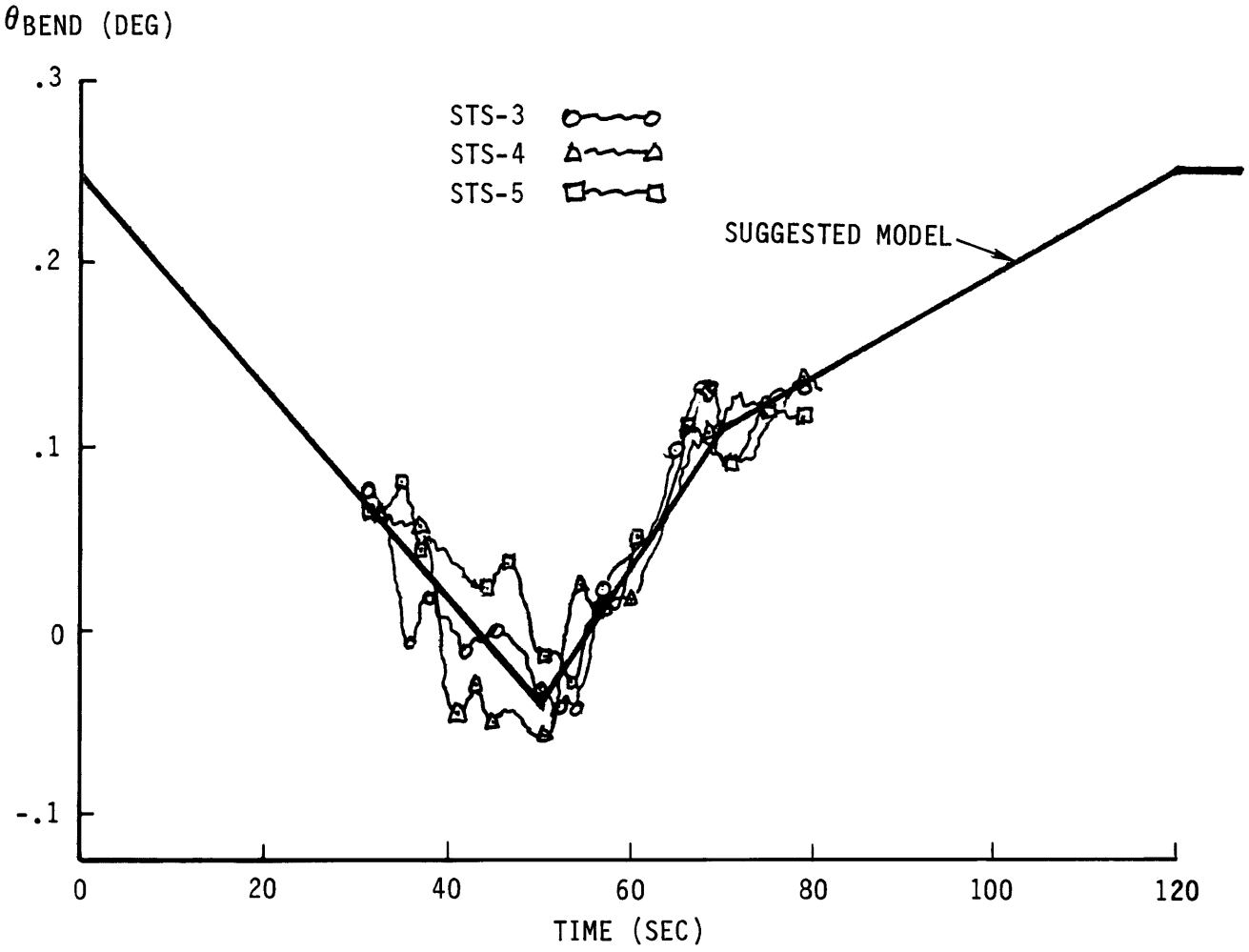

FIGURE 10-2

SRB TAIL-OFF PITCH MOMENT

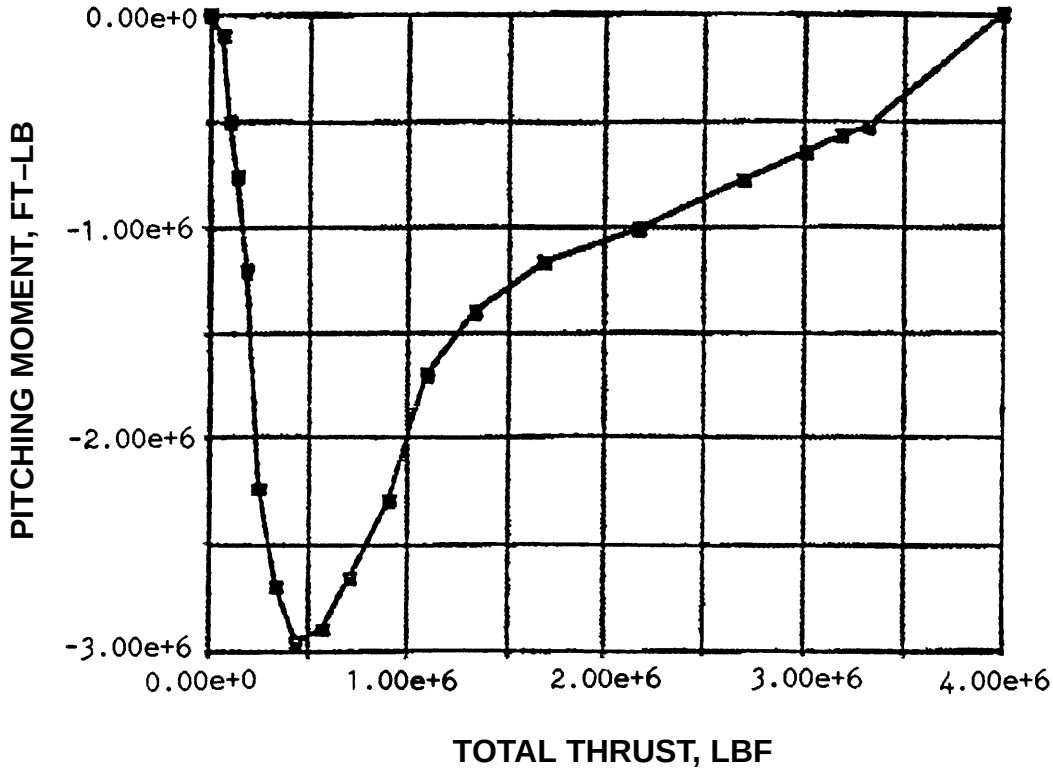

FIGURE 10-3

PREDICTED CREW VIBRATION AS A FUNCTION OF PAYLOAD CG